

Spring 2021

# Fate of Persistent Contaminants and Emerging Algal Toxins in Drinking Water and the Environment

Danielle Christine Westerman

Follow this and additional works at: <https://scholarcommons.sc.edu/etd>



Part of the [Chemistry Commons](#)

---

## Recommended Citation

Westerman, D. C.(2021). *Fate of Persistent Contaminants and Emerging Algal Toxins in Drinking Water and the Environment*. (Doctoral dissertation). Retrieved from <https://scholarcommons.sc.edu/etd/6431>

This Open Access Dissertation is brought to you by Scholar Commons. It has been accepted for inclusion in Theses and Dissertations by an authorized administrator of Scholar Commons. For more information, please contact [digres@mailbox.sc.edu](mailto:digres@mailbox.sc.edu).

Fate of Persistent Contaminants and Emerging Algal Toxins in Drinking Water and the  
Environment

by

Danielle Christine Westerman

Bachelor of Science  
University of Puget Sound, 2016

---

Submitted in Partial Fulfillment of the Requirements

For the Degree of Doctor of Philosophy in

Chemistry

College of Arts and Sciences

University of South Carolina

2021

Accepted by:

Susan D. Richardson, Major Professor

S. Michael Angel, Committee Member

Sheryl Wiskur, Committee Member

Peter Binev, Committee Member

Tracy L. Weldon, Interim Vice Provost and Dean of the Graduate School

© Copyright by Danielle Christine Westerman, 2021  
All Rights Reserved

## DEDICATION

I dedicate this dissertation to my amazing family: my parents, Theresa and Erik, my sister Cheyenne, and my brother Erik. You have continuously supported me through the marathon that has been my academic career, and I will forever appreciate you. Also, to Ms. Bailey Dog Westerman; love you my gal.

## ACKNOWLEDGEMENTS

First, I want to thank my incredible research mentor, Susan Richardson. Your guidance not only helped me to learn and grow as a researcher, but also as a person. These last five years have taught me how to face adversity with grace and composure (at least more than I was able before), to persist and stay curious even through failure, and to find inspiration from anywhere and everywhere. I am also truly grateful for the overwhelming kindness and hospitality felt from you and Andy; you made joining this lab feel like joining your family.

I would like to thank the many graduate students I have had the privilege to work with over the years: Josh Allen, Madison Kilpatrick, Caroline Granger, Amy Cuthbertson, Hannah Liberatore, Kristin Cochran, Md. Tareq Aziz, Dallas Abraham, Allie Forster, and Ashley Perkins (during your undergraduate and graduate career). Special thanks also to Dayla Rich, Meagan Smith, Sam Putnam, and the endless colleagues and friends I was able to grow alongside throughout this experience. I am also very grateful for my committee members: Drs. Mike Angel, Sheryl Wiskur, and Peter Binev, along with my lecture professors Dr. John Ferry and Dr. Tim Shaw, for their helpful feedback and comments.

## ABSTRACT

Population growth and global climate change has resulted in the degradation of pristine water sources, causing issues like saltwater intrusion, persistent harmful algal blooms, and drought from population growth. Future reliance on alternative sources of drinking water to is expected globally, therefore, nontraditional sources of drinking water are becoming increasingly vital sources of potable water around the world. For example, desalination (typically by reverse osmosis), despite its high energy demands and high cost, is being utilized all over the world to meet drinking water demand. Wastewater reuse, the additional treatment of wastewater to produce drinking water, either directly or indirectly, is also being explored, with the largest indirect potable reuse system in the world producing one hundred million gallons of water a day in California. Traditional drinking water treatment is also being impacted; harmful algal blooms are increasing in both frequency and abundance, putting additional strain on drinking water treatment needs and impacting drinking water quality in ways that are not fully understood.

Desalination, in an effort to maintain and extend the lifetime of filters and membranes, pre-chlorinate intake waters, forming chlorinated brines that are released back into the aquatic environment without additional treatment. Wastewater reuse is required to remove contaminants traditional wastewater treatment does not, resulting in the use of both traditional (UV/H<sub>2</sub>O<sub>2</sub>) and novel (UV/NO<sub>3</sub><sup>-</sup>/HCO<sub>3</sub><sup>-</sup>) advanced oxidation processes (AOPs) to remove emerging contaminants (ECs) without forming equally concerning transformation products. Harmful algal blooms and their resulting toxins must

be assessed in the environment before steps can be taken toward remediation, but quantitative approaches for individual toxins have previously been unavailable.

Three studies presented here integrate newly developed analytical methods for the assessment of desalination, advanced oxidation, and harmful algal bloom impacted water systems. Pre-chlorination practices in desalination facilities impact both public health and the aquatic environment through the production of toxic disinfection by-products (DBPs). Wastewater reuse via two different AOPs are shown to degrade ECs, but do so incompletely, forming new transformation products that impact toxicity. Toxins specific to *Lyngbya wollei*, a freshwater algae impacting drinking water sources across the United States, are analyzed by high resolution mass spectrometry that resulted in a new, selective, and sensitive method for the quantification of *Lyngbya wollei* toxins.

## TABLE OF CONTENTS

Dedication.....	iii
Acknowledgements.....	iv
Abstract.....	v
List of Tables .....	viii
List of Figures.....	x
Chapter 1: Introduction.....	1
Chapter 2: Desalination Wastewaters as a Source of Disinfection By-Products in Aquatic Environments .....	3
Chapter 3: Investigation of New Green Technologies for Improving the Safety of Drinking Water: Non-Target Analysis of Transformation Products from Emerging Contaminants.....	26
Chapter 4: Emerging <i>Lyngbya wollei</i> toxins: A New High Resolution Mass Spectrometry Method to Elucidate a Potential Environmental Threat .....	46
References.....	63
Appendix A – Supporting Information for Chapter 2.....	77
Appendix B – Supporting Information for Chapter 3 .....	114
Appendix C – Supporting Information for Chapter 4.....	139
Appendix D – Reprint Permissions.....	145
Appendix E – Publications.....	151



## LIST OF TABLES

Table 2.1 – Water Quality Parameters in Desalination Plants.....	22
Table 3.1 – Contaminants of Emerging Concern.....	39
Table 4.1 – High Resolution Fragmentation Data for Saxitoxin .....	54
Table 4.2 – High Resolution Fragmentation Data for LWT1 .....	56
Table 4.3 – High Resolution Fragmentation Data for LWT4.....	57
Table 4.4 – High Resolution Fragmentation Data for LWT5 .....	58
Table 4.5 – High Resolution Fragmentation Data for LWT6.....	59
Table A.1 – GC-MS Details and Vendor Information for Quantified DBPs.....	79
Table A.2 – Summary of analytical methods for Desalination.....	81
Table A.3 – DBP known cytotoxicity values (LC <sub>50</sub> ) .....	82
Table A.4 – DBP known genotoxicity values (MTM) .....	85
Table A.5 – DBP Concentrations for Desalination Plant 1 (µg/L).....	87
Table A.6 – DBP Calculated Cytotoxicity Index Value for Desalination Plant 1 .....	90
Table A.7 – DBP Calculated Genotoxicity Index Value for Desalination Plant 1 .....	93
Table A.8 – DBP Concentrations for Desalination Plant 2 (µg/L).....	96
Table A.9 – DBP Calculated Cytotoxicity Index Value for Desalination Plant 2 .....	99
Table A.10 – DBP Calculated Genotoxicity Index Value for Desalination Plant 2 .....	102
Table A.11 – DBP Concentrations for Desalination Plant 3 (µg/L).....	105
Table A.12 – DBP Calculated Cytotoxicity Index Value for Desalination Plant 3 .....	108

Table A.13 – DBP Calculated Genotoxicity Index Value for Desalination Plant 3 .....	111
Table B.1 – UHPLC Parameters .....	115
Table B.2 – UHPLC-QTOF Parameters .....	116
Table B.3 – Detected transformation products of bisphenol-A during UV/H <sub>2</sub> O <sub>2</sub> treatment.....	117
Table B.4 – Detected transformation products of estrone during UV/H <sub>2</sub> O <sub>2</sub> treatment ...	121
Table B.5 – Detected transformation products of diclofenac during UV/H <sub>2</sub> O <sub>2</sub> treatment.....	123
Table B.6 – Detected transformation products of triclosan during UV/H <sub>2</sub> O <sub>2</sub> treatment .	126
Table B.7 – Individual cytotoxicity of BPA, IBP, DCF, TCS, and E1 during the UV/H <sub>2</sub> O <sub>2</sub> treatment in Milli-Q water .....	129
Table B.8 – Detected transformation products of bisphenol-A in UV/NO <sub>3</sub> <sup>-</sup> /HCO <sub>3</sub> <sup>-</sup> . .....	130
Table B.9 – Detected transformation products of triclosan in UV/NO <sub>3</sub> <sup>-</sup> /HCO <sub>3</sub> <sup>-</sup> .....	132
Table B.10 – Detected transformation products of diclofenac in UV/NO <sub>3</sub> <sup>-</sup> /HCO <sub>3</sub> <sup>-</sup> . .....	136
Table B.11 – Detected transformation products of estrone in UV/NO <sub>3</sub> <sup>-</sup> /HCO <sub>3</sub> <sup>-</sup> . .....	138

## LIST OF FIGURES

Figure 2.1 – Treatment Train Depiction of Desalination Plant .....	23
Figure 2.2 – Stack plots of DBP concentration by class, calculated cytotoxicity index values, and genotoxicity index values for Plants 1, 2, and 3 .....	24
Figure 2.3 – Stack plots of DBP concentration by halogenation for Plants 1, 2, and 3.....	25
Figure 3.1 – Possible degradation pathways of bisphenol-A in UV/H <sub>2</sub> O <sub>2</sub> .....	40
Figure 3.2 – Possible degradation pathways of estrone in UV/H <sub>2</sub> O <sub>2</sub> .....	41
Figure 3.3 – Possible degradation pathways of diclofenac in UV/H <sub>2</sub> O <sub>2</sub> .....	42
Figure 3.4 – Possible degradation pathways of triclosan in UV/H <sub>2</sub> O <sub>2</sub> .....	43
Figure 3.5 – Possible degradation pathways of ibuprofen in UV/H <sub>2</sub> O <sub>2</sub> .....	44
Figure 3.6 – Possible degradation pathways of triclosan, diclofenac, bisphenol-A, and estrone in UV/NO <sub>3</sub> <sup>-</sup> /HCO <sub>3</sub> <sup>-</sup> .....	45
Figure 4.1 – Molecular structures of the Lyngbya wollei toxins (LWTs) 1-6.....	61
Figure 4.2 – LC-MS chromatogram for LWT1,4,5,6 .....	62
Figure B.1 – High resolution MS/MS mass spectrum and tentative structure of B <sub>243</sub> .....	119
Figure B.2 – High resolution MS/MS mass spectrum and tentative structure of B <sub>167</sub> .....	119
Figure B.3 – High resolution MS/MS mass spectrum and tentative structure of B <sub>245</sub> .....	120
Figure B.4 – High resolution MS/MS mass spectrum and tentative structure of E <sub>285</sub> .....	122
Figure B.5 – High resolution MS/MS mass spectrum and tentative structure of D <sub>212</sub> ....	124
Figure B.6 – High resolution MS/MS mass spectrum and tentative structure of D <sub>214</sub> ....	125
Figure B.7 – High resolution MS/MS mass spectrum and tentative structure of D <sub>244</sub> ....	125

Figure B.8 – High resolution MS/MS mass spectrum and tentative structure of T <sub>235</sub> .....	127
Figure B.9 – High resolution MS/MS mass spectrum and tentative structure of T <sub>143</sub> .....	128
Figure B.10 – High resolution MS/MS mass spectrum and tentative structure of B <sub>287</sub> ...	131
Figure B.11 – High resolution MS/MS mass spectrum and tentative structure of T <sub>235</sub> ...	134
Figure B.12 – High resolution MS/MS mass spectrum and tentative structure of T <sub>249</sub> ...	134
Figure B.13 – High resolution MS/MS mass spectrum and tentative structure of T <sub>283</sub> ...	135
Figure B.14 – High resolution MS/MS mass spectrum and tentative structure of T <sub>317</sub> ...	135
Figure B.15 – High resolution MS/MS mass spectrum and tentative structure of T <sub>253</sub> ...	136
Figure B.16 – High resolution MS/MS mass spectrum and tentative structure of D <sub>260</sub> ..	137
Figure B.17 – High resolution MS/MS mass spectrum and tentative structure of D <sub>214</sub> ..	137
Figure C.1 – +ESI High resolution mass spectra of LWT 2/3 at 3.87 mins obtained from the UHPLC-QTOF.....	140
Figure C.2 – +ESI High resolution mass spectra of LWT1 at 3.87 mins obtained from the UHPLC-QTOF.....	141
Figure C.3 – +ESI High resolution mass spectra of LWT 2/3 at 3.87 mins obtained from the UHPLC-QTOF.....	142
Figure C.4 – +ESI High resolution mass spectra of LWT4 at 6.13 mins obtained from the UHPLC-QTOF.....	143
Figure C.5 – +ESI High resolution mass spectra of LWT5 at 5.84 mins obtained from the UHPLC-QTOF.....	144
Figure C.6 – +ESI High resolution mass spectra of LWT6 at 4.96 mins obtained from the UHPLC-QTOF.....	145

## CHAPTER 1

### INTRODUCTION

Chapter 2 provides results from a case study on the presence of organic contaminants in desalination waters, both treated drinking water and wastewaters released into the environment, to elucidate both environmental and public health impacts. More than 50 regulated and priority, unregulated disinfection by-products (DBPs) were quantified across three different desalination plants, where toxic brominated and iodinated DBPs were observed at higher ratios than from traditional drinking water sources, which was attributed to the incorporation of the inorganic bromide and iodide present in seawater. Also, DBPs present in desalination wastewaters were also quantified in the source water, showing their persistence in the aquatic environment.

Chapter 3 investigates the use of both traditional (UV/H<sub>2</sub>O<sub>2</sub>) and novel (UV/NO<sub>3</sub><sup>-</sup>/HCO<sub>3</sub><sup>-</sup>) advanced oxidation processes (AOPs) and their ability to degrade emerging contaminants (ECs). ECs known to be unaffected by traditional wastewater treatment that persist at environmentally relevant levels were evaluated, with both AOPs exhibiting at least some degradation of ECs. Many ECs were not completely mineralized, therefore, high resolution mass spectrometry was used to identify transformation products formed in both AOPs. Chapter 4 provides the first high resolution mass spectral data for toxins produced by the benthic freshwater algae, *Lyngbya wollei* (LWTs). Not only does this information provide detailed structural information through the identification of

fragment ions, but also resulted in the optimization of a sensitive method to quantify LWTs via liquid chromatography (LC)-mass spectrometry (MS).

CHAPTER 2  
DESALINATION WASTEWATERS AS A SOURCE OF DISINFECTION  
BY-PRODUCTS IN AQUATIC ECOSYSTEMS

Westerman, D. C.; Powers, L. C.; Gonsior, M.; Richardson, S. D., Desalination Wastewaters as a Source of Disinfection By-Products in Aquatic Ecosystems. To be submitted to *Environ. Sci. Technol.*

## **ABSTRACT**

Future reliance on desalination to provide suitable drinking water is expected globally as a result of population growth and increased freshwater scarcity. Desalination, specifically via reverse osmosis (RO) is expected to be a major source of reliable drinking water along coastal regions. Before the desalination process, water is disinfected by chlorine to limit membrane biofouling. While there is some information on disinfection by-products (DBPs) in finished drinking water following desalination, little is known about the DBPs formed in the reject waters that generally get discharged back to sea. Elevated levels of bromide and iodide in seawater may form brominated and iodinated DBPs, most of which are highly toxic. Desalination plants are allowed to discharge chlorinated reject water into the coastal environment, dispersing the newly formed DBPs in the process. Samples that both were and were not subject to pre-chlorination were evaluated (when available) for each location in order to differentiate between environmental contaminants and disinfection by-products, a strategy that was found to be necessary where outfall is located near seawater intake systems. Quantification of 53 known DBPs was performed by liquid-liquid extraction followed by gas chromatography-mass spectrometry (GC-MS). Quantification data was then utilized to calculate predicted relative cytotoxicity and genotoxicity for each sample in order to provide insight into the formation of DBPs in seawater treatment and their potential impacts on public health and aquatic environments. Pre-chlorinated samples (including lab chlorinated samples) have higher levels of DBPs than their non-chlorinated counterparts. Brominated DBPs were found to be much more abundant than iodinated DBPs in desalination reject waters, with either brom- and/or bromo-chloro-DBPs as the most abundant halogenation at all locations. In locations where the outfall is located near seawater intake, DBPs were found in influent seawater



before chlorination, suggesting the potential persistence of DBPs released from desalination facilities in the coastal environment. This project is the first to show the presence and potential stability of DBPs as environmental contaminants resulting from desalination and their potential impacts on aquatic ecosystems.

## **INTRODUCTION**

Drinking water disinfection is vital to public health, and is considered the greatest public health achievement of the 20th century.<sup>1-2</sup> An unintended consequence of disinfection is the formation of disinfection by-products (DBPs) through the reaction of disinfectants with natural organic matter (NOM), bromide, and iodide.<sup>3-5</sup> Epidemiologic studies have linked DBPs to cancer, birth defects, and miscarriage.<sup>4,6-12</sup> In the U.S., regulations are enforced for four trihalomethanes (THMs), five haloacetic acids (HAAs), bromate, and chlorite under the Stage 2 Disinfectants and DBP Rule.<sup>13</sup>

Due to the increase in freshwater scarcity, either from the degradation of pristine water sources or increased demand from population growth, nontraditional sources of drinking water are becoming increasingly vital around the world. Desalination, despite its high energy demands and high cost, is being utilized at many locations (and even inland locations) to meet drinking water demand. With 1.2 billion people currently living under physical water scarcity, and 40% of the global population residing within 100 km from the coast, the global dependence on desalination is expected to grow.<sup>14-16</sup>

There are three main desalination methods for the production of drinking water: thermal distillation, electrodialysis, and reverse osmosis. Desalination plants now commonly perform reverse osmosis (RO) due to the comparatively low capital costs and higher freshwater production.<sup>16-18</sup> Brines formed during RO are typically concentrated

two-fold (up to 5x concentrated) and are typically discharged back into the environment (e.g., the sea).<sup>19</sup> In order to maintain and extend the life of RO membranes, plants typically include a disinfection step (often chlorine) at the beginning of the treatment train to prevent biofouling, but this can form DBPs.<sup>20-21</sup> DBPs are formed when the disinfectant reacts with the organic matter, bromide, and iodide present in source water. Little is known about DBP formation in treated seawater, and consequently, their potential environmental and human health impacts have not been fully addressed. Seawater is a different matrix than surface or ground water, therefore the disinfection of seawater can produce different relative amounts of known DBPs and entirely new DBPs, compared to freshwater.<sup>22-23</sup> Previous studies have analyzed RO permeate/finished water, with a focus on regulated THMs and HAAs,<sup>24-30</sup> with some including haloacetonitriles (HANs),<sup>24,26-28,31-32</sup> iodo-trihalomethanes (I-THMs),<sup>33</sup> or bromophenols.<sup>24,27-28,32,34</sup> DBP speciation between chlorinated seawater and surface water is very different, with brominated species predominant in the former, and chlorinated in the latter.<sup>33,35-36</sup> Not only have bromo-DBPs been associated with chlorinated seawater,<sup>28,30,37-38</sup> but there are many still to be investigated. When studying electro-chlorination of ballast water of an ocean-going vessel, 462 new and previously unknown, brominated compounds were identified, including 2,2,4-tribromo-5-hydroxy-4-cyclopentene-1,3-dione, which constituted 22% of the relative abundance of DBPs formed. The same study found dibromomethane at 1% relative abundance, which supports the need to evaluate small organics during the chlorination of seawaters.<sup>39</sup>

The differences in DBPs from saltwater and freshwater disinfection may result in different, currently unknown, toxicity. Brominated and iodinated disinfection by-products

are known to be more toxic than their chlorinated analogues,<sup>4,40</sup> but iodinated disinfection by-products (I-DBPs) do not typically form in chlorinated freshwaters because hypochlorous acid will readily oxidize iodide to iodate, which is non-toxic.<sup>41</sup> It is well established that Br-DBPs are formed in seawater chlorination,<sup>21</sup> but the possibility for formation of I-DBPs during the chlorination of seawater cannot be ignored due to the elevated concentration of iodide in seawater ( $\sim 60 \mu\text{g L}^{-1}$ )<sup>42-43</sup> as compared to the trace levels found in freshwater (median iodide of  $1.9 \mu\text{g/L}$ ).<sup>44</sup> The increased toxicity and potential for formation of brominated and iodinated DBPs make them a priority for investigation in desalinated waters. DBPs from desalination is of particular concern because they not only impact human health through finished drinking water, but they also may pose a potential threat to nearby aquatic ecosystems. Discharge of the brine waste to the environment is an acceptable form of disposal,<sup>19</sup> therefore, DBPs are released when pre-chlorinated reject waters are discharged into the environment. It is currently unknown what effects DBPs will have on the surrounding ecosystems.

This project seeks to understand the production, speciation, and environmental fate of DBPs produced at desalination plants, with a focus on chlorinated RO reject water. We report for the first time, the measurement of 53 regulated and unregulated DBPs in reject waters from three full-scale desalination plants, including haloacetonitriles (HANs), haloamides (HAMs), halonitromethanes (HNMs), haloacetaldehydes (HALs), haloketones (HKs), trihalomethanes (THMs), and iodinated THMs (I-THMs), and the calculated toxicity associated with the DBPs.

## MATERIALS AND METHODS

**Chemical Reagents.** General reagents were ACS reagent grade and were purchased from Sigma-Aldrich (St. Louis, MO), VWR International (Radnor, PA), and Fisher Scientific (Waltham, MA). DBP standards were purchased or custom synthesized from Sigma-Aldrich, CanSyn Chem. Corp. (Toronto, ON), Aldlab Chemicals (Woburn, MA), and TCI America (Waltham, MA) at the highest level of purity available. All solvents (acetonitrile (ACN), methyl *tert*-butyl ether (MTBE), methanol (MeOH), and ethyl acetate) were of highest purity and were purchased from Sigma-Aldrich, VWR International (Radnor, PA), or Fisher Scientific. Artificial seawater salts were manufactured by Instant Ocean (Blacksburg, VA) and diluted in laboratory as necessary.

**Sampling.** All samples were collected in amber glass bottles, filled headspace free. After collection, samples were shipped on ice and processed (or chlorinated) within 48 h of collection. Samples subject to chlorination at the treatment plant were quenched with ammonium chloride (5 mg/L) and pH adjusted (pH 3.5-4) with sulfuric acid at time of collection and extracted/reacted within 24 h. Sample parameters and locations can be found in Table 2.1.

**Plant 1: Water Collection and Treatment.** Plant 1 was the only plant utilizing pre-chlorination during the time of sampling. For this reason, it was especially important to take samples at multiple locations throughout the treatment train (Figure 2.1). Samples were collected before treatment (raw), after pre-chlorination pre-treatment (PT), both RO permeate and reject waters, and finally finished drinking water. Due to the use of pre-chlorination on site, in lab chlorination reactions were not performed for this location.

**Plant 2: Water Collection and Treatment.** Raw seawater was collected in the aquatic environment next to the intake valve supplying seawater to the Plant 2 desalination facility. The plant RO reject waters (denoted as “brine”) were collected at the outfall pipe where they are released to the environment. At the time of sampling, the desalination facility was not performing pre-chlorination as part of the treatment train, therefore, raw and reject samples were chlorinated (24 h) in the laboratory to mimic the DBP formation.

**Plant 3: Water Collection and Treatment.** Plant influent (denoted as “raw”) from Plant 3 is a brackish groundwater source, not a marine environment. The plant reject waters (denoted as “brine”) were collected as the post-RO wastewater in the desalination facility. Finished drinking water was also acquired at the plant. At the time of sampling, Plant 3 was not performing pre-chlorination as part of the treatment train, therefore, samples were chlorinated (24 h reaction) in the laboratory to provide insight on the DBP formation of pre-chlorinated waters.

**Lab chlorination reactions.** A 500 mg L<sup>-1</sup> combusted NaCl (extra pure, Acros chemicals) solution was chlorinated for 15 min using an electrochlorination unit (ChlorMaker saltwater chlorine generator, ControlOMatic, Inc). Free chlorine (Cl<sub>2</sub>) concentrations were determined using HACH Method 8021 (USEPA DPD method for free chlorine) with a HACH autoanalyzer. Chlorine was diluted when necessary and added to samples (described by “+ Cl<sub>2</sub>”) and reacted for 24 h, after which the samples were quenched with ammonium chloride in 10 fold excess.

**Analytical Methods. Bulk Parameters.** The analytical methods for dissolved organic carbon (DOC), specific UV absorbance (SUVA), total dissolved nitrogen (TDN), and salinity measurements are summarized in Appendix A.2.

*DBP quantification.* Liquid-liquid extraction (LLE), modified from a previously published method,<sup>45</sup> was used to quantify 53 DBPs in all samples. Analyte stock solutions were made by dissolving DBP standards in acetonitrile, methanol, or MTBE. DBP standard solutions were prepared by diluting individual DBP stocks together to make 100 mg/L mixtures of each DBP class in MeOH, then diluting again to 10 mg/L in MeOH. In both cases, fluorobenzaldehyde and 1,2-dibromopropane were used as the surrogate standard and the internal standard, respectively.

During extraction, a 100 mL aliquot of sample was pH adjusted with H<sub>2</sub>SO<sub>4</sub> to pH < 2 and 30 g sodium sulfate was added, followed by 3x LLE of 5 mL MTBE. Extracts were concentrated under nitrogen, spiked with surrogate/internal standard, and analyzed using gas chromatography (GC)-mass spectrometry (MS) with electron ionization (EI) and selected ion monitoring (SIM) (7890 GC, 5977A mass spectrometer, Agilent Technologies, Santa Clara, CA) using an Rtx-200 column (30 m x 0.25 mm x 0.25 μm film thickness; Restek Corporation, Bellefonte, PA). Additional extraction details can be found in Appendix A.

Finished drinking water was quantified via internal calibration in nanopure (18 MΩ) water for finished drinking water; other samples were analyzed using a 3-point standard addition (0, 1.0, 2.0 μg/L) curve. Standard addition was applied within a previously determined linear range (0.1 – 40 μg/L) for each analyte in artificial seawater (Instant Ocean). Artificial seawater was made by dissolving aquarium salt to three times the recommended concentration (105 PSU), since that was the highest acceptable concentration factor during RO set by the participating desalination plants. Spiked seawater matrix was quantified in triplicate via standard addition to evaluate method

accuracy, and values were only reported for analytes with linear coefficients ( $R^2$ ) of 0.8 and above (see Appendix A.3).

**TIC-Tox Calculations.** Calculated toxicity associated with DBPs in each sample was based on the “TIC-Tox” method.<sup>46</sup> Molar concentrations of each DBP were multiplied by their corresponding cyto- and genotoxicity index values for Chinese hamster ovary cells (CHO) and summed together for cytotoxicity and genotoxicity values for each sample. Haloketones, tribromoacetonitrile, and iodoacetonitrile were not included in TIC-Tox calculations due to the lack of previously measured toxicity index values. TIC-Tox cytotoxicity and genotoxicity values can be found in Appendix A.4 and A.5, respectively.

## **RESULTS AND DISCUSSION**

Plants 1, 2, and 3 sampled during this project each had different source water characteristics, high DOC seawater, low DOC seawater, and brackish groundwater, respectively (Table 2.1). For all plants, DBPs were found on both sides of the RO membrane, with DBP precursor material impacting both sides of the membrane, resulting in an increase in DBP formation after chlorination of both RO permeate and reject waters. Chloro- and chloro-bromo-DBPs were the dominant halogen incorporation across all plants, with some I-DBPs formed in seawater intake locations (Plant 1 and Plant 2).

### **DBP Formation at Three Desalination Plants.**

*Plant 1.* Plant 1 had the highest level of total DBPs of any plant, with a total DBP concentration around 100  $\mu\text{g/L}$ , whereas all other plants were below 40  $\mu\text{g/L}$  (Figure 2.2) which was only achieved after lab chlorination experiments. The relatively high levels of DBPs is likely due to the use of pre-chlorination at Plant 1 at the time of sampling. The

pre-treatment (PT) sample was collected immediately after adding disinfectant, with the brackish water (BW) and RO permeate collected on either side of the RO membrane. The RO permeate is blended with water from a nearby freshwater source and disinfected to generate the finished drinking water (FW). The RW was found to contain predominantly 1,1-dichloropropanone (1.4  $\mu\text{g/L}$ ), with 1-bromo-1,1-dichloropropanone and dibromoacetamide also quantified at 0.3  $\mu\text{g/L}$  and 0.2  $\mu\text{g/L}$ , respectively. The addition of chlorine resulted mostly in the formation of chloroform (1.1  $\mu\text{g/L}$ ) in the PT, and further down the treatment train, samples with increased contact time (BW and ROP) showed an increased formation of DBPs, predominantly in the form of trihalomethanes. Trihalomethanes were found on both sides of the RO membrane, but predominantly in ROP with 23.7  $\mu\text{g/L}$  bromoform quantified, demonstrating its ability to pass through the RO membrane. The hydrophobic nature of trihalomethanes, along with their relatively small molecular volume, allows them to undergo hydrophobic adsorption onto the RO membrane, increasing their ability to pass through. This is consistent with previous desalination studies that quantified trihalomethanes, specifically bromoform, in desalination finished waters.<sup>48</sup> Bromoform was also previously found to have a ~50% rejection rate from RO membranes, which means that 50% passes through the RO membrane.<sup>47</sup> Haloketones and haloacetamides were found in BW, with dibromoacetamide (2.9  $\mu\text{g/L}$ ) and 1,1-dichloropropanone (2.4  $\mu\text{g/L}$ ) the most abundant in each category, but no haloacetamides and only one haloketone (1,1-dichloropropanone, 1.0  $\mu\text{g/L}$ ) were quantified in ROP, suggesting haloacetamides and haloketones are mostly rejected by RO membranes and therefore impacting aquatic environments over drinking water during desalination. Haloacetamides and haloketones have been previously found



to have high percent rejection by RO membranes, with all haloacetamides and haloketones studied exhibiting over 80% rejection.<sup>47</sup> The greatest formation of DBPs was in the finished water, likely due to the addition of surface water, which contains more reactive aromatic groups (higher SUVA) than seawater, and therefore, is more likely to form DBPs. Haloacetamides, trihalomethanes, haloacetaldehydes, and haloketones were the dominant classes quantified in finished water at Plant 1, with levels of 30.8 µg/L, 26.5 µg/L, 15.6 µg/L, and 14.7 µg/L, respectively. The increase in haloacetaldehydes and haloketones, specifically bromodichloroacetaldehyde (14.3 µg/L) and 1-bromo-1,1-dichloropropanone (6.0 µg/L), compared to ROP is likely due to the blending of finished waters, since neither class is expected to permeate RO membranes at a high fraction, and since additional bromide has been shown to incorporate after RO with the addition of DOM.<sup>48</sup>

*Plant 2.* Plant 2 is the only plant with a high quantity (>5 µg/L) of DBPs in the untreated raw seawater (Figure 2.2). The presence of DBPs in the source water shows that the reject water discharged by the plant is contributing DBPs to the aquatic ecosystem and they are stable enough in the environment to persist and re-enter the treatment plant.<sup>33</sup> In fact, of the six classes of DBPs quantified in the chlorinated reject water (BW + Cl<sub>2</sub>), all but haloacetaldehydes were present in the raw water. The decrease in haloacetamides, haloacetonitriles, and haloacetaldehydes from chlorinated wastewater to raw water suggests these classes do not persist as long in the aquatic environment, compared to haloketones, halonitromethanes, and trihalomethanes, which stay the same or increase in concentration. In fact, the greater concentration of trihalomethanes and

halonitromethanes in the raw water suggests these classes may even accumulate in this environment when chlorinated RO permeate is discharged by the desalination plant.

After chlorination, an increase in DBPs was observed, with the greatest increase from halonitromethanes. Before chlorination, a total of 1.2  $\mu\text{g/L}$  halonitromethanes was quantified in the raw water (predominantly tribromonitromethane at 0.9  $\mu\text{g/L}$ ), but after chlorination, bromodichloronitromethane, dibromochloronitromethane, and tribromonitromethane were all individually above the previous total for all halonitromethanes (1.1, 3.0, and 2.8  $\mu\text{g/L}$ , respectively). The considerable concentration of halonitromethanes (7.0  $\mu\text{g/L}$ ) compared to all other DBPs quantified (3.4  $\mu\text{g/L}$ ) suggests that raw water contains precursor material for halonitromethanes more than any other class quantified. Nitrite is a known precursor to halonitromethane formation,<sup>49-50</sup> and would not be expected to permeate an RO membrane due to its overall charge of minus one. No increase in haloacetonitriles, haloketones, and haloacetamides was found following the addition of chlorine (indicating their formation is not favored compared to halonitromethanes). DBPs that were consistent from RW to RW + Cl<sub>2</sub> increased in reject water after chlorination. The increased formation of haloacetonitriles, haloketones, and haloacetamides in the brackish water compared to the raw is likely due to the removal of HNM precursor material (nitrite) during RO, allowing the disinfectant to react and form the aforementioned DBP classes instead.

The observation of DBPs in the raw water, even without the use of pre-chlorination, provides insight regarding which DBPs will be rejected by the RO membrane and which will be present in the RO permeate. The increase in halonitromethanes from RW to BW suggests they are rejected by the RO membrane,

increasing their concentration in the process. Trihalomethanes and haloketones, however, decreased from raw water to reject, implying they either transform or pass through the RO membrane. Haloamides and haloacetonitriles had relatively consistent concentrations from raw to reject water. Little change in concentration assumes an equal likelihood to pass through the RO membrane as rejection.

*Plant 3.* Plant 3, being a brackish groundwater source, had the lowest DBP concentrations in non-chlorinated raw water of the three plants assessed in this study. Upon chlorination, however, Plant 3 was found to have almost 40 µg/L total DBPs in chlorination raw water, and >10 µg/L in the brackish RO permeate. This is higher than the other two plants where the raw and brackish water samples did not surpass 15 µg/L for any sample, even though they had higher DOC and salinity than Plant 3. Although there is less precursor material in the source water (low DOC), the DBP formation potential was higher at Plant 3, likely due to the increased aromaticity (SUVA 14 m<sup>-1</sup> L mg<sup>-1</sup>) compared to Plant 1 (2.8 m<sup>-1</sup> L mg<sup>-1</sup>) or Plant 2 (1.3 m<sup>-1</sup> L mg<sup>-1</sup>). This is consistent with previous knowledge that natural organic matter (NOM) in freshwater sources is usually more aromatic than ocean NOM.<sup>22-23</sup>

The chlorinated raw water formed halonitromethanes, haloacetonitriles, trihalomethanes, and haloketones in similar quantities, ranging from 6.0 to 11.9 µg/L, with haloacetonitriles the largest contributor at 11.9 µg/L. Precursor material rejected by the RO membrane (in brackish water samples) formed predominantly haloketones (6.9 µg/L), followed by halonitromethanes (2.2 µg/L), haloacetonitriles (2.2 µg/L), and trihalomethanes (1.1 µg/L). The lack of haloacetaldehydes and relative decrease of trihalomethanes, haloacetonitriles, and halonitromethanes from raw to brackish water

suggests that precursor material for those DBP classes is able to pass through the RO membrane and impact finished water. The increase of haloketones from chlorinated raw to chlorinated brackish samples is attributed to the concentration factor that results from the RO process.

### **DBP Formation by Halogenation.**

*Plant 1.* At the time of RO, Br-DBPs were the dominant halogenated species in both the RO permeate and reject waters, with Cl-DBPs only observed in the permeate, and I-DBPs only in the reject water (Figure 2.3). Finished water is where Cl-DBPs become the most abundant class of halogenated DBPs, likely due to the increased ratio of reactive chlorine to reactive bromine or iodine.

*Plant 2.* Plant 2 formed iodinated DBPs in real samples from the treatment plant, as well as after in-lab chlorination. Triiodomethane was found at 0.9 µg/L in raw water, which is indicative of its presence in the affected aquatic environment (Figure 2.3). I-DBPs were also observed in the plant reject water, with iodoacetamide quantified at 0.6 µg/L. Both triiodomethane and iodoacetamide were observed in the chlorinated reject water. Dibromiodomethane is the mixed-halogen, iodine containing DBP that was also observed in the chlorinated reject water (0.3 µg/L).

Raw and reject samples had the same halogen speciation, with Br-DBPs the primary species quantified. After chlorination, the raw water was then dominated by the presence of Cl/Br-DBPs. A >3 fold increase (3.34x) in Cl-DBPs was also observed after the chlorination of raw water from Plant 2. The implementation of pre-chlorination at this plant, therefore, is likely to produce more chlorine containing DBPs, but shifts to Br-

DBPs when pre-chlorination is not used. The increase in both single and mixed halogen species of DBPs from BW to BW + Cl<sub>2</sub>, however, implies most DBPs formed are not reaching the RO permeate but are rejected and expelled into the environment.

*Plant 3.* Chlorine containing DBPs were overall the most predominant halogen species of DBPs in Plant 3 (Figure 2.3), which can be explained by the low salinity in the source water (5 PSU). The lack of natural bromide and iodide in the source water results in chlorine, both naturally present as inorganic chlorine and that added during chlorination, is the predominant halogen species in this plant. Chlorine containing DBPs were the most abundant at Plant 3 overall, with chloro-bromo- and Br-DBPs also present (and predominant in the finished water). Iodinated DBPs were not detected until the finished water, where dichloriodomethane and bromochloriodomethane were quantified at 0.2 and 0.4 µg/L, respectively. The increase in Br-DBP concentration from chlorinated raw to brackish water is likely due to the concentration of precursor material (and bromide) during the RO process, whereas the decrease in chlorine containing DBPs shows inorganic chlorine is more likely to pass through the RO membrane compared to bromine, which is supported by their relative size.<sup>47</sup>

### **Calculated Toxicity.**

*Plant 1.* Samples with the lowest DBP formation (RW and PT) from Plant 1 also have the lowest calculated cyto- and genotoxicity, with values two orders of magnitude lower than samples obtained further down the treatment train (Figure 2.2). A similar trend was observed for DBP formation and calculated toxicity, with the exception of cytotoxicity for the RO reject water (BW), which was found to be higher than that of ROP. The RO permeate, consisting of primarily THMs (76% by mass), was not as cytotoxic as the RO

reject waters, which was driven almost entirely by haloacetamides (81%). Both BW and ROP, however, were lower in both calculated cyto- and genotoxicity than the finished drinking water, likely due to the addition of treated surface water during blending. Finished water from Plant 1 formed much higher levels of haloacetaldehydes than any other sample (15.6 µg/L), which contributed to the increase in both cyto- and genotoxicity of the finished water. Other than the presence of haloacetaldehydes in the finished water, Plant 1 shows the impact of N-DBPs on calculated toxicity; with haloacetamides driving calculated cytotoxicity, followed by haloacetonitriles, then halonitromethanes. Haloacetonitriles were the primary drivers of calculated genotoxicity, followed by haloacetamides and halonitromethanes.

*Plant 2.* Both the calculated cyto- and genotoxicity from Plant 2 followed the same trend as the overall DBP formation for each sampling location. RW to BW shows a decrease in calculated cytotoxicity, but this is likely due to the lack of cytotoxicity values for tribromoacetonitrile, the only haloacetonitrile found in BW, whereas RW had a variety of haloacetonitriles present that contributed to the toxicity calculations (Figure 2.2). The cyto- and genotoxicity for RW is driven primarily by haloacetonitriles (44% cyto, 36% geno), followed by haloacetamides (31% cyto, 22% geno), which differs from BW that is almost entirely driven by halonitromethanes, both in cytotoxicity (91%) and genotoxicity (95%). After chlorination, the calculated toxicity of the raw water shifts from haloacetonitrile-driven for both toxicity calculations to halonitromethane-driven, due to the almost 6-fold increase (5.9x) in concentration of halonitromethanes after chlorination. Brackish water, however, shifts from almost entirely halonitromethane-driven in both cyto- and genotoxicity, to Haloacetamide- and haloacetonitrile-driven; accounting for

88% and 89% of both calculated cyto- and genotoxicity, respectively. Chlorinated brackish water is also where haloacetaldehydes are first formed in Plant 2, contributing to the calculated cytotoxicity (8%) more than the genotoxicity (2%) of the plant reject water.

*Plant 3.* At Plant 3, the lack of DBPs quantified in RW and BW result in zero calculated cyto- and genotoxicity for the non-chlorinated samples collected at this site (Figure 2.2). All other samples, however, were driven by haloacetonitriles and halonitromethanes for both calculated cyto- and genotoxicity, representing a combined >75% in every sample up to 100% of the toxicity calculation. Chlorinated brackish water and finished water were both more genotoxic than chlorinated raw water, which is opposite the trend observed for DBP concentration. The haloacetonitriles in RW+Cl<sub>2</sub> consist of dichloroacetonitrile (9.2 µg/L) and bromochloroacetonitrile (2.3 µg/L), both of which are less toxic than bromoacetonitrile, found in both chlorinated brackish water (2.2 µg/L) and finished water (0.7 µg/L). The shift toward more bromine containing DBPs in BW+Cl<sub>2</sub> and FW, especially for the haloacetonitriles, is responsible for the increase in calculated toxicity. The iodo-trihalomethanes and the haloacetaldehydes, present in both chlorinated raw and finished water, are more cytotoxic than genotoxic, with the greatest impact for cytotoxicity of finished drinking water. Chlorinated brackish water was the most cyto- and genotoxic (calculated) sample at Plant 3, suggesting the ability to negatively impact ecosystems once these waters are discharged to the environment.

## **CONCLUSIONS**

Desalination of water will increase in necessity over time as a reliable source of drinking water, therefore, its comparative quality to conventional drinking water is a necessary

indicator of the future of water quality. Compared to traditional drinking water sources, desalinated waters assessed in this study had increased DBP formation and calculated toxicity. For example, in finished drinking water, previous DBP studies reported iodotrihalomethanes at 0.4  $\mu\text{g/L}$  (median value) for 12 drinking water treatment plants across the U.S.,<sup>51</sup> which is much lower than what was found in desalination waters in this study (3.9  $\mu\text{g/L}$  total I-THMs). A combined median concentration of 1.3  $\mu\text{g/L}$  dichloriodomethane and bromochloriodomethane was found after sampling 23 iodide-impacted freshwater drinking water systems.<sup>44</sup> Desalinated finished water in this study formed 2.5  $\mu\text{g/L}$  combined dichloriodomethane and bromochloriodomethane, double the reported freshwater median. There is a similar trend for nitrogen containing DBPs (N-DBP) formation as well, with the same 12-plant study reporting median concentrations of 3  $\mu\text{g/L}$  haloacetonitriles, 2.5  $\mu\text{g/L}$  haloacetamides, and 3  $\mu\text{g/L}$  halonitromethanes.<sup>51</sup> However, in the current desalination study, finished water from Plant 1 formed double the amount of total haloacetonitriles and halonitromethanes and 10x the total haloacetamide concentrations compared to freshwater sources.

The calculated cytotoxicity index (CTI) for Plant 1 (seawater source utilizing pre-chlorination) was also higher than those calculated for traditional drinking water sources. Cuthbertson et al reports a CTI of >9000 in chlorinated drinking water from traditional freshwater sources,<sup>52</sup> another report shows 500 nM total DBPs formed resulting in a CTI of about 8000,<sup>53</sup> compared to Plant 1 with 600 nM and 14,500 CTI for finished drinking water. The difference in DBP formation and CTI implies that even though desalination only formed 100 nM additional DBPs in finished water, the greater bromide levels in



seawater form DBPs that are more toxic than those formed during traditional drinking water treatment.

Although this study utilized full-scale desalination plants to understand the impact pre-chlorination has on DBP formation and environmental impact, it does have limitations. When plants were not utilizing pre-chlorination (Plants 2, and 3), precursor material was rejected by the RO membrane, therefore, it is not an exact representation of the DBPs that will permeate the membrane or be rejected. Rather, including locations that were not performing pre-chlorination provide a high estimate for DBPs that are expelled into the aquatic environment, since RO membranes are more likely to reject large NOM precursors than DBPs formed in pre-chlorination. However, because many plants do not continuously pre-chlorinate, this is still a useful comparison to determine potential human health implications of desalination as a source for drinking water, since RO permeate is chlorinated before distribution.

## **ACKNOWLEDGEMENTS**

We thank the desalination plants for their willingness to participate in this project and their support and assistance in collecting samples. This work was supported by National Science Foundation Environmental Chemical Sciences Grants 1708461 and 1708766 (to Susan Richardson and Michael Gonsior, respectively).

## TABLES AND FIGURES

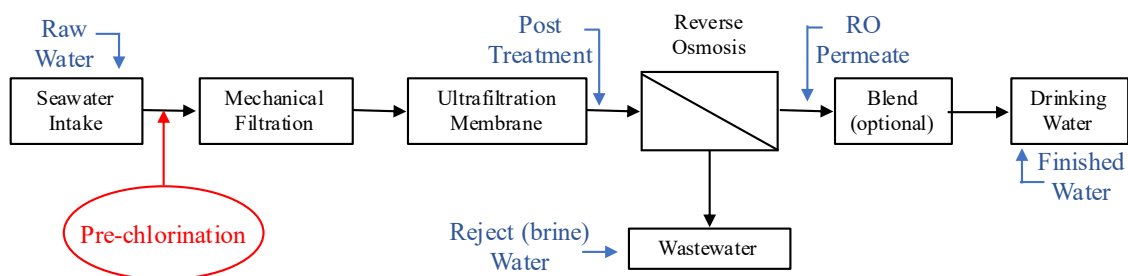
**Table 2.1.** Water Quality Parameters\*

Plant	Source water	Sample	Sample ID	DOC (mg/L)	Salinity (PSU)	TDN (mg/L)	SUVA (m <sup>-1</sup> L mg <sup>-1</sup> )
<b>Plant 1</b>	High DOC seawater	Raw Water	RW	4.3	21	0.41	2.8
		Post Treatment	PT	3.9	21	0.3	1.9
		Reject (brine) water	BW	10.2	60	0.68	1.9
		RO Permeate	ROP	<0.1	0	ND	ND
		Finished water	FW	<0.1	0	ND	11
<b>Plant 2</b>	Low DOC seawater	Raw Water	RW	0.5	34	0.07	1.3
		Raw + Cl <sub>2</sub>	RW + Cl <sub>2</sub>	0.5	34	0.06	1.4
		Reject Water	BW	0.6	38	0.10	1.3
		Reject + Cl <sub>2</sub>	BW + Cl <sub>2</sub>	0.5	38	0.07	1.3
<b>Plant 3</b>	Brackish groundwater	Raw Water	RW	<0.1	5	0.1	14
		Raw + Cl <sub>2</sub> <sup>†</sup>	RW + Cl <sub>2</sub>	<0.1	5	0.1	1.1
		Reject (brine) water	BW	0.6	12	0.3	2.8
		Reject + Cl <sub>2</sub>	BW + Cl <sub>2</sub>	0.6	12	0.3	3.3
		Finished water	FW	<0.1	3	0.47	3.7

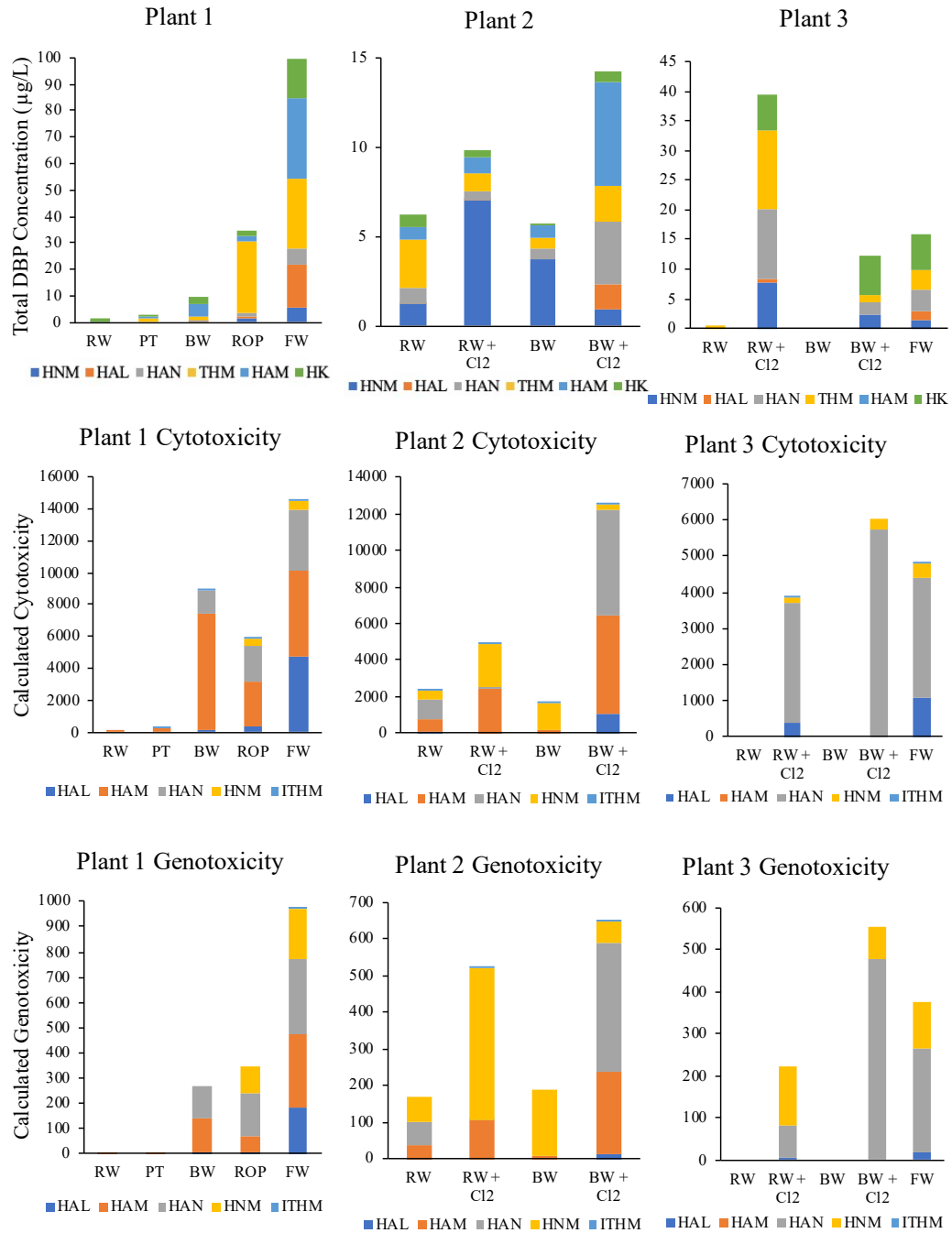
ND = not detected

\*PT, BW, and ROP from Plant 1 were subject to pre-chlorination at the treatment plant.

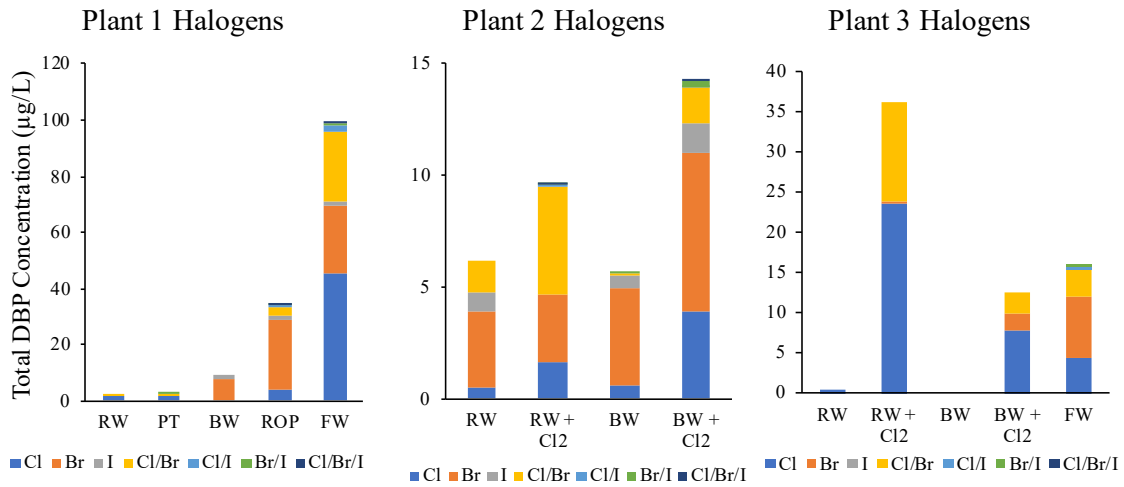
<sup>†</sup> The “+ Cl<sub>2</sub>” notation indicates in-lab chlorination experiments via electrochlorination.



**Figure 2.1.** Treatment train depiction of desalination plant with the use of pre-chlorination (red) and sampling locations (blue) identified throughout the process. Plant 1 includes all sampling locations and utilized pre-chlorination during sampling, whereas Plant 2 and Plant 3 do not include pre-chlorination and were only sampled at the Raw Water, and Reject (brine) Water locations.



**Figure 2.2.** Stack plots of DBP concentration by class, calculated cytotoxicity index values, and genotoxicity index values for Plants 1, 2, and 3.



**Figure 2.3.** Stack plots of DBP concentration by halogenation for Plants 1, 2, and 3.

CHAPTER 3  
INVESTIGATION OF NEW GREEN TECHNOLOGIES FOR IMPROVING  
THE SAFETY OF DRINKING WATER: NON-TARGET ANALYSIS OF  
TRANSFORMATION PRODUCTS

Huang, Y.; Kong, M.; Westerman, D. C.; Xu, E. G.; Coffin, S; Cochran, K. H.; Liu, Y.; Richardson, S. D.; Schlenk, D.; Dionysiou, D. D.: Effects of  $\text{HCO}_3^-$  on Degradation of Toxic Contaminants of Emerging Concern by UV/ $\text{NO}_3^-$  *Environ. Sci. Technol.* **2018**, *52*, 12697–12707.

Huang, Y.; Kong, M.; Coffin, S.; Cochran, K. H.; Westerman, D. C.; Schlenk, D.; Richardson, S. D.; Lei, L.; Dionysiou, D. D. Degradation of contaminants of emerging concern by UV/ $\text{H}_2\text{O}_2$  for water reuse: kinetics, mechanisms, and cytotoxicity analysis. *Water Res.* **2020**, *174*, 115587.

## INTRODUCTION

The environmental health of drinking water sources is becoming of increasing importance due to stressors like population growth, drought, and increased contamination. Even though municipal wastewater is treated before being discharged into nearby surface/ground water, conventional wastewater treatment does not fully remove emerging contaminants (ECs), which impact downstream drinking water sources. Moreover, population increases and water scarcity have increased the need for nontraditional sources of drinking water. Reuse of wastewater following treatment by advanced oxidation processes (AOPs) is being explored as a safe, reliable source of drinking water.<sup>56</sup>

Advanced wastewater treatment for the purpose of drinking water typically includes microfiltration (MF) and nanofiltration (NF) to remove microorganisms and particulates, followed by reverse osmosis (RO) and subsequent UV/hydrogen peroxide (UV/H<sub>2</sub>O<sub>2</sub>) advanced oxidation process (AOP) to disinfect and degrade emerging contaminants.<sup>57-58</sup> The primary concern with wastewater reuse is the incomplete removal of certain organic contaminants from conventional wastewater treatment, like pharmaceuticals, antibacterial compounds, hormones, and plasticizers.<sup>59</sup> The State of California recommended a list of contaminants of emerging concern to monitor during indirect potable and non-potable water reuse based on toxicity, environmental concentration, and persistence through conventional wastewater treatment processes.<sup>60-61</sup> These contaminants should then be removed by the AOP in order to provide safe potable water.

UV/ H<sub>2</sub>O<sub>2</sub> is the most widely utilized AOP for water reuse due to the efficient production of hydroxyl radicals ( $\cdot\text{OH}$ ), a strong oxidant that is non-selective and reacts very quickly ( $> 10^9 \text{ M}^{-1} \text{ s}^{-1}$ ).<sup>62</sup> UV/H<sub>2</sub>O<sub>2</sub> is known to degrade individual contaminants,<sup>58-59,63-64</sup> but its degradation of priority ECs in complex mixtures needs additional investigation.<sup>59,65</sup> A more novel AOP, UV photolysis with nitrate and carbonate (UV/NO<sub>3</sub><sup>-</sup>/HCO<sub>3</sub><sup>-</sup>), also has the potential to degrade/transform emerging contaminants due to the presence of not only hydroxyl radical ( $\cdot\text{OH}$ ), but also reactive nitrogen species (RNS) and carbonate radical (CO<sub>3</sub><sup>\cdot-</sup>). RNS has been shown to decompose ECs from wastewater during UV irradiation in the presence of NO<sub>3</sub><sup>-</sup>,<sup>66-69</sup> but studies about the effects of HCO<sub>3</sub><sup>-</sup> on various EC degradation are limited,<sup>66,68-69</sup> even though electron-rich aromatic compounds are preferred for CO<sub>3</sub><sup>\cdot-</sup> attack and have relatively high reaction rates, especially phenolic and aromatic amine moieties<sup>70-72</sup> which are important functional groups of ECs and natural organic matter (NOM).

Because advanced oxidation does not always completely mineralize contaminants, exploring incomplete degradation, or transformation, of these contaminants requires investigation because transformation products (TPs) can be equally toxic and environmentally persistent as the contaminant itself.<sup>73-75</sup> Previous studies have found mixtures of ECs after advanced oxidation to be toxic to aquatic organisms (e.g. *Daphnia similis* and *Carassius auratus L.*)<sup>65,73</sup> and microorganisms (e.g. *V. fischeri*).<sup>76-77</sup> Prediction models (e.g. ECOSAR program) also indicate the potential toxicity of TPs.<sup>77-78</sup>

The goal of this research is to comprehensively assess the application of UV/H<sub>2</sub>O<sub>2</sub> and UV/NO<sub>3</sub><sup>-</sup>/HCO<sub>3</sub><sup>-</sup> to remove multiple ECs for water reuse, including bisphenol-A (BPA), diclofenac (DCF), ibuprofen (IBP), triclosan (TCS), and estrone (E1). TPs formed



during EC degradation by UV/H<sub>2</sub>O<sub>2</sub> and UV/NO<sub>3</sub><sup>-</sup>/HCO<sub>3</sub><sup>-</sup> were measured to compare their degradation effectiveness and degradation pathways.

A novel sample workflow was optimized for evaluating TPs from three ECs of interest, where samples were analyzed using ultrahigh performance liquid chromatography (UHPLC) paired with electrospray ionization (ESI) and accurate mass quadrupole time-of-flight (Q-TOF) mass spectrometry. UHPLC-ESI/Q-TOF MS provides the appropriate resolution and sensitivity to identify unknown transformation products in these treated waters. Molecular formulas obtained by high resolution-MS can be used together with formulas for fragment (product) ions generated by MS/MS to determine the unknown chemical structures. The tentative identification of transformation products of ECs by both UV/H<sub>2</sub>O<sub>2</sub> and UV/NO<sub>3</sub><sup>-</sup>/HCO<sub>3</sub><sup>-</sup> advanced oxidation are provided.

## **MATERIALS AND METHODS**

**Chemical Reagents.** Analytical standards of bisphenol-A (BPA), diclofenac (DCF), ibuprofen (IBP), triclosan (TCS), and estrone (E1) were purchased from Sigma-Aldrich (St. Louis, MO, U.S.A.) at the highest available purity. Their structures and properties are listed in Table 3.1.

**Sample Preparation.** Photolysis experiments were conducted in a bench scale photochemical apparatus using one UV light-emitting diode (LED) lamp (Aquisense Technologies) for peroxide experiments, and two 15 W low-pressure mercury UV lamps (Cole-Parmer) for carbonate to emit monochromatic UV at 254 nm. The average UV fluence rate through the reaction solutions under LP-UV and LED-UV was measured as 0.1 mW cm<sup>-2</sup> and 0.13 mW cm<sup>-2</sup>, respectively. The initial concentration of the ECs was

20  $\mu\text{M}$  in both types of AOP experiments, with 10 mM of phosphate buffer to control the pH. UV/ $\text{H}_2\text{O}_2$  reactions were quenched with 200  $\mu\text{L}$  of pure methanol. For UV/ $\text{NO}_3^-/\text{HCO}_3^-$ , the initial concentrations of  $\text{NO}_3^-$  and  $\text{HCO}_3^-$  were 10 mM and 3 mM, respectively, and was quenched with 50  $\mu\text{L}$  of methanol, before being analyzed by UHPLC-MS/MS.

**Analytical Methods.** Reacted standards of estrone, triclosan, ibuprofen, diclofenac, and bisphenol-A were analyzed directly using an Agilent 1290 Infinity II UHPLC system coupled to an Agilent 6545 quadrupole time-of-flight (Q-TOF) mass spectrometer with electrospray ionization (ESI). The UHPLC system used an Agilent 1290 Infinity II binary pump (G7120A), a temperature-controlled Agilent Infinity II multisampler (G7167B), an Agilent Infinity II isocratic pump (G7110), and a temperature-controlled multicolumn compartment (G7116B). Both positive and negative ionization were used to identify potential transformation products.

Standards for triclosan, diclofenac, and bisphenol-A were used to optimize UHPLC conditions for unknown transformation product analysis. Table B.1 provides the settings and parameters for the UHPLC analysis. Samples were held at 20  $^\circ\text{C}$  before injecting a 10  $\mu\text{L}$  sample volume. LC flow was set to 0.35 mL/min through a Poroshell 120 EC-C18 column (2.1 mm  $\times$  50 mm  $\times$  1.9  $\mu\text{m}$ , Agilent InfinityLab) held at 30  $^\circ\text{C}$ . Analyte separation was performed using the following solvent gradient: 5% solvent B held for the first minute, ramped to 95% by minute 10, held at 95% for 2 min, then ramped back to 5% B over 0.1 min, where solvents A and B are water and methanol, respectively, with 0.1% formic acid with 5 mM ammonium acetate in positive mode, and 0.02% ammonium hydroxide in negative mode.

Continuous internal calibration was performed during the analysis. A mix of analytes was used for mass calibration (Santa Clara, CA, USA), with  $m/z$  121.050873 and 922.009798 in positive ion mode, and  $m/z$  112.985587 and 1033.988109 in negative ion mode used to account for instrument drift in real time. Mass spectra were obtained for a mass range of  $m/z$  100 to 3,200 at a rate of 5.5 spectra/s. A wider fragmentation window (4 amu) was deliberately chosen so that isotopic patterns could be observed, since halogenated TPs were expected. Precursor ions with a minimum of 200 counts were selected for targeted MS/MS. The MS/MS acquisition mass range was between  $m/z$  50 and 1,000. Table B.2 shows the settings used for the MS/MS analysis. Appendix B provides additional detail regarding data acquisition and analysis.

**Toxicity.** Cytotoxicity for DCF, TCS, E1, IBU and BPA treated by both UV/H<sub>2</sub>O<sub>2</sub> and UV/NO<sub>3</sub><sup>-</sup>/HCO<sub>3</sub><sup>-</sup> were carried out using the 3-(4,5-dimethylthiazol-2-yl)-2,5-diphenyltetrazolium bromide (MTT) assay in GeneBLAzer CYP1A1-bla LS-180 cells (Life Technologies, Carlsbad, CA)<sup>37</sup>. Green (650 nm) and blue (595 nm) absorbance was measured on a SpectraMax+ 384 plate reader (Molecular Devices, San Jose, CA). The resulting blue:green ratio provides a normalized reporter response, with the higher value indicating lower cytotoxicity.

## RESULTS AND DISCUSSION

**UV/H<sub>2</sub>O<sub>2</sub>: Transformation Product Identification.** Transformation products (TPs) of four ECs (BPA, E1, DCF, TCS) were tentatively identified in UV/H<sub>2</sub>O<sub>2</sub> advanced oxidation. No TPs of ibuprofen (IBP) were detected, which could be due to IBP having high resistance to removal by UV/H<sub>2</sub>O<sub>2</sub>.<sup>79</sup> Many of the transformation resulting from treatment of BPA, E1, DCF, and TCS derived from addition of hydroxy groups and/or

cleavage of the parent compound. For TCS, replacement of chlorine with a hydroxy group was also noted. The proposed degradation pathways for BPA, DCF, IBP, TCS, and E1 are shown in Figures 3.1-3.6. Tables of identified transformation products, along with their high resolution mass spectra, can be found in Appendix B.

Hydroxylation was the main route observed for BPA degradation by UV/H<sub>2</sub>O<sub>2</sub> (Figure 3.1), producing hydroxylated BPA, B<sub>243</sub>. Figure B.1 shows the MS/MS spectrum and proposed structure of tentatively identified TP B<sub>243</sub>. The observed accurate mass ([M-H]<sup>-</sup> m/z 243.1021, C<sub>15</sub>H<sub>16</sub>O<sub>3</sub>) is within 2.5 ppm of the theoretical mass, m/z 243.1027, and fragment ion m/z 149.0592 shows the cleavage between the two aromatic rings and corresponds to loss of phenol.

Quinone derivatives were also observed during BPA degradation, which are formed after further <sup>•</sup>OH oxidation of hydroxylation products (like B<sub>243</sub>).<sup>80-82</sup> Bond breakage then occurred at the methyl bridge of BPA via <sup>•</sup>OH oxidation,<sup>82</sup> and underwent further oxidation to generate B<sub>167</sub> (Figure B.1). TP B<sub>167</sub> was tentatively identified, with the observed accurate mass ([M-H]<sup>-</sup> m/z 167.0704, C<sub>9</sub>H<sub>12</sub>O<sub>3</sub>) is within 6 ppm of the theoretical mass, m/z 167.0714. Loss of water (fragment m/z 149.0608), common among molecules with phenolic moieties, supports the proposed structure (Figure B.2).

B<sub>245</sub> is a newly identified product, produced by the loss of a central methyl group and hydroxylated on both sides of the parent molecule. The elimination of the CH<sub>3</sub> group was attributed to the <sup>•</sup>OH oxidation of the central C atom on the methyl bridge of BPA, which has been previously observed during formation of other BPA byproducts, such as 4-hydroxyacetophenone.<sup>83</sup> TP B<sub>245</sub>, was observed with an accurate mass ([M-H]<sup>-</sup> m/z 245.0817, C<sub>14</sub>H<sub>14</sub>O<sub>4</sub>) within 1 ppm of the theoretical mass, m/z 245.0819 (Figure B.3).

The fragment ion  $m/z$  227.0712 is due to loss of water from a phenolic moiety, and the fragment ion  $m/z$  109.0317 can be attributed to cleavage between the two aromatic rings and corresponding observed dihydroxybenzene.

During E1 degradation, only hydroxylation products were observed by high resolution mass spectrometry (Table B.4). TP E<sub>285</sub> is likely the result of continuous attack of  $\cdot\text{OH}$  on the phenolic ring (Figure 3.2). Figure B.4 shows the MS/MS spectrum and proposed structure of tentatively identified TP E<sub>285</sub>. The observed accurate mass ( $[\text{M-H}]^-$   $m/z$  285.1492,  $\text{C}_{18}\text{H}_{22}\text{O}_3$ ) is within 2 ppm of the theoretical mass,  $m/z$  285.1496. Fragment with  $m/z$  267.1388 represents a loss of water and is consistent with a phenolic moiety. The other three fragments ( $m/z$  245.1148, 153.0558, and 123.0437) are likely due to charge-driven rearrangements; commonly observed during collision-induced fragmentation.<sup>84</sup> The proposed structure of E<sub>285</sub> has several possible isomers from the placement of the additional hydroxy group on the aromatic ring, but the isomers are indistinguishable by MS/MS without confirming with standards.

Due to the complex structure of diclofenac and the non-selective property of  $\cdot\text{OH}$ , several degradation routes were observed during DCF degradation in UV/ $\text{H}_2\text{O}_2$  (Figure 3.3). DCF was in the deprotonated form at the reaction pH, which could spontaneously dechlorinate from its triplet state under UV irradiation, leading to ring closure and forming a five-membered cyclic product, which would then decarboxylate to form D<sub>212</sub>.<sup>85</sup> Decarboxylation was initiated with  $\cdot\text{OH}$ -involved electron transfer on the carboxylic acid, followed by removal of  $\text{CO}_2$  and an electron.<sup>86</sup> The proposed structure for D<sub>212</sub> ( $[\text{M-H}]^-$   $m/z$  212.0712,  $\text{C}_{13}\text{H}_{11}\text{NO}_2$ ) is supported by fragment ion  $m/z$  194.0576, corresponding to loss of water, which is common in compounds with hydroxyl functional

groups (Figure B.5). Subsequent dechlorination and hydroxylation of the cyclic form of DCF would then produce TPs D<sub>214</sub>, D<sub>244</sub>, which were also observed (Figures B.6-7). The observed fragmentation, as well as the [M-H]<sup>-</sup> isotopic pattern where the <sup>37</sup>Cl isotope can be seen, support the proposed structure of D<sub>214</sub> ([M-H]<sup>-</sup> *m/z* 214.0427, C<sub>13</sub>H<sub>10</sub>ClN). Fragment ion *m/z* 178.0654 corresponds to loss of HCl, and consequently, the <sup>37</sup>Cl isotopic pattern is no longer observed in this fragment. The proposed structure of D<sub>244</sub> ([M-H]<sup>-</sup> *m/z* 244.0613, C<sub>13</sub>H<sub>11</sub>NO<sub>4</sub>) is supported by two fragment ions at *m/z* 226.0491 and 158.0612, corresponding to loss of water and cleavage of the ring with three hydroxy groups, respectively.

Dechlorination-hydroxylation of triclosan was observed with the formation of T<sub>235</sub>. TP T<sub>235</sub>, shown in Figure B.8, has an observed accurate mass ([M-H]<sup>-</sup> *m/z* 235.0160, C<sub>12</sub>H<sub>9</sub>ClO<sub>3</sub>) within 3 ppm of the theoretical mass, *m/z* 235.0167. The two fragments, *m/z* 217.0050 and 181.0275, correspond to loss of water and subsequently loss of HCl.

The continuous attack of •OH could lead to the breakdown of the ether bond, generating T<sub>143</sub> after additional dechlorination-hydroxylation.<sup>87</sup> Figure B.9 shows the MS/MS spectrum and proposed structure of tentatively identified TP T<sub>143</sub>. The observed accurate mass ([M-H]<sup>-</sup> *m/z* 142.9904, C<sub>6</sub>H<sub>5</sub>ClO<sub>2</sub>) and the chlorine isotopic pattern support the proposed structure; since the accurate mass is within 1 ppm of the theoretical, and the <sup>37</sup>Cl isotope can be seen in the spectrum. A loss of HCl (*m/z* 107.0142) is shown by the mass difference, lack of chlorine isotope pattern on the fragment ion, and mass defect. The negative mass defect confirms the presence of chlorine on the molecule, and the positive mass defect on the fragment ion confirms loss of chlorine through fragmentation.

**UV/NO<sub>3</sub><sup>-</sup>/HCO<sub>3</sub><sup>-</sup> Transformation Product Identification.** Transformation products of bisphenol-A, diclofenac, and triclosan were tentatively identified in UV/NO<sub>3</sub><sup>-</sup>/HCO<sub>3</sub><sup>-</sup> advanced oxidation. No TPs of estrone were identified by high resolution mass spectrometry in this study. Many of the transformation products resulting from treatment of BPA, DCF, and TCS are derived from the addition of hydroxy groups, oxidation of hydroxy groups to ketones, and/or cleavage of the parent compound. The proposed degradation pathways for BPA, DCF, IBP, TCS, and E1 are shown in Figure 3.6.

Hydroxylation was observed during BPA degradation, which could be initiated with <sup>•</sup>OH addition and further oxidized by <sup>•</sup>OH to generate the quinone-like transformation product B<sub>287</sub>. This TP was tentatively identified ([M-H]<sup>-</sup> m/z 287.0558, C<sub>15</sub>H<sub>12</sub>O<sub>6</sub>) after observing the loss of water (m/z 269.0450), followed by two CH<sub>3</sub> and two CO losses overall (Figure B.10). The loss of two methyl groups corresponds to those present on the methyl bridge, and the loss of CO is likely from ring opening, losing the ketone. B<sub>287</sub> has not been previously reported, and was likely generated via further hydroxylation on formed quinone derivatives.<sup>80</sup>

Dechlorination-hydrogenation products were observed during triclosan degradation via UV/NO<sub>3</sub><sup>-</sup>/HCO<sub>3</sub><sup>-</sup> advanced oxidation (Table B.9). The dechlorination-hydroxylation that led to the generation of isomers of T<sub>235</sub> could be initiated by <sup>•</sup>OH, since this chemistry is well-established in the reaction of <sup>•</sup>OH with halobenzenes,<sup>88</sup> trimethoprim,<sup>89</sup> and ATZ.<sup>90-91</sup> Transformation product T<sub>235</sub> ([M-H]<sup>-</sup> m/z 235.0150, C<sub>12</sub>H<sub>9</sub>ClO<sub>3</sub>) is 7 ppm difference to the theoretical m/z 235.0167. The isotopic pattern where the <sup>37</sup>Cl isotope can be seen in the fragment corresponding to a loss of water at m/z

217.0049, but after the loss of HCl ( $m/z$  181.0281) is no longer observed, supports the proposed structure for T<sub>235</sub> (Figure B.11).

Additionally, quinone derivatives, T<sub>249</sub>, T<sub>283</sub>, and T<sub>317</sub>, were observed during TCS degradation. The *p*-hydroquinone of triclosan is a common transformation product in  $\cdot\text{OH}$ -based oxidation of triclosan, due to the  $\cdot\text{OH}$  attack at *para*-position<sup>87,92</sup> and can be further oxidized by  $\cdot\text{OH}$  to form T<sub>249</sub>, T<sub>283</sub>, and T<sub>317</sub> through dechlorination-hydrogenation, dechlorination-hydroxylation, and hydroxylation, respectively (Figure 3.6). T<sub>249</sub> ( $[\text{M}-\text{H}]^-$   $m/z$  248.9960, C<sub>12</sub>H<sub>7</sub>ClO<sub>4</sub>) had a loss of CO<sub>2</sub> ( $m/z$  ), followed by a loss of CO ( $m/z$  177.0111), which are commonly observed for hydroxyl groups and quinones. The fragment at  $m/z$  126.9954 was also observed (Figure B.12), corresponding to a break in the ether bond and retaining the C<sub>6</sub>H<sub>4</sub>ClO half of the structure. T<sub>283</sub> ( $[\text{M}-\text{H}]^-$   $m/z$  282.9589, C<sub>12</sub>H<sub>6</sub>Cl<sub>2</sub>O<sub>4</sub>) is within 7 ppm of the theoretical  $m/z$  282.9570 for the proposed structure. The presence of the fragment  $m/z$  218.9846, corresponding to a loss of HCl and CO, along with both halves of the ether ( $m/z$  156.9695 and  $m/z$  142.9896), supports the assignment of the proposed structure (Figure B.13). T<sub>317</sub> ( $[\text{M}-\text{H}]^-$   $m/z$  316.9180, C<sub>12</sub>H<sub>5</sub>Cl<sub>3</sub>O<sub>4</sub>) also shows a fragment at the ether bond ( $m/z$  160.9562), along with  $m/z$  279.9837 showing the loss of HCl (Figure B.14). The agreement within fragment structure assignments, along with good agreement between the observed and theoretical masses (0.3 ppm), supports the predicted structure.

The same cyclization product that was reported for DCF decomposition in UV/H<sub>2</sub>O<sub>2</sub>, was observed for UV/NO<sub>3</sub><sup>-</sup>/HCO<sub>3</sub><sup>-</sup>. TP D<sub>260</sub> ( $[\text{M}-\text{H}]^-$   $m/z$  258.0327, C<sub>14</sub>H<sub>10</sub>ClNO<sub>2</sub>) shows the loss of the carboxylic acid ( $m/z$  214.0428) followed by HCl (178.0660) in Figure B.17. The chlorine isotopic pattern is also lost with the loss of HCl,



confirming the presence and subsequent loss of chlorine. This structure can undergo decarboxylation with  $\cdot\text{OH}$ , but the addition of carbonate in this system can lead to the quinone-like product,  $\text{D}_{214}$ .<sup>70-71,86,93-94</sup> Transformation product  $\text{D}_{214}$  (Figure B.17) was observed in positive ion mode ( $[\text{M}+\text{H}]^+$   $m/z$  214.0416,  $\text{C}_{13}\text{H}_8\text{ClN}$ ), which is 1 ppm from the theoretical  $m/z$  214.0418. The fragment  $m/z$  178.0650 corresponds to a loss of  $\text{HCl}$ , which is followed by a ring break and the loss of the nitrogen ( $-\text{CN}$ ,  $m/z$  151.0546).

**Broader Implications.** Transformation products of emerging contaminants from two different AOPs were tentatively identified using high resolution mass spectrometry. TPs were tentatively identified to better understand the toxicity of selected ECs during individual degradation by  $\text{UV}/\text{H}_2\text{O}_2$ . For BPA degradation by  $\text{UV}/\text{H}_2\text{O}_2$ , hydroxylation and quinone products were detected; these showed little cytotoxicity compared to their starting material. For DCF degradation, the cytotoxicity was elevated, which might be ascribed to the generated hydroxylation and cyclization products. During TCS degradation, dechlorination, cyclization, and dechlorination-hydroxylation products were tentatively identified. However, the resulting cytotoxicity did not change significantly compared to TCS. As for E1 degradation, only three TPs were detected with unchanged cytotoxicity.

This research also demonstrates the important role of  $\text{HCO}_3^-$  in  $\text{UV}/\text{NO}_3^-$  treatment in the removal of ECs with electron-rich moieties such as phenolic and aniline groups. The combined effects of UV photolysis,  $\cdot\text{OH}$ , and  $\text{CO}_3^{\cdot-}$  all contributed to the degradation of ECs in  $\text{UV}/\text{NO}_3^-/\text{HCO}_3^-$ . Among the selected ECs, the cytotoxicity was significantly decreased during BPA degradation in  $\text{UV}/\text{NO}_3^-/\text{HCO}_3^-$  treatment. Moreover, the selectivity of  $\text{CO}_3^{\cdot-}$  made them less affected by NOM than traditional

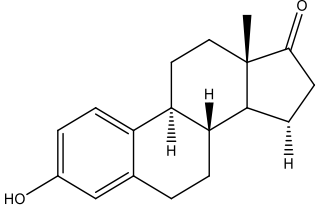
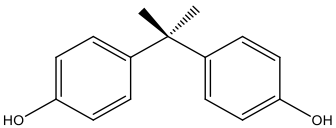
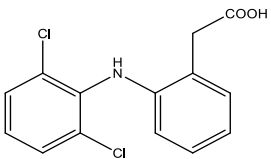
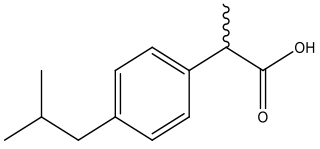
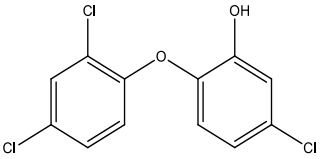
UV/H<sub>2</sub>O<sub>2</sub> technologies. Therefore, UV/NO<sub>3</sub><sup>-</sup>/HCO<sub>3</sub><sup>-</sup> has the potential to be a successful alternative AOP to UV/H<sub>2</sub>O<sub>2</sub> in wastewater reuse.

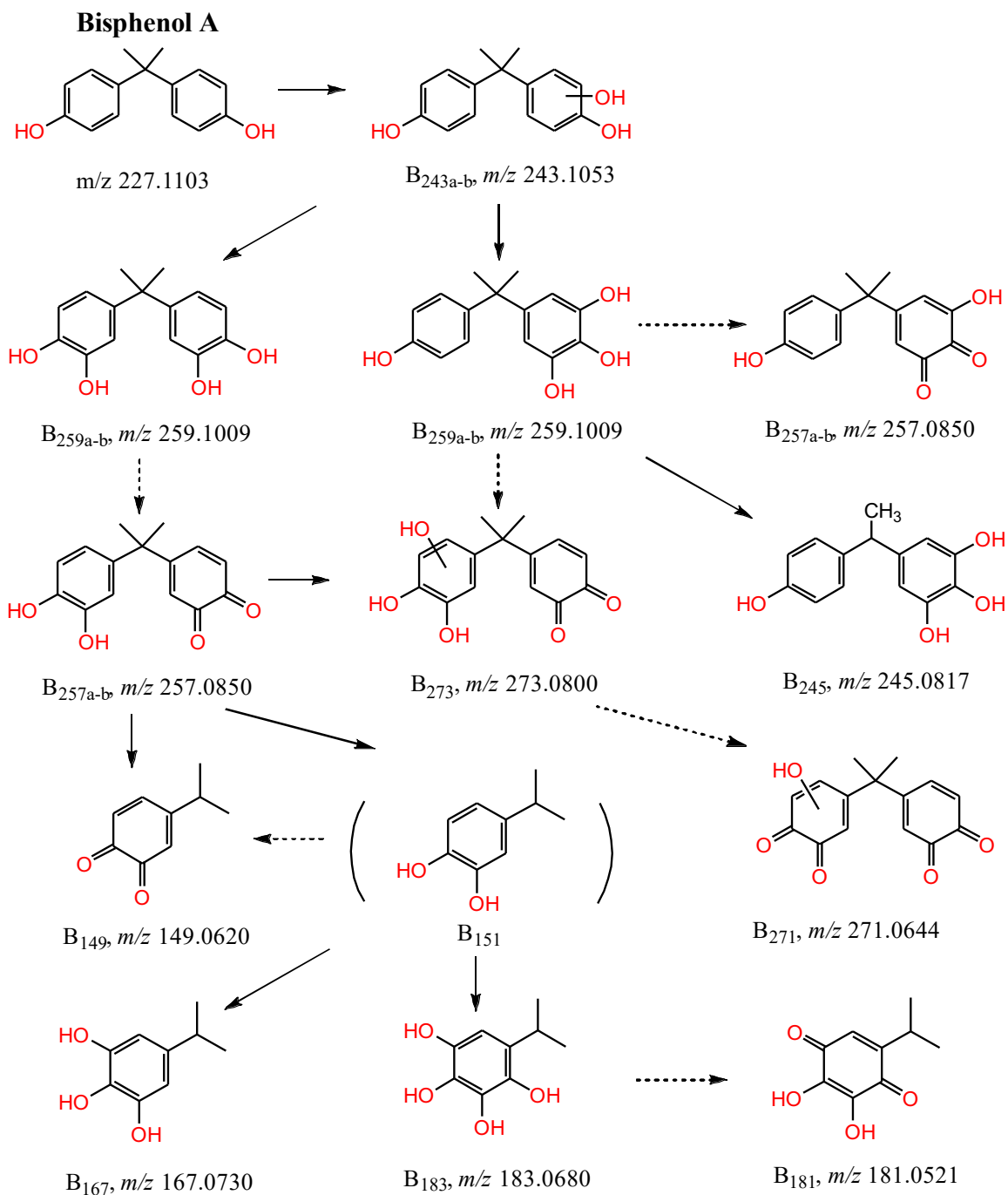
### **ACKNOWLEDGEMENTS**

The authors acknowledge financial support from the U.S. Geological Survey (USGS)-Water Resources Research Institute (WRRI) (2015SC101G) for this research.

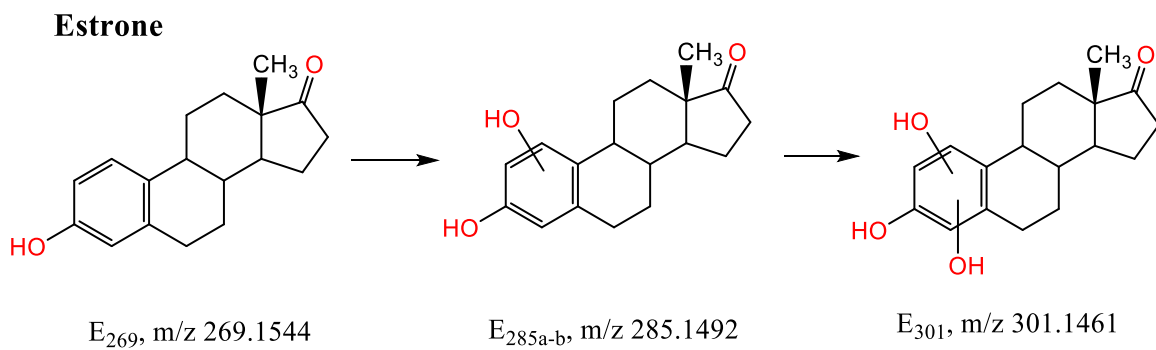
## TABLES AND FIGURES

**Table 3.1.** Contaminants of emerging concern (ECs).

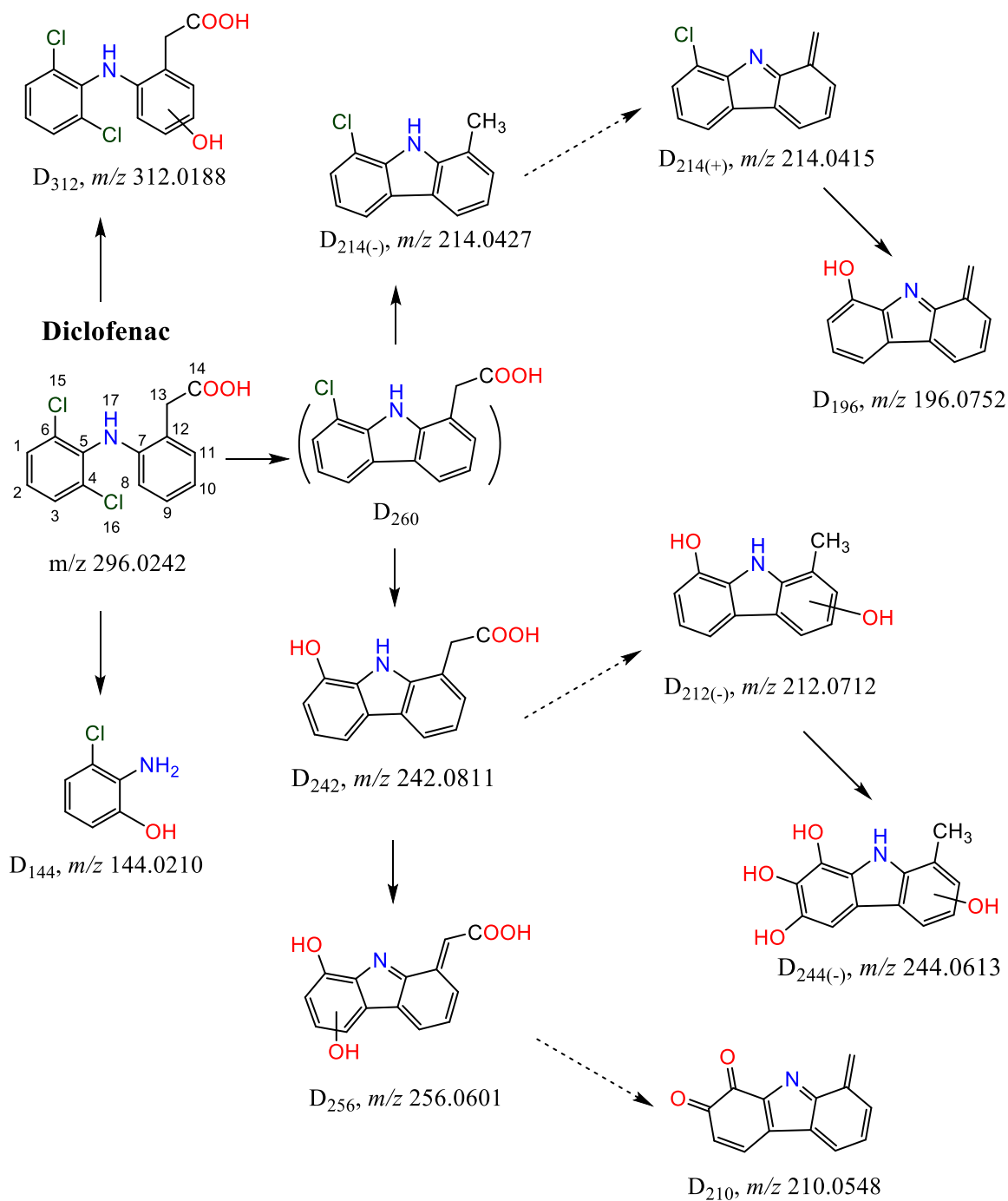
EC	pKa	Structure
<b>Estrone (E1)</b>	10.7	
<b>Bisphenol A (BPA)</b>	9.6	
<b>Diclofenac (DCF)</b>	4.2	
<b>Ibuprofen (IBP)</b>	4.9	
<b>Triclosan (TCS)</b>	7.9	



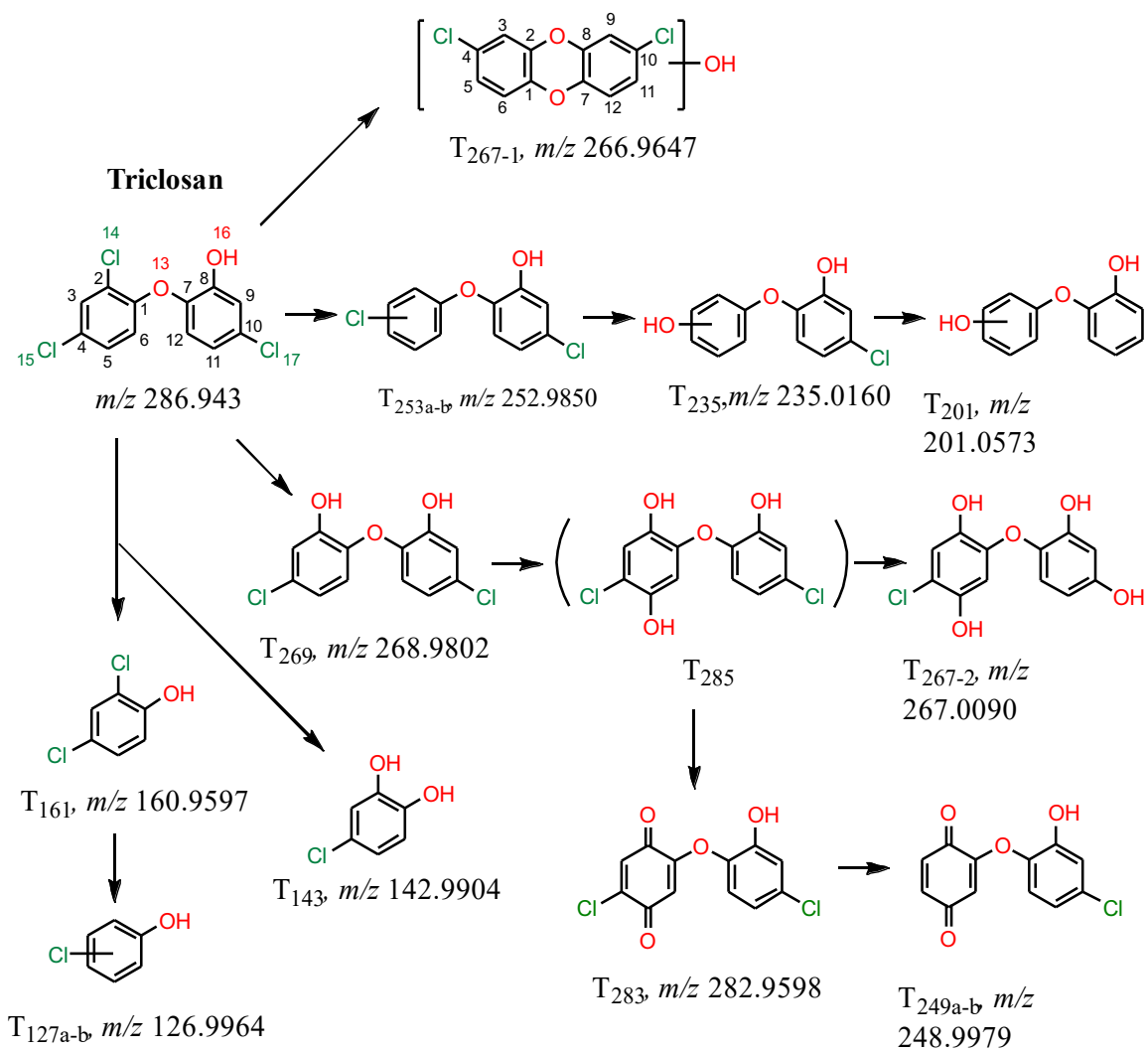
**Figure 3.1.** Possible degradation pathways of bisphenol-A in UV/H<sub>2</sub>O<sub>2</sub>.



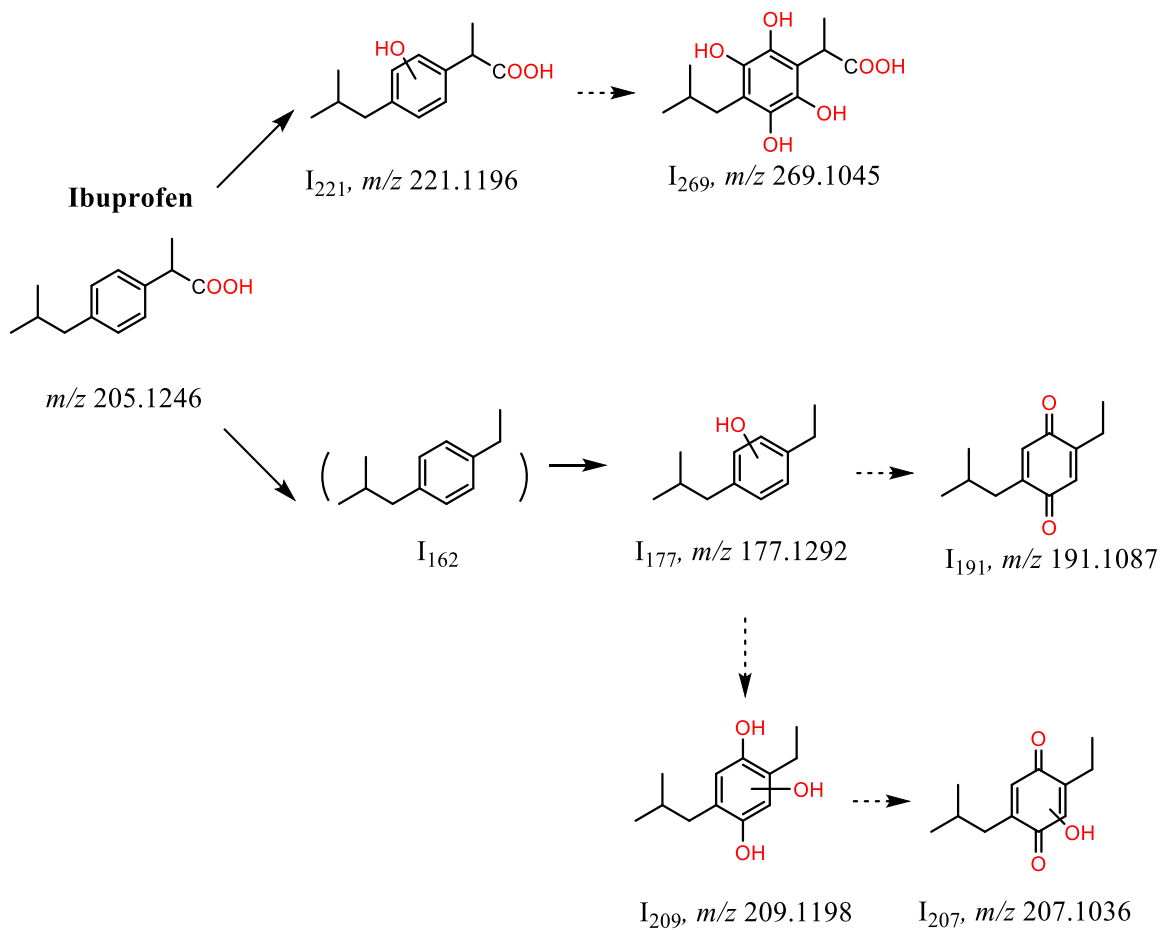
**Figure 3.2.** Possible degradation pathways of estrone in UV/H<sub>2</sub>O<sub>2</sub>.



**Figure 3.3.** Possible degradation pathways of diclofenac in UV/H<sub>2</sub>O<sub>2</sub>.

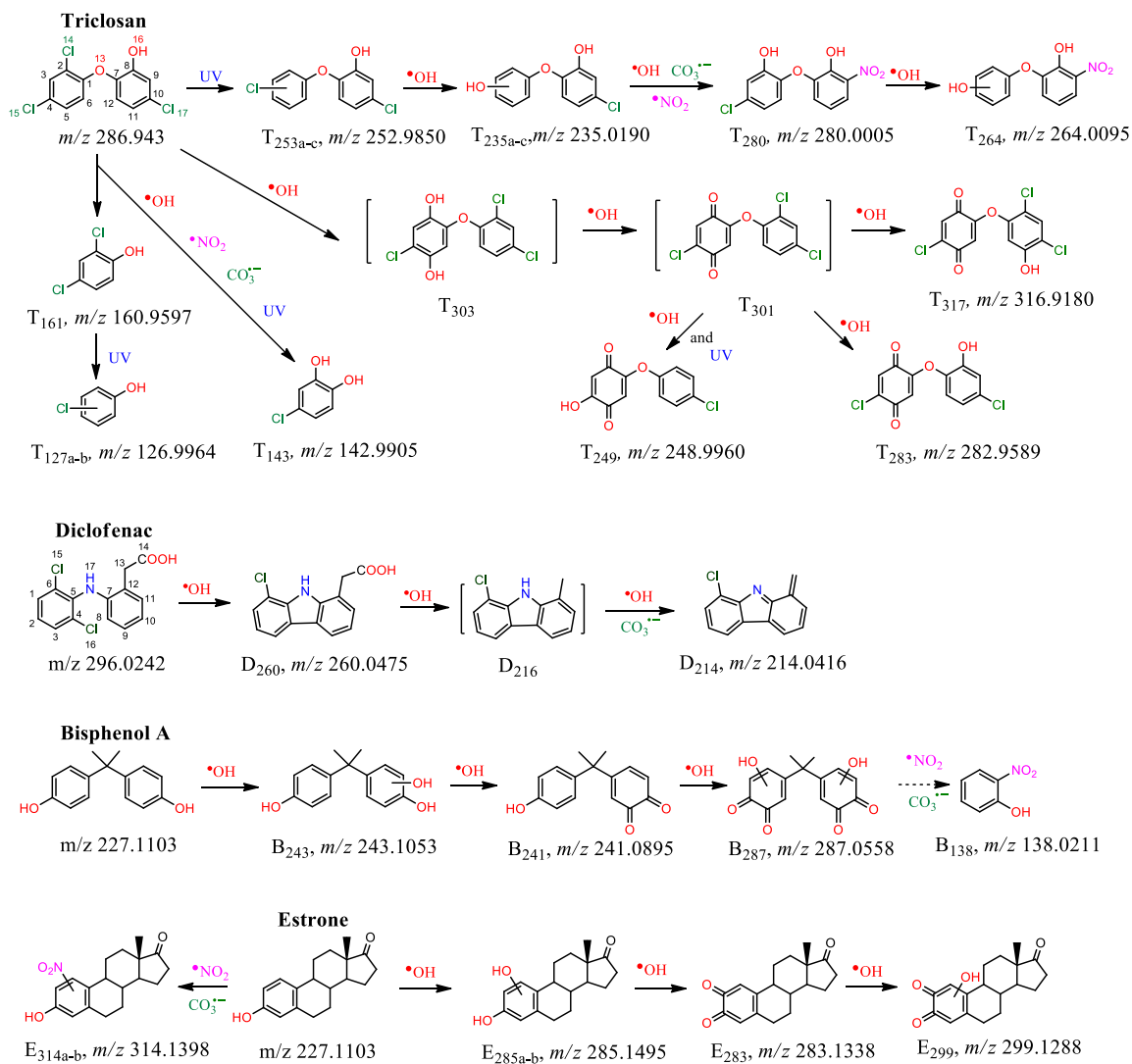


**Figure 3.4.** Possible degradation pathways of triclosan in UV/H<sub>2</sub>O<sub>2</sub>.



**Figure 3.5.** Possible degradation pathways of ibuprofen in UV/H<sub>2</sub>O<sub>2</sub>.





**Figure 3.6.** Possible degradation pathways of triclosan, diclofenac, bisphenol-A, and estrone in UV/NO<sub>3</sub><sup>-</sup>/HCO<sub>3</sub><sup>-</sup>.

CHAPTER 4  
EMERGING LYNGBYA WOLLEI TOXINS: A NEW HIGH RESOLUTION MASS  
SPECTROMETRY METHOD TO ELUCIDATE A POTENTIAL  
ENVIRONMENTAL THREAT

Smith, M. L.; Westerman, D. C.; Putnam, S. P.; Richardson, S. D.; Ferry, J. L.; Emerging Lyngbya wollei toxins: A new high resolution mass spectrometry method to elucidate a potential environmental threat. *Harmful Algae* **2019**, 90, 101700.

## ABSTRACT

Biological assays are commonly used to detect the presence of saxitoxin analogues, but lack the ability to quantify individual toxins in complex mixtures and environmental samples, making harmful algal bloom remediation difficult. Mass spectrometry has the ability to solve this issue and quantify toxins individually. Here we present an extraction procedure designed to identify specific algal toxins in samples of *Lyngbya wollei*, a filamentous benthic algae known to produce several saxitoxin analogues. *Lyngbya wollei* samples were collected from a persistent harmful algal bloom in Lake Wateree, SC. Six known *Lyngbya wollei*-specific toxins (LWT1-6) were successfully resolved, identified, and quantified against saxitoxin using hydrophilic interaction liquid chromatography coupled with triple quadrupole and quadrupole time-of-flight mass spectrometry. The first high resolution mass spectra showing unique fragmentation ions for LWTs 1-6, and an optimized sample extraction method and instrument parameters for quantification ( $R^2 > 0.96$ ) are presented.

## INTRODUCTION

Saxitoxin analogues, also known as paralytic shellfish toxins, are produced by both freshwater cyanobacteria and marine dinoflagellates.<sup>96-97</sup> These compounds are extremely toxic to humans as well as other mammalian species that work by blocking sodium channels in the body.<sup>98-102</sup> Saxitoxin analogues are known to have a variety of toxicity levels and are produced by many different algal species: *Anabaena*,<sup>103-105</sup> *Cylindospermopsis*,<sup>106</sup> *Aphanizomenon*,<sup>107-109</sup> *Planktothrix*,<sup>110</sup> and *Lyngbya*. Specifically, *Lyngbya wollei* is a filamentous, benthic, freshwater algae that is known to produce six different *Lyngbya wollei* toxins (LWTs),<sup>105,112-114</sup> shown in Figure 4.1.

Currently, biological assays are the most common technique for the quantification and qualification of LWTs.<sup>116-128</sup> However, these assays cannot differentiate between individual LWTs, reporting only a summed saxitoxin equivalent value. The lack of individual LWT abundance data limits the understanding of how and when these toxins are produced and their impact on aquatic environments. Liquid chromatography mass spectrometry can be a useful alternative to biological assays due to its ability to separate and analyze compounds of interests individually, while also providing key structural information for each analyte.<sup>111,114,129-132</sup> Here we report the development of a new mass spectrometry method for the accurate and precise measurement of *Lyngbya wollei* toxins at ng/L detection limits, along with the first published high resolution mass spectra for LWTs.

## **MATERIALS AND METHODS**

**Chemical Reagents.** All aqueous solutions used 18 M $\Omega$  cm<sup>-1</sup> (Barnstead E-pure) water. Acetonitrile (HPLC grade) was obtained from VWR BDH chemicals. Ammonium formate (98+%) was purchased from Alfa Aesar. Formic acid (certified ACS), glacial acetic acid (certified ACS PLUS), and hydrochloric acid (certified ACS Plus) were purchased from Fisher. Saxitoxin dihydrochloride in dilute hydrochloride standard solutions were obtained from NIST and Abraxis Inc. Due to the lack of commercially available standards, all *Lyngbya wollei* toxins were analyzed from environmental samples.

**Sampling.** *Lyngbya wollei* grab samples were collected on November 6, 2018 from a surface floating mat on Lake Wateree, SC. Samples were collected in sterile 500-mL

collection bottles and stored at 0 °C until processed (<3 h). Samples were rinsed with deionized water to remove debris before being freeze-dried.

**Extraction Procedure.** Freeze-dried samples were homogenized and weighed before extraction. Algae was mixed with 10 mL 0.1 M acetic acid, sonicated for 15 minutes and centrifuged for 5 minutes. The aqueous layer was removed from the solid material and filtered to 0.45 µm and analyzed by ultrahigh performance liquid chromatography mass spectrometry (UHPLC-MS).

**High Resolution Mass Spectrometry.** Samples were analyzed using an Agilent (Santa Clara, CA, USA) 1290 Infinity II UHPLC system coupled to an Agilent 6545 Accurate Mass Q-TOF with electrospray ionization (ESI) operated in positive ion mode. High resolution Q-TOF data was processed using Agilent B.08.00 software. Separations were performed on a BEH Amide (2.1x150 mm x 1.7 µm) column (Waters, Milford, MA, USA) using aqueous 5.6 mM formate buffered pH 3.5 (A) and 95:5 acetonitrile:water 5.6 mM formate buffer pH 3.5 (B) as the mobile phase. The gradient was performed as follows: 80% B held for one min, ramped to 60% B for 3 min and held for 2 min, at 7 min ramped back to the original conditions for one min (80% B) and held for re-equilibration for 8 min (16 min total). The mass spectrometer was operated at a fragmentation voltage of 110 V, capillary voltage of 4000 V, gas temperature of 300 °C, drying gas flow of 12 L min<sup>-1</sup>, and nebulizer pressure of 35 psi, with a scan range of m/z 50 to 750. During initial analyte screening, the collision energy was ramped from 0, 20, to 40 eV every scan to obtain both MS and MS/MS spectra for each chromatographic peak. Once LWTs of interest were identified in algae extracts, targeted analysis was performed with a collision energy of 30 eV to obtain high resolution MS/MS spectra.

Toxins were quantified using a Waters (Milford, MA, USA) Acquity ultra performance liquid chromatograph (UPLC) coupled with a Xevo triple quadrupole (TQ) mass spectrometer equipped with an electrospray ionization (ESI) source in positive ion mode. Saxitoxin was optimized manually by direct infusion into the source, using an optimized cone voltage of 0.5 kV and cone energy of 80 V. The source temperature was 150 °C. The source parameters were as follows: desolvation temperature 400 °C, extractor voltage of 3 V, desolvation gas flow 600 L/hr, cone gas flow 25 L/hr, capillary voltage of 0.5 kV, and collision gas flow 0.15 L/hr. The instrument was optimized with respect to saxitoxin, since LWTs are not available as commercial standards, therefore, the limit of detection on the UPLC-TQ instrument was 0.1 ppb for saxitoxin. To minimize in-source fragmentation, the cone potential was set at 30 V in the retention time window corresponding to LWT1 elution. The other LWTs did not experience this issue, and a cone energy of 80 V was optimal for LWT4, LWT5, and LWT6.

## RESULTS AND DISCUSSION

Previously published work on LWT analysis using mass spectrometry relied on unit-mass resolution, with secondary confirmation by nuclear magnetic resonance (NMR) spectroscopy.<sup>114,130,133-134</sup> This is the first study where high resolution mass spectral data is evaluated for LWTs. The high resolution analysis identified over 10 fragment ions for each LWT, providing ample options for sensitivity and selectivity optimization for selected reaction monitoring (SRM) analysis in quantification. Also, the high number of fragments identified has the potential to quantify LWTs in a variety of sample matrices; if an interferent is present in the sample matrix for one fragment ion, changing the ion used to quantify and qualitatively confirm *Lyngbya wollei* toxins is now an option.

High resolution analysis was utilized for confirmation of the identity of saxitoxin and the suspected LWTs on the unit resolution UPLC-TQ instrument. High resolution data using the UHPLC-QTOF mass spectrometer provided exact masses of precursor and product ions, correlating to a specific molecular formula for each peak, which allowed additional confidence in the chemical structures for these toxins (Figure C.1-6).

Due to their structural similarities, similar product ion fragments were identified for saxitoxin and LWTs. For example, fragments with theoretical values  $m/z$  72.0556 and  $m/z$  60.0556, corresponding to elemental formulae of  $C_2H_6N_3$  and  $CH_6N_3$ , respectively, were observed for all LWTs (Tables 4.2-6). Similarly, six identical product ions were observed between LWT4 and LWT6. The analysis of LWT1 resulted in ten fragment ions. The sulfur-containing functional group was lost from each fragment ion observed. Thirteen fragment ions were observed for LWT4 (Table 1). Similarly to LWT1, the most abundant fragment was from loss of the OH functional group, corresponding to the ester and hydroxyl groups on the toxins, as well loss of nitrogen-containing groups (such as  $CH_5N_3$  and  $CH_4N_3$ ).

Fragment ions obtained for LWT5 and saxitoxin were nearly identical (Tables 4.1, 4.6), which is consistent with their similar structures; the difference being an amide instead of the ester for saxitoxin. Eleven fragment ions were observed for LWT5, of those eleven, eight were also present for saxitoxin. The three unique product ions were the result of losses from locations other than the carbamate ester (for saxitoxin) or the acetyl ester (for LWT5). The structural similarity complicates fragment ion identification since mass differences in these product ions differed by 1 Da. For example, the loss of water from LWT5 resulted in the product ion  $m/z$  281.1357, whereas the loss of water from

saxitoxin resulted in  $m/z$  282.1309. The similar fragmentation of saxitoxin and LWT5 provides confidence in the analyte identification and suggests parallels between the ionization chemistry of these two families of analytes, supporting the use of saxitoxin as a quantification standard for the LWTs.

LWT2 and LWT3 are structural isomers (referred to as LWT2/3) with the same molecular weight. One isomer was detected with the QTOF mass spectrometer during the high resolution analysis of the algae extract (Table 4.4), but the exact structure cannot be elucidated without a pure standard. LWT2/3 are structural isomers, and likely were not separable with the chromatographic approaches used in this study; thus, it is possible that both isomers were present, but coeluted. Similar to LWT1, LWT2/3 has a sulfur-containing functional group which was lost in four out of the six product ions observed. LWT2/3 were 2 orders of magnitude lower in peak intensity, relative to LWT1, 4, 5, and 6 (which had peak intensities on the order of  $10^5$ ) on the QTOF mass spectrometer, and LWT2/3 were undetectable at these concentrations on the UPLC-TQ mass spectrometer.

## **CONCLUSION**

Accurate risk assessments for *Lyngbya wollei* are extremely difficult due to reference standards for the mixture of toxins produced by this algae being commercially unavailable. Effect-based assays for the analysis of these toxins remain largely non-specific, fail to provide a molecular toxin profile, and often require secondary verification by mass spectrometry. The combination of a lack of standards for quantification and qualification make risk assessment and remediation difficult each time this species is encountered, as historical data shows the relative concentrations of LWTs are variable and unpredictable. The high-resolution fragmentation analysis presented here provides an



unprecedented range of fragment ion options that can be used to conclusively indicate the presence and retention time of LWTs 1 through 6 in a sample, as shown in the included quantification method.

## TABLES AND FIGURES

**Table 4.1.** High resolution fragmentation data for saxitoxin.

m/z	Formula	Mass loss	Formula Loss	Theoretical m/z	ppm Mass Error
300.1413	C <sub>10</sub> H <sub>18</sub> N <sub>7</sub> O <sub>4</sub>			300.14148	0.600
282.1309	C <sub>10</sub> H <sub>16</sub> N <sub>7</sub> O <sub>3</sub>	18.0104	-H <sub>2</sub> O	282.13091	0.035
258.1196	C <sub>9</sub> H <sub>16</sub> N <sub>5</sub> O <sub>4</sub>	42.0217	-CH <sub>2</sub> N <sub>2</sub>	258.11968	0.310
240.1100	C <sub>9</sub> H <sub>14</sub> N <sub>5</sub> O <sub>3</sub>	60.0313	-CH <sub>2</sub> N <sub>2</sub> , -H <sub>2</sub> O	240.10912	3.665
221.1145	C <sub>9</sub> H <sub>13</sub> N <sub>6</sub> O	79.0268	-CH <sub>3</sub> NO, -H <sub>2</sub> O	221.11454	0.181
204.0879	C <sub>9</sub> H <sub>10</sub> N <sub>5</sub> O	96.0534	-CH <sub>2</sub> NO, -NH <sub>2</sub> , -H <sub>2</sub> O, -H <sub>2</sub> O	204.08799	0.441
197.1032	C <sub>8</sub> H <sub>13</sub> N <sub>4</sub> O <sub>2</sub>	103.0381	-CH <sub>3</sub> NO <sub>2</sub> , -CH <sub>2</sub> N <sub>2</sub>	197.10330	0.507
179.0928	C <sub>8</sub> H <sub>11</sub> N <sub>4</sub> O	121.0485	-CH <sub>3</sub> NO <sub>2</sub> , -CH <sub>2</sub> N <sub>2</sub> , -H <sub>2</sub> O	179.09274	0.335
169.072	C <sub>6</sub> H <sub>9</sub> N <sub>4</sub> O <sub>2</sub>	131.0693	-CH <sub>3</sub> N <sub>3</sub> , -C <sub>3</sub> H <sub>6</sub> O <sub>2</sub>	169.072	0.000
157.0719	C <sub>5</sub> H <sub>9</sub> N <sub>4</sub> O <sub>2</sub>	143.0694	-C <sub>5</sub> H <sub>9</sub> N <sub>3</sub> O <sub>2</sub>	157.0720	0.637
144.0768	C <sub>5</sub> H <sub>10</sub> N <sub>3</sub> O <sub>2</sub>	156.0645	-C <sub>5</sub> H <sub>8</sub> N <sub>4</sub> O <sub>2</sub>	144.07675	0.347
138.0674	C <sub>6</sub> H <sub>8</sub> N <sub>3</sub> O	162.0739	-H <sub>2</sub> O, -CH <sub>2</sub> N <sub>2</sub> , -C <sub>3</sub> H <sub>6</sub> N <sub>2</sub> O <sub>2</sub>	138.06619	8.764
96.0458	C <sub>5</sub> H <sub>6</sub> NO	204.0955	-CH <sub>2</sub> NO, -CH <sub>2</sub> N <sub>2</sub> , -CH <sub>4</sub> N <sub>3</sub> , -C <sub>2</sub> H <sub>4</sub> O <sub>2</sub>	96.04439	14.681

83.0606	C <sub>4</sub> H <sub>7</sub> N <sub>2</sub>	217.0807	-CH <sub>2</sub> NO <sub>2</sub> , -C <sub>5</sub> H <sub>9</sub> N <sub>4</sub> O <sub>2</sub>	83.06037	2.769
72.0554	C <sub>2</sub> H <sub>6</sub> N <sub>3</sub>	228.0859	-C <sub>8</sub> H <sub>12</sub> N <sub>4</sub> O <sub>4</sub>	72.05562	3.053
60.0556	CH <sub>6</sub> N <sub>3</sub>	240.0857	-C <sub>9</sub> H <sub>12</sub> N <sub>4</sub> O <sub>4</sub>	60.05562	0.333

**Table 4.2.** High resolution fragmentation data for LWT1.

m/z	Formula	Mass loss	Formula Loss	Theoretical m/z	ppm Mass Error
379.1040	C <sub>11</sub> H <sub>19</sub> N <sub>6</sub> O <sub>7</sub> S			379.1030	2.53
299.1464	C <sub>11</sub> H <sub>19</sub> N <sub>6</sub> O <sub>4</sub>	79.9576	-SO <sub>3</sub>	299.1462	0.67
281.1350	C <sub>11</sub> H <sub>17</sub> N <sub>6</sub> O <sub>3</sub>	97.9690	-SO <sub>3</sub> , -H <sub>2</sub> O	281.1351	0.43
240.0981	C <sub>10</sub> H <sub>14</sub> N <sub>3</sub> O <sub>4</sub>	157.9895	-SO <sub>3</sub> , -H <sub>2</sub> O, -C <sub>2</sub> H <sub>4</sub> O <sub>2</sub>	240.0979	0.92
221.1145	C <sub>9</sub> H <sub>13</sub> N <sub>6</sub> O	175.0161	-SO <sub>3</sub> , -H <sub>2</sub> O, -C <sub>2</sub> H <sub>4</sub> O <sub>2</sub> , -NH <sub>3</sub>	221.1145	0.00
204.0880	C <sub>9</sub> H <sub>10</sub> N <sub>5</sub> O	139.0059	-SO <sub>3</sub> , -CH <sub>5</sub> N <sub>3</sub>	204.0880	0.20
197.1034	C <sub>8</sub> H <sub>13</sub> N <sub>4</sub> O <sub>2</sub>	182.0006	-SO <sub>3</sub> , -CH <sub>4</sub> N <sub>2</sub> , -C <sub>2</sub> H <sub>3</sub> O <sub>2</sub>	197.1033	0.51
180.0771	C <sub>8</sub> H <sub>10</sub> N <sub>3</sub> O <sub>2</sub>	199.0269	-SO <sub>3</sub> , -CH <sub>5</sub> N <sub>3</sub> , -C <sub>2</sub> H <sub>4</sub> O <sub>2</sub>	180.0768	1.94
162.0663	C <sub>8</sub> H <sub>8</sub> N <sub>3</sub> O	217.0377	-SO <sub>3</sub> , -CH <sub>5</sub> N <sub>3</sub> , -C <sub>2</sub> H <sub>4</sub> O <sub>2</sub> , -H <sub>2</sub> O	162.0662	0.68
110.0712	C <sub>5</sub> H <sub>8</sub> N <sub>3</sub>	269.0328	-SO <sub>3</sub> , -C <sub>2</sub> H <sub>4</sub> O <sub>2</sub> , -C <sub>4</sub> H <sub>8</sub> N <sub>3</sub> O <sub>2</sub>	110.0713	0.64
102.0661	C <sub>3</sub> H <sub>8</sub> N <sub>3</sub> O	277.0379	-C <sub>2</sub> H <sub>3</sub> O, -C <sub>6</sub> H <sub>8</sub> N <sub>3</sub> O <sub>5</sub> S	102.0662	0.88
72.0556	C <sub>2</sub> H <sub>6</sub> N <sub>3</sub>	307.0484	-C <sub>9</sub> H <sub>13</sub> N <sub>3</sub> O <sub>7</sub> S	72.0556	0.28
60.0557	CH <sub>6</sub> N <sub>3</sub>	319.0483	-C <sub>10</sub> H <sub>13</sub> N <sub>3</sub> O <sub>7</sub> S	60.0556	1.33

**Table 4.3.** High resolution fragmentation data for LWT4.

m/z	Formula	Mass loss	Formula Loss	Theoretical m/z	ppm Mass Error
241.1405	C <sub>9</sub> H <sub>17</sub> N <sub>6</sub> O <sub>2</sub>			241.1408	1.04
223.1295	C <sub>9</sub> H <sub>15</sub> N <sub>6</sub> O	18.0110	-H <sub>2</sub> O	223.1302	3.09
205.1192	C <sub>9</sub> H <sub>13</sub> N <sub>6</sub>	36.0213	-H <sub>2</sub> O, -H <sub>2</sub> O	205.1196	2.05
177.0886	C <sub>7</sub> H <sub>9</sub> N <sub>6</sub>	64.0519	-H <sub>2</sub> O, -H <sub>2</sub> O, -C <sub>2</sub> H <sub>4</sub>	177.0883	1.58
164.0821	C <sub>8</sub> H <sub>10</sub> N <sub>3</sub> O	77.0584	-H <sub>2</sub> O, -CH <sub>5</sub> N <sub>3</sub>	164.0818	1.58
152.0819	C <sub>7</sub> H <sub>10</sub> N <sub>3</sub> O	89.0586	-CH <sub>4</sub> N <sub>3</sub> , -CH <sub>3</sub> O	152.0818	0.39
136.0867	C <sub>7</sub> H <sub>10</sub> N <sub>3</sub>	105.0538	-CH <sub>4</sub> N <sub>3</sub> , -H <sub>2</sub> O, -CH <sub>2</sub> O	136.0869	1.62
122.0711	C <sub>6</sub> H <sub>8</sub> N <sub>3</sub>	119.0694	-CH <sub>4</sub> N <sub>3</sub> , -CH <sub>3</sub> O, -CH <sub>2</sub> O	122.0713	1.39
110.0712	C <sub>5</sub> H <sub>8</sub> N <sub>3</sub>	131.0693	-C <sub>4</sub> H <sub>8</sub> N <sub>3</sub> O, -OH	110.0713	0.64
94.0650	C <sub>6</sub> H <sub>8</sub> N	147.0755	-C <sub>3</sub> H <sub>9</sub> N <sub>5</sub> O <sub>2</sub>	94.0651	1.28
80.0492	C <sub>5</sub> H <sub>6</sub> N	161.0913	-C <sub>4</sub> H <sub>11</sub> N <sub>5</sub> O <sub>2</sub>	80.0495	3.44
72.0556	C <sub>2</sub> H <sub>6</sub> N <sub>3</sub>	169.0849	-C <sub>4</sub> H <sub>11</sub> N <sub>5</sub> O <sub>2</sub>	72.0556	0.28
69.0447	C <sub>3</sub> H <sub>5</sub> N <sub>2</sub>	172.0958	-CH <sub>3</sub> O, -C <sub>5</sub> H <sub>9</sub> N <sub>4</sub> O	69.0447	0.29
60.0555	CH <sub>6</sub> N <sub>3</sub>	181.0850	-C <sub>8</sub> H <sub>11</sub> N <sub>3</sub> O <sub>2</sub>	60.0556	2.00

**Table 4.4.** High resolution fragmentation data for LWT5.

m/z	Formula	Mass loss	Formula Loss	Theoretical m/z	ppm Mass Error
299.1460	C <sub>11</sub> H <sub>19</sub> N <sub>6</sub> O <sub>4</sub>			299.1462	0.77
281.1353	C <sub>11</sub> H <sub>17</sub> N <sub>6</sub> O <sub>3</sub>	18.0107	-H <sub>2</sub> O	281.1357	1.28
257.1240	C <sub>10</sub> H <sub>17</sub> N <sub>4</sub> O <sub>4</sub>	42.0220	-CH <sub>2</sub> N <sub>2</sub>	257.1244	1.67
239.1157	C <sub>10</sub> H <sub>15</sub> N <sub>4</sub> O <sub>3</sub>	60.0303	-H <sub>2</sub> O, -CH <sub>2</sub> N <sub>2</sub>	239.1139	7.65
204.0880	C <sub>9</sub> H <sub>10</sub> N <sub>5</sub> O	95.0580	-H <sub>2</sub> O, - H <sub>2</sub> O, -NH <sub>2</sub> , -C <sub>2</sub> H <sub>3</sub> O	204.0880	0.05
197.1030	C <sub>8</sub> H <sub>13</sub> N <sub>4</sub> O <sub>2</sub>	102.0430	-C <sub>2</sub> H <sub>4</sub> O <sub>2</sub> , -CH <sub>2</sub> N <sub>2</sub>	197.1033	1.52
179.0927	C <sub>8</sub> H <sub>11</sub> N <sub>4</sub> O	120.0533	-C <sub>2</sub> H <sub>4</sub> O <sub>2</sub> , -CH <sub>2</sub> N <sub>2</sub> , -H <sub>2</sub> O	179.09274	0.22
138.0673	C <sub>6</sub> H <sub>8</sub> N <sub>3</sub> O	161.0787	-C <sub>2</sub> H <sub>4</sub> O <sub>2</sub> , -CH <sub>2</sub> N <sub>2</sub> , -H <sub>2</sub> O, -C <sub>2</sub> H <sub>3</sub> N	138.0662	8.04
96.0442	C <sub>5</sub> H <sub>6</sub> NO	203.1018	-CH <sub>2</sub> N <sub>2</sub> , - CH <sub>4</sub> N <sub>3</sub> , -C <sub>2</sub> H <sub>4</sub> O <sub>2</sub> , -C <sub>2</sub> H <sub>3</sub> O	96.0444	1.98
83.0604	C <sub>4</sub> H <sub>7</sub> N <sub>2</sub>	216.0856	-C <sub>2</sub> H <sub>3</sub> O <sub>2</sub> , -C <sub>5</sub> H <sub>9</sub> N <sub>4</sub> O <sub>2</sub>	83.0604	0.36
72.0552	C <sub>2</sub> H <sub>6</sub> N <sub>3</sub>	227.0908	-C <sub>9</sub> H <sub>13</sub> N <sub>3</sub> O <sub>4</sub>	72.0556	5.83
60.0557	CH <sub>6</sub> N <sub>3</sub>	239.0903	-C <sub>10</sub> H <sub>13</sub> N <sub>3</sub> O <sub>4</sub>	60.0556	1.33

**Table 4.5.** High resolution fragmentation data for LWT6.

m/z	Formula	Mass loss	Formula Loss	Theoretical m/z	ppm Mass Error
283.1513	C <sub>11</sub> H <sub>19</sub> N <sub>6</sub> O <sub>3</sub>			283.1513	0.04
241.1301	C <sub>10</sub> H <sub>17</sub> N <sub>4</sub> O <sub>3</sub>	42.0212	-CH <sub>2</sub> N <sub>2</sub>	241.12952	2.41
224.1032	C <sub>10</sub> H <sub>14</sub> N <sub>3</sub> O <sub>3</sub>	59.0481	-CH <sub>5</sub> N <sub>3</sub>	224.1030	1.03
205.1194	C <sub>9</sub> H <sub>13</sub> N <sub>6</sub>	78.0319	-H <sub>2</sub> O, -C <sub>2</sub> H <sub>4</sub> O <sub>2</sub>	205.1196	1.07
190.0958	C <sub>8</sub> H <sub>10</sub> N <sub>6</sub>	93.0555	-H <sub>2</sub> O, -C <sub>2</sub> H <sub>4</sub> O <sub>2</sub> , -CH <sub>3</sub>	190.0962	1.84
181.1082	C <sub>8</sub> H <sub>13</sub> N <sub>4</sub> O	102.0431	-C <sub>2</sub> H <sub>4</sub> O <sub>2</sub> , -CH <sub>2</sub> N <sub>2</sub>	181.1084	1.05
177.0883	C <sub>7</sub> H <sub>9</sub> N <sub>6</sub>	106.0630	-C <sub>2</sub> H <sub>4</sub> O <sub>2</sub> , -H <sub>2</sub> O, -C <sub>2</sub> H <sub>4</sub>	177.0883	0.11
164.0825	C <sub>8</sub> H <sub>10</sub> N <sub>3</sub> O	119.0688	-C <sub>2</sub> H <sub>4</sub> O <sub>2</sub> , -CH <sub>5</sub> N <sub>3</sub>	164.0818	4.02
146.0713	C <sub>8</sub> H <sub>8</sub> N <sub>3</sub>	137.0800	-C <sub>2</sub> H <sub>4</sub> O <sub>2</sub> , -CH <sub>5</sub> N <sub>3</sub> , -H <sub>2</sub> O	146.0713	0.21
136.08679	C <sub>7</sub> H <sub>10</sub> N <sub>3</sub>	147.0645	-C <sub>2</sub> H <sub>4</sub> O <sub>2</sub> , -CH <sub>3</sub> N <sub>3</sub> , -CH <sub>2</sub> O	136.0869	0.96
122.0713	C <sub>6</sub> H <sub>8</sub> N <sub>3</sub>	161.0800	-C <sub>2</sub> H <sub>4</sub> O <sub>2</sub> , -CH <sub>3</sub> N <sub>3</sub> , -C <sub>2</sub> H <sub>4</sub> O	122.0713	0.25
110.0713	C <sub>5</sub> H <sub>8</sub> N <sub>3</sub>	173.0800	-C <sub>2</sub> H <sub>4</sub> O <sub>2</sub> , -C <sub>4</sub> H <sub>8</sub> N <sub>3</sub> O	110.0713	0.27
102.0655	C <sub>5</sub> H <sub>8</sub> N <sub>3</sub>	181.0858	-C <sub>2</sub> H <sub>3</sub> O, -C <sub>4</sub> H <sub>8</sub> N <sub>3</sub> O <sub>3</sub>	102.0662	6.76
94.0651	C <sub>6</sub> H <sub>8</sub> N	189.0862	-C <sub>5</sub> H <sub>9</sub> N <sub>5</sub> O <sub>2</sub> , -H <sub>2</sub> O	94.0651	0.21
80.0495	C <sub>5</sub> H <sub>6</sub> N	203.1018	-C <sub>6</sub> H <sub>11</sub> N <sub>5</sub> O <sub>2</sub> , -H <sub>2</sub> O	80.0495	0.31
72.0554	C <sub>2</sub> H <sub>6</sub> N <sub>3</sub>	211.0959	-C <sub>9</sub> H <sub>13</sub> N <sub>3</sub> O <sub>3</sub>	72.0556	3.05

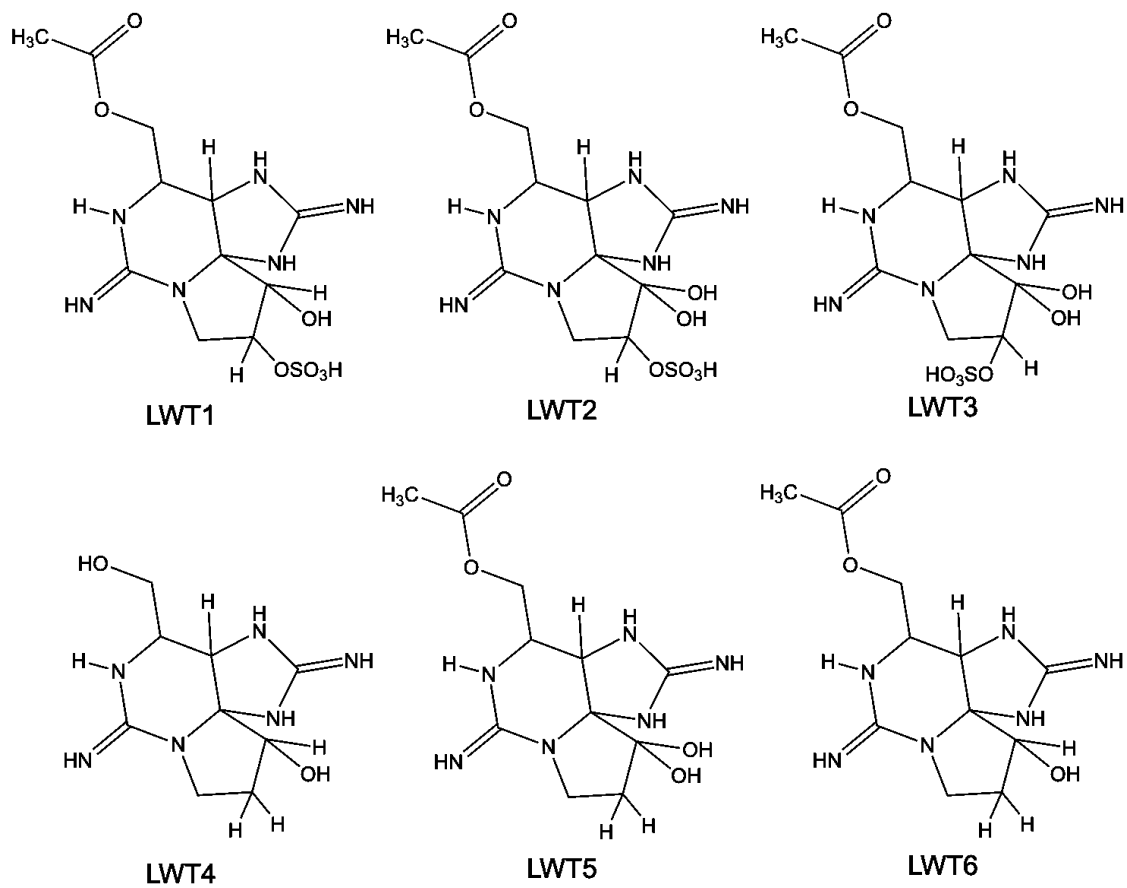
60.0556	CH <sub>6</sub> N <sub>3</sub>	223.0957	-C <sub>10</sub> H <sub>13</sub> N <sub>3</sub> O <sub>3</sub>	60.0556	0.33
---------	--------------------------------	----------	--	---------	------

---

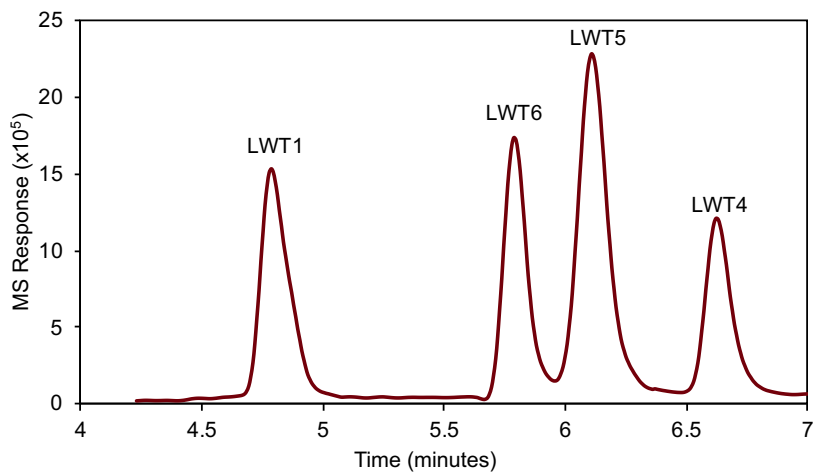
60.0556	CH <sub>6</sub> N <sub>3</sub>	223.0957	-C <sub>10</sub> H <sub>13</sub> N <sub>3</sub> O <sub>3</sub>	60.0556	0.33
---------	--------------------------------	----------	--	---------	------

---





**Figure 4.1.** Molecular structures of the *Lyngbya wollei* toxins (LWTs) 1-6 (free base).



**Figure 4.2.** UPLC-MS chromatogram for LWT1 (RT = 4.79 min), LWT4 (RT = 6.64 min), LWT5 (RT = 6.11 min), and LWT6 (RT = 5.79 min).

## REFERENCES

1. Otterstetter, H.; Craun, G. Disinfection in the Americas: A Necessity. *J. Am. Water Works Assoc.* **1997**, *89*, 8–10.
2. Calderon, R. L. The Epidemiology of Chemical Contaminants of Drinking Water. *Food Chem. Toxicol.* **2000**, *38* (SUPPL.1).
3. Rook, J. J. *J. Water Treat. Exam.* **1974**, *23*, 234–243.
4. Richardson, S. D.; Plewa, M. J.; Wagner, E. D.; Schoeny, R.; DeMarini, D. M. Occurrence, genotoxicity, and carcinogenicity of regulated and emerging disinfection by-products in drinking water: a review and roadmap for research. *Mutat. Res., Rev. Mutat. Res.* **2007**, *636*, 178–242.
5. Richardson, S. D.; Ternes, T. A. Water Analysis: Emerging Contaminants and Current Issues. *Anal. Chem.* **2011**, 4616–4648.
6. Cantor, K. P.; Lynch, C. F.; Hildesheim, M. E.; Dosemeci, M.; Lubin, J.; Alavanja, M.; Craun, G. Drinking water source and chlorination byproducts. I. Risk of bladder cancer. *Epidemiology* **1998**, *9*, 21–28.
7. Nieuwenhuijsen, M. J.; Toledano, M. B.; Eaton, N. E.; Fawell, J.; Elliott, P. Chlorination disinfection byproducts in water and their association with adverse reproductive outcomes: a review. *Occup. Environ. Med.* **2000**, *57*, 73–85.
8. Villanueva, C. M.; Cantor, K. P.; Grimalt, J. O.; Malats, N.; Silverman, D.; Tardon, A.; Garcia-Closas, R.; Serra, C.; Carrato, A.; Castano-Vinyals, G.; Marcos, R.; Rothman, N.; Real, F. X.; Dosemeci, M.; Kogevinas, M. Bladder cancer and exposure to water disinfection by-products through ingestion, bathing, showering, and swimming in pools. *Am. J. Epidemiol.* **2006**, *165*, 148–156.
9. Waller, K.; Swan, S. H.; DeLorenze, G.; Hopkins, B. Trihalomethanes in drinking water and spontaneous abortion. *Epidemiology* **1998**, *9*, 134–140.

10. Krasner, S. W.; Kostopoulou, M.; Toledano, M. B.; Wright, J.; Patelarou, E.; Kogevas, M.; Villanueva, C. M.; Turigas, G. C.; Santa Marina, L.; Fernandez-Somoano, A.; et al. Occurrence of DBPs in Drinking Water of European Regions for Epidemiology Studies. *J. Am. Water Works Assn.* **2016**, *108*, E501–E512.
11. Evans, A. M.; Wright, J. M.; Meyer, A.; Rivera-Nunez, Z. Spatial variation of disinfection by-product concentrations: Exposure assessment implications. *Water Res.* **2013**, *47*, 6130–6140.
12. Grellier, J.; Bennett, J.; Patelarou, E.; Smith, R. B.; Toledano, M. B.; Rushton, L.; Briggs, D. J.; Nieuwenhuijsen, M. J. Exposure to Disinfection By-products, Fetal Growth, and Prematurity A Systematic Review and Meta-analysis. *Epidemiology* **2010**, *21*, 300–313.
13. U.S. Environmental Protection Agency. *National Primary Drinking Water Regulations: Stage 2 Disinfectants and Disinfection Byproducts Rule*; Fed. Reg., 2006, 71.
14. *United Nations World Water Development Report 4. Volume 1: Managing Water under Uncertainty and Risk*
15. Jury, W. A.; Vaux Jr, H. J., The Emerging Global Water Crisis: Managing Scarcity and Conflict Between Water Users. In *Advances in Agronomy*, Academic Press: 2007, 95, 1-76.
16. Elimelech, M.; Phillip, W.A. The future of seawater desalination: energy, technology, and the environment. *Science* **2011**, *333*, 712-717.
17. S. V. Veerapaneni et al., Reducing Energy Consumption for Seawater Desalination, *J. Am. Water Works Assn.* **2007**, *99*, 95.
18. Watson, K.; Farre, M.J.; Knight, N. Strategies for the removal of halides from drinking water sources, and their applicability in disinfection by-product minimization: a critical review. *J. Environ. Manag.* **2012**, *110*, 276-298.
19. Brown Jr., E. G.; Laird, J.; Cowin, M. California Water Plan - Update 2013; State of California, Natural Resources Agency, Department of Water Resources: 2013.

20. Agus, E.; Voutchkov, N.; Sedlak, D. L. Disinfection byproducts and their potential impact on the quality of water produced by desalination systems: A literature review, *Desalination*, **2009**, *237*, 214–237.
21. Kim, D.; Amy G. L.; Karan, T. Disinfection by-product formation during seawater desalination: A review, *Water Res.*, **2015**, *81*, 343–355.
22. Carpenter, K.D., Kraus, T.E.C., Goldman, J.H., Saraceno, J.F., Downing, B.D., Bergamaschi, B.A., McGhee, G. and Triplett, T. (2013). Sources and characteristics of organic matter in the Clackamas River, Oregon, related to the formation of disinfection by-products in treated drinking water. U.S. Geological Survey Scientific Investigation Report 2013–5001, 78.
23. Owen, D.M., Amy, G.L., Chowdhury, Z.K., Paode, R., McCoy, G. and Viscosil, K. NOM characterization and treatability. *J. Am. Water Works Assoc.*, **1995**, *87* 46–63.
24. Allonier, A.-S.; Khalanski, M.; Camel, V.; Bermond, A. Characterization of chlorination by-products in cooling effluents of coastal nuclear power stations. *Mar. Pollut. Bull.* **1999**, *38*, 1232-1241.
25. Dalvi, A.G.; Al-Rasheed, R.; Javeed, M.A. Haloacetic acids (HAAs) formation in desalination processes from disinfectants. *Desalination* **2000**, *129*, 261-271.
26. Fabbicino, M.; Korshin, G.V. Formation of disinfection by-products and applicability of differential absorbance spectroscopy to monitor halogenation in chlorinated coastal and deep ocean seawater. *Desalination* **2005**, *176*, 57-69.
27. Agus, E.; Sedlak, D.L. Formation and fate of chlorination by-products in reverse osmosis desalination systems. *Water Res.* **2010**, *44*, 1616-1626.
28. Werschkun, B.; Sommer, Y.; Banerji, S. Disinfection by-products in ballast water treatment: an evaluation of regulatory data. *Water Res.* **2012**, *46*, 4884-4901.
29. Parinet, J.; Tabaries, S.; Coulomb, V.; Vassalo, L.; Boudenne, J.-L. Exposure levels to brominated compounds in seawater swimming pools treated with chlorine. *Water Res.* **2012**, *46*, 828-836.

30. Shi, H.; Qiang, Z.; Adama, C. Formation of haloacetic acids, halonitromethanes, bromate, and iodate during chlorination and ozonation of seawater and saltwater of marine aquaria systems. *Chemosphere* **2013**, *90*, 2485-2492.
31. Jenner, H.A.; Taylor, C.J.L.; van Donk, M.; Khalanski, M.; Chlorination by-products in chlorinated cooling water of some European coastal power stations. *Mar. Environ. Res.* **1997**, *43*, 479-493.
32. Taylor, C.J.L. The effects of biological fouling control at coastal and estuarine power stations. *Mar. Pollut. Bull.* **2006**, *53*, 30-48.
33. Le Roux, J., Nada, N., Khan, M. T., Croue, J.-P. Tracing disinfection byproducts in full-scale desalination plants. *Desalination* **2015**, *359*, 141-148.
34. Albaladejo, G.; Ros, J.A.; Romero, A.; Navarro, S. Effect of bromophenols on the taste and odour of drinking water obtained by seawater desalination in south-eastern Spain. *Desalination* **2012**, *307*, 1-8.
35. Sorlini, S., Collivignarelli, C. Trihalomethane formation during chemical oxidation with chlorine, chlorine dioxide and ozone of ten Italian natural waters. *Desalination* **2005**, *176*, 103-111.
36. Kim, J.; Chung, Y.; Shin, D.; Kim, M.; Lee, Y.; Lim, Y.; Lee, D. Chlorination byproducts in surface water treatment process. *Desalination* **2002**, *151*, 1-9.
37. Echardt, J.; Kornmueller, A. The advanced EctoSys electrolysis as an integral part of a ballast water treatment system. *Water Sci. Technol.* **2009**, *60*, 2227-2234.
38. Oh, B.S.; Oh, S.G.; Hwang, Y.Y.; Yu, H.-W.; Kang, J.-W.; Kim, I.S. Formation of hazardous inorganic by-products during electrolysis of seawater as a disinfection process for desalination. *Sci. Total Environ.* **2010**, *408*, 5958-5965.
39. Gonsior, M.; Mitchelmore, C.; Heyes, A.; Harir, M.; Richardson, S. D.; Petty, W. T.; Wright, D. A.; Schmitt-Kopplin, P., Bromination of Marine Dissolved Organic Matter following Full Scale Electrochemical Ballast Water Disinfection. *Environ. Sci. Technol.* **2015**, *49*, 9048-9055.
40. Komaki, Y.; Pals, J.; Wagner, E. D.; Mariñas, B. J.; Plewa, M. J., Mammalian Cell DNA Damage and Repair Kinetics of Monohaloacetic Acid Drinking Water Disinfection By-Products. *Environ. Sci. Technol.* **2009**, *43*, 8437-8442.

41. Bichsel, Y.; von Gunten, U. Formation of iodo-trihalomethanes during disinfection and oxidation of iodide containing waters. *Environ. Sci. Technol.* **2000**, *34*, 2784-2791. <https://doi.org/10.1021/es9914590>
42. Ito, K.; Nomura, R.; Fujii, T.; Tanaka, M.; Tsumura, T.; Shibata, H.; Hirokawa, T. Determination of nitrite, nitrate, bromide, and iodide in seawater by ion chromatography with UV detection using dilauryldimethylammonium-coated monolithic ODS columns and sodium chloride as an eluent, *Anal. Bioanal. Chem.*, **2012**, *404*, 2513–2517.
43. Millero, F. J.; Feistel, R.; Wright, D. G.; McDougall, T. J. The composition of Standard Seawater and the definition of the Reference-Composition Salinity Scale, *Deep Sea Res., Part I*, **2008**, *55*, 50–72.
44. Richardson, S. D.; Thruston, A. D.; Krasner, S. W.; Weinberg, H. S.; Miltner, R. J.; Schenck, K. M.; Narotsky, M. G.; McKague, A. B.; Simmons, J. E. Integrated Disinfection By-Products Mixtures Research: Comprehensive Characterization of Water Concentrates Prepared from Chlorinated and Ozonated/Postchlorinated Drinking Water. *J. Toxicol. Environ. Heal. - Part A Curr. Issues* **2008**, *71*, 1165–1186.
45. Cuthbertson, A. A.; Liberatore, H. K.; Kimura, S. Y.; Allen, J. M.; Bensussan, A. V.; Richardson, S. D. Trace Analysis of 61 Emerging Br-, Cl-, and I-DBPs: New Methods to Achieve Part-Per-Trillion Quantification in Drinking Water. *Anal. Chem.* **2020**, *92*, 3058–3068.
46. Plewa, M. J.; Wagner, E. D.; Richardson, S. D. TIC-Tox: A Preliminary Discussion on Identifying the Forcing Agents of DBP-Mediated Toxicity of Disinfected Water. *J. Environ. Sci.* **2017**, *58*, 208–216.
47. Doederer, K.; Farré, M. J.; Pidou, M.; Weinberg, H. S.; Gernjak, W.; Rejection of disinfection by-products by RO and NF membranes: Influence of solute properties and operational parameters *Journal of Membrane Science* **2014**, *467*, 195–205.
48. Kitis, M.; Karanfil, T.; Wigton, A.; Kilduff, J.E. Probing reactivity of dissolved organic matter for disinfection by-product formation using XAD-8 resin adsorption and ultrafiltration fractionation. *Water Res.* **2002**, *36*, 3834-3848.
49. Hong, H.; Qian, L.; Xiao, Z.; Zhang, J.; Chen, J.; Lin, H.; Yu, H.; Shen, L.; Liang, Y. Effect of nitrite on the formation of halonitromethanes during chlorination of organic matter from different origin, *J. Hydrol.*, **2015**, *531*, 802-809.

50. Hu, J.; Song, H.; Karanfil, T.; Comparative Analysis of Halonitromethane and Trihalomethane Formation and Speciation in Drinking Water: The Effects of Disinfectants, pH, Bromide, and Nitrite. *Environ. Sci. Technol.* **2010**, *44*, 794–799.
51. Krasner, S. W.; Weinberg, H. S.; Richardson, S. D.; Pastor, S.; Chinn, R.; Sclimenti, M. J.; Onstad, G.; Thruston, A. D., Jr. The occurrence of a new generation of disinfection byproducts. *Environ. Sci. Technol.* **2006**, *40*, 7175–7185.
52. Cuthbertson, A. A.; Kimura, S. Y.; Liberatore, H. K.; Summers, R. S.; Knappe, D. R. U.; Stanford, B. D.; Maness, J. C.; Mulhern, R. E.; Selbes, M.; Richardson, S. D. Does Granular Activated Carbon with Chlorination Produce Safer Drinking Water? From Disinfection Byproducts and Total Organic Halogen to Calculated Toxicity. *Environ. Sci. Technol.* **2019**, *53*, 5987–5999.
53. Cuthbertson, A. A.; Kimura, S. Y.; Liberatore, H. K.; Knappe, D. R. U.; Stanford, B.; Summers, R. S.; Dickenson, E. R.; Maness, J. C.; Glover, C.; Selbes, M.; et al. GAC to BAC: Does It Make Chloraminated Drinking Water Safer? *Water Res.* **2020**, *172*.
54. Huang, Y.; Kong, M.; Westerman, D. C.; Xu, E. G.; Coffin, S.; Cochran, K. H.; Liu, Y.; Richardson, S. D.; Schlenk, D.; Dionysiou, D. D.: Effects of  $\text{HCO}_3^-$  on Degradation of Toxic Contaminants of Emerging Concern by UV/ $\text{NO}_3^-$  *Environ. Sci. Technol.* **2018**, *52*, 12697–12707.
55. Huang, Y.; Kong, M.; Coffin, S.; Cochran, K. H.; Westerman, D. C.; Schlenk, D.; Richardson, S. D.; Lei, L.; Dionysiou, D. D. Degradation of contaminants of emerging concern by UV/ $\text{H}_2\text{O}_2$  for water reuse: kinetics, mechanisms, and cytotoxicity analysis. *Water Res.* **2020**, *174*, 115587.
56. Binz, C., Harris-Lovett, S., Kiparsky, M., Sedlak, D.L. and Truffer, B. The thorny road to technology legitimation - Institutional work for potable water reuse in California. *Technological Forecasting and Social Change* **2016**, *103*, 249-263.
57. Chuang, Y.-H., Chen, S., Chinn, C.J., Mitch, W.A.; Comparing the UV/monochloramine and UV/free chlorine advanced oxidation processes (AOPs) to the UV/hydrogen peroxide AOP under scenarios relevant to potable reuse. *Environ. Sci. Technol.* **2017**, *51*, 13859-13868.
58. Patton, S., Romano, M., Naddeo, V., Ishida, K.P., Liu, H.; Photolysis of mono- and dichloramines in UV/hydrogen peroxide: Effects on 1,4-dioxane removal and relevance in water reuse. *Environ. Sci. Technol.*, **2018**, *52*, 11720–11727.



59. Wols, B.A., Hofman-Caris, C.H.M., Harmsen, D.J.H. and Beerendonk, E.F.; Degradation of 40 selected pharmaceuticals by UV/H<sub>2</sub>O<sub>2</sub>. *Water Res.* **2013**, *47*, 5876-5888.
60. Anderson, P., Denslow, N., Drewes, J., Olivieri, A., Schlenk, D., Snyder, S.A.; *Final report: Monitoring strategies for chemicals of emerging concern (CECs) in recycled water*. Recommendations of a science advisory panel convened by the California State Water Resources Control Board, Sacramento, Calif., **2010**.
61. Maruya, K.A., Schlenk, D., Anderson, P.D., Denslow, N.D., Drewes, J.E., Olivieri, A.W., Scott, G.I. and Snyder, S.A.; An adaptive, comprehensive monitoring strategy for chemicals of emerging concern (CECs) in California's aquatic ecosystems. *Integrated Environmental Assessment and Management*, **2014**, *10*, 69-77.
62. He, X., Zhang, G., de la Cruz, A.A., O'Shea, K.E. and Dionysiou, D.D.; Degradation mechanism of cyanobacterial toxin cylindrospermopsin by hydroxyl radicals in homogeneous UV/H<sub>2</sub>O<sub>2</sub> process. *Environ. Sci. Technol.* **2014**, *48*, 4495-4504.
63. Gligorovski, S., Streckowski, R., Barbati, S. and Vione, D.; Environmental implications of hydroxyl radicals (•OH). *Chem. Rev.* **2015**, *115*, 13051-13092.
64. Huang, Y., Liu, Y., Kong, M., Xu, E.G., Coffin, S., Schlenk, D. and Dionysiou, D.D.; Efficient degradation of cytotoxic contaminants of emerging concern by UV/H<sub>2</sub>O<sub>2</sub>. *Environ. Sci.: Water Res. Technol.*, **2018**, *4*, 1272-1281.
65. Shu, Z., Singh, A., Klamerth, N., McPhedran, K., Bolton, J.R., Belosevic, M. and Gamal El-Din, M.; Pilot-scale UV/H<sub>2</sub>O<sub>2</sub> advanced oxidation process for municipal reuse water: Assessing micropollutant degradation and estrogenic impacts on goldfish (*Carassius auratus* L.). *Water Res.* **2016**, *101*, 157-166.
66. Lambropoulou, D. A.; Nollet, L. M. L.; Ohio, L.; Information, N., *Transformation products of emerging contaminants in the environment: analysis, processes, occurrence, effects and risks*. John Wiley and Sons Ltd: Chichester, West Sussex, United Kingdom, 2014.
67. Walse, S. S.; Morgan, S. L.; Kong, L.; Ferry, J. L., Role of dissolved organic matter, nitrate, and bicarbonate in the photolysis of aqueous fipronil. *Environ. Sci. Technol.* **2004**, *38*, 3908-3915.
68. Mao, L.; Meng, C.; Zeng, C.; Ji, Y.; Yang, X.; Gao, S., The effect of nitrate, bicarbonate and natural organic matter on the degradation of sunscreen agent p-aminobenzoic acid by simulated solar irradiation. *Sci. Total Environ.* **2011**, *409*, 5376-5381.

69. Ren, D.; Bi, T.; Gao, S.; Li, X.; Huang, B.; Pan, X., Photodegradation of 17 $\alpha$ -ethynylestradiol in nitrate aqueous solutions. *Environ. Eng. Res.* **2016**, *21*, 188-195.
70. Liu, Y.; He, X.; Duan, X.; Fu, Y.; Fatta-Kassinos, D.; Dionysiou, D. D., Significant role of UV and carbonate radical on the degradation of oxytetracycline in UV-AOPs: Kinetics and mechanism. *Water Res.* **2016**, *95*, 195-204.
71. Larson, R. A.; Zepp, R. G., Reactivity of the carbonate radical with aniline derivatives. *Environ. Toxicol. Chem.* **1988**, *7*, 265-274.
72. Umschlag, T.; Herrmann, H., The carbonate radical ( $\text{HCO}_3^{\cdot}/\text{CO}_3^{\cdot-}$ ) as a reactive intermediate in water chemistry: Kinetics and modelling. *Acta Hydrochim. Hydrobiol.* **1999**, *27*, 214-222.
73. de Luna, L.A.V., da Silva, T.H.G., Nogueira, R.F.P., Kummrow, F. and Umbuzeiro, G.A. Aquatic toxicity of dyes before and after photo-Fenton treatment. *J. Hazard. Mater.* **2014**, *276*, 332-338.
74. Li, W., Xu, E., Schlenk, D. and Liu, H.; Cyto- and geno-toxicity of 1,4-dioxane and its transformation products during ultraviolet-driven advanced oxidation processes. *Environmental Science: Water Research & Technology* **2018**, *4*, 1213-1218.
75. Mariani, M.L., Romero, R.L. and Zalazar, C.S.; Modeling of degradation kinetic and toxicity evaluation of herbicides mixtures in water using the UV/H<sub>2</sub>O<sub>2</sub> process. *Photochemical & Photobiological Sciences* **2015**, *14*, 608-617.
76. Olmez-Hanci, T., Dursun, D., Aydin, E., Arslan-Alaton, I., Girit, B., Mita, L., Diano, N., Mita, D.G. and Guida, M.; S<sub>2</sub>O<sub>8</sub><sup>2-</sup>/UV-C and H<sub>2</sub>O<sub>2</sub>/UV-C treatment of Bisphenol A: Assessment of toxicity, estrogenic activity, degradation products and results in real water. *Chemosphere* **2015**, *119*, S115-S123.
77. Yin, K., Deng, L., Luo, J., Crittenden, J., Liu, C., Wei, Y. and Wang, L.; Destruction of phenicol antibiotics using the UV/H<sub>2</sub>O<sub>2</sub> process: Kinetics, byproducts, toxicity evaluation and trichloromethane formation potential. *Chem. Eng. J.* **2018**, *351*, 867-877.
78. Gao, Y., Ji, Y., Li, G. and An, T.; Mechanism, kinetics and toxicity assessment of OH-initiated transformation of triclosan in aquatic environments. *Water Res.* **2014**, *49*, 360-370.
79. Westerhoff, P., Yoon, Y., Snyder, S., and Wert, E.; Fate of endocrine-disruptor, pharmaceutical, and personal care product chemicals during simulated drinking water processes. *Environ. Sci. Technol.* **2005**, *39*, 6649-6663.

80. Dhara, A.K., Singh, U.P. and Ghosh, K. (2016) Radical pathways and O<sub>2</sub> participation in benzyl alcohol oxidation, and catechol and o-aminophenol oxidase activity studies with novel zinc complexes: an experimental and theoretical investigation. *Inorg. Chem. Front.* **2016**, 3, 1543-1558.
81. Gligorovski, S., Strekowski, R., Barbati, S. and Vione, D. (2015) Environmental implications of hydroxyl radicals ( $\bullet$ OH). *Chem. Rev.* **2015**, 115, 13051-13092.
82. Li, H., Long, Y., Zhu, X., Tian, Y. and Ye, J.; Influencing factors and chlorinated byproducts in electrochemical oxidation of bisphenol A with boron-doped diamond anodes. *Electrochim. Acta* **2017**, 246, 1121-1130.
83. Abdelraheem, W.H.M., Patil, M.K., Nadagouda, M.N. and Dionysiou, D.D.; Hydrothermal synthesis of photoactive nitrogen- and boron- codoped TiO(2) nanoparticles for the treatment of bisphenol A in wastewater: Synthesis, photocatalytic activity, degradation byproducts and reaction pathways. *Applied Catalysis B-Environmental* **2019**, 241, 598-611.
84. Wooding, K.M., Barkley, R.M., Hankin, J.A., Johnson, C.A., Bradford, A.P., Santoro, N., and Murphy, R.C. Mechanism of formation of major estradiol product ions following collisional activation of the molecular anion in a tandem quadrupole mass spectrometer. *JASMS* **2013**, 24, 1451-1455.
85. Musa, K.A.K. and Eriksson, L.A.; Photodegradation mechanism of the common non-steroid anti-inflammatory drug diclofenac and its carbazole photoproduct. *Phys. Chem. Chem. Phys.* **2009**, 11, 4601-4610.
86. Pérez-Estrada, L.A., Malato, S., Gernjak, W., Agüera, A., Thurman, E.M., Ferrer, I. and Fernández-Alba, A.R.; Photo-Fenton degradation of diclofenac: Identification of main intermediates and degradation pathway. *Environ. Sci. Technol.* **2005**, 39, 8300-8306.
87. Munoz, M., de Pedro, Z.M., Casas, J.A. and Rodriguez, J.J.; Triclosan breakdown by Fenton-like oxidation. *Chem. Eng. J.* **2012**, 198-199, 275-281.
88. Naik, D. B.; Mohan, H., Radiolysis of aqueous solutions of dihalobenzenes: studies on the formation of halide ions by ion chromatography. *Radiation Physics and Chemistry* **2005**, 73, 218-223.
89. Wu, Z.; Fang, J.; Xiang, Y.; Shang, C.; Li, X.; Meng, F.; Yang, X., Roles of reactive chlorine species in trimethoprim degradation in the UV/chlorine process: Kinetics and transformation pathways. *Water Res.* **2016**, 104, 272-282.

90. Huang, Y.; Han, C.; Liu, Y.; Nadagouda, M. N.; Machala, L.; O'Shea, K. E.; Sharma, V. K.; Dionysiou, D. D., Degradation of atrazine by  $Zn_xCu_{1-x}Fe_2O_4$  nanomaterial-catalyzed sulfite under UV-vis light irradiation: Green strategy to generate  $SO_4^{\cdot-}$ . *Applied Catalysis B: Environmental* **2018**, *221* (Supplement C), 380-392.
91. Khan, J. A.; He, X.; Shah, N. S.; Khan, H. M.; Hapeshi, E.; Fatta-Kassinos, D.; Dionysiou, D. D., Kinetic and mechanism investigation on the photochemical degradation of atrazine with activated  $H_2O_2$ ,  $S_2O_8^{2-}$  and  $HSO_5^-$ . *Chem. Eng. J.* **2014**, *252* (Supplement C), 393-403.
92. Xin, L.; Sun, Y.; Feng, J.; Wang, J.; He, D., Degradation of triclosan in aqueous solution by dielectric barrier discharge plasma combined with activated carbon fibers. *Chemosphere* **2016**, *144* (Supplement C), 855-863.
93. Busset, C.; Mazellier, P.; Sarakha, M.; De Laat, J., Photochemical generation of carbonate radicals and their reactivity with phenol. *J. Photochem. Photobiol. A: Chem.* **2007**, *185*, 127-132.
94. Sein, M. M.; Zedda, M.; Tuerk, J.; Schmidt, T. C.; Golloch, A.; von Sonntag, C., Oxidation of diclofenac with ozone in aqueous solution. *Environ. Sci. Technol.* **2008**, *42*, 6656-6662.
95. Smith, M. L.; Westerman, D. C.; Putnam, S. P.; Richardson, S. D.; Ferry, J. L.; Emerging Lyngbya wollei toxins: A new high resolution mass spectrometry method to elucidate a potential environmental threat. *Harmful Algae* **2019**, *90*, 101700.
96. Harada, T., Oshima, Y., Yasumoto, T., Studies on paralytic shellfish poisoning in tropical waters .4. Structures of 2 paralytic shellfish toxins, gonyautoxin-V and gonyautoxin-VI isolated from a tropical dinoflagellate, pyrodinium bahamense var compressa. *Agr. Biol. Chem.* **1982**, *46*, 1861-1864.
97. Oshima, Y., Hasegawa, M., Yasumoto, T., Hallegraeff, G., Blackburn, S., Dinoflagellate *Gymnodinium catenatum* as the source of paralytic shellfish toxins in tasmanian shellfish. *Toxicon* **1987**, *25*, 1105-1111.
98. Carmichael, W.W., Toxins of cyanobacteria. *Sci.Am.* **1994**, *270*, 78-86.
99. Jochimsen, E.M., Carmichael, W.W., An, J.S., Cardo, D.M., Cookson, S.T., Holmes, C.E.M., Antunes, M.B.D., de Melo, D.A., Lyra, T.M., Barreto, V.S.T., Azevedo, S., Jarvis, W.R., Liver failure and death after exposure to microcystins at a hemodialysis center in Brazil. *N. Engl. J. Med.* **1998**, *338*, 873-878.
100. Kao, C.Y., Paralytic shellfish poisoning. In *Algal toxins in seafood and drinking water.*; Falconer, I. R.; Academic Press: Cambridge, MA, **1993**, 75-86.

101. Landsberg, J.H., 2002. The effects of harmful algal blooms on aquatic organisms. *Rev. Fish. Sci.* **2002**, *10*, 113-390.
102. Negri, A.P., Jones, G.J., Hindmarsh, M., Sheep mortality associated with paralytic shellfish poisons from the cyanobacterium *Anabaena circinalis*. *Toxicon* **1995**, *33*, 1321-1329.
103. Al-Tebrineh, J., Mihali, T.K., Pomati, F., Neilan, B.A., Detection of Saxitoxin-Producing Cyanobacteria and *Anabaena circinalis* in Environmental Water Blooms by Quantitative PCR. *Appl. Environ. Microbiol.* **2010**, *76*, 7836-7842.
104. Humpage, A.R., Magalhaes, V.F., Froscio, S.M., Comparison of analytical tools and biological assays for detection of paralytic shellfish poisoning toxins. *Anal. Bioanal. Chem.* **2010**, *397*, 1655-1671.
105. Onodera, H., Satake, M., Oshima, Y., Yasumoto, T., Carmichael, W.W., New saxitoxin analogues from the freshwater filamentous cyanobacterium *Lyngbya wollei*. *Nat. Toxins* **1997**, *5*, 146-151.
106. Lagos, N., Onodera, H., Zagatto, P.A., Andrinolo, D., Azevedo, S., Oshima, Y., The first evidence of paralytic shellfish toxins in the freshwater cyanobacterium *Cylindrospermopsis raciborskii*, isolated from Brazil. *Toxicon*, **1999**, *37*, 1359-1373.
107. Jackim, E., Gentile, J., Toxins of a blue green alga - similarity to saxitoxin. *Science* **1968**, *162*, 915.
108. Mahmood, N.A., Carmichael, W.W., Paralytic shellfish poisons produced by the freshwater cyanobacterium *Aphanizomenon-flos-aquae* NH-5. *Toxicon* **1986**, *24*, 175.
109. Sawyer, P.J., Gentile, J.H., Sasner, J.J., Demonstration of a toxin from *Aphanizomenon flos aquae* (L) Ralfs. *Can. J. Microbiol.* **1968**, *14*, 1199.
110. Pomati, F., Sacchi, S., Rosetti, C., Giovannardi, S., Onodera, H., Oshima, Y., Neilan, B.A., The freshwater cyanobacterium *Planktothrix* Sp. FP1: Molecular identification and detection of paralytic shellfish poisoning toxins. *J. Phycol.* **2003**, *36*, 553-562.

111. Dell'Aversano, C., Hydrophilic Interaction Liquid Chromatography-Mass Spectrometry (HILIC-MS) of Paralytic Shellfish Poisoning Toxins, Domoic Acid, and Assorted Cyanobacterial Toxins, In: Wang, P.G., He, W. (Eds.), Hydrophilic Interaction Liquid Chromatography. Crc Press-Taylor & Francis Group, Boca Raton, **2011**, 105-132.
112. Carmichael, W.W., Evans, W.R., Yin, Q.Q., Bell, P., Moczydlowski, E., Evidence for paralytic shellfish poisons in the freshwater cyanobacterium *Lyngbya wollei* (Farlow ex Gomont) comb. nov. *Appl. Environ. Microbiol.* **1997**, *63*, 3104-3110.
113. Cowell, B.C., Botts, P.S., Factors influencing the distribution, abundance and growth of *Lyngbya wollei* in central Florida. *Aquat. Bot.* **1994**, *49*, 1-17.
114. Foss, A.J., Phlips, E.J., Yilmaz, M., Chapman, A., 2012b. Characterization of paralytic shellfish toxins from *Lyngbya wollei* dominated mats collected from two Florida springs. *Harmful Algae* **2012a**, *16*, 98-107.
115. Yin, Q.Q., Carmichael, W.W., Evans, W.R., Factors influencing growth and toxin production by cultures of the freshwater cyanobacterium *Lyngbya wollei* Farlow ex Gomont. *J. Appl. Phycol.* **1997**, *9*, 55-63.
116. Cusick, K.D., Saylor, G.S., An Overview on the Marine Neurotoxin, Saxitoxin: Genetics, Molecular Targets, Methods of Detection and Ecological Functions. *Mar. Drugs* **2013**, *11*, 991-1018.
117. Schantz, E.J., McFarren, E.F., Schafer, M.L., Lewis, K.H., Purified shellfish poison for bioassay standardization. *JAOAC* **1958**, *41*, 160-168.
118. Turner, A.D., Dhanji-Rapkova, M., Algoet, M., Suarez-Isla, B.A., Cordova, M., Caceres, C., Murphy, C.J., Casey, M., Lees, D.N., Investigations into matrix components affecting the performance of the official bioassay reference method for quantitation of paralytic shellfish poisoning toxins in oysters. *Toxicon* **2012**, *59*, 215-230.
119. Gallacher, S., Birkbeck, T.H., A tissue culture assay for direct detection of sodium-channel blocking toxins in bacterial culture supernates. *FEMS Microbiol. Lett.* **1992**, *92*, 101-108.
120. Jellett, J.F., Marks, L.J., Stewart, J.E., Dorey, M.L., Watsonwright, W., Lawrence, J.F., Paralytic shellfish poison (saxitoxin family) bioassays - automated end-point determination and standardization of the invitro tissue-culture bioassay, and comparison with the standard mouse bioassay. *Toxicon* **1992**, *30*, 1143-1156.

121. Kogure, K., Tamplin, M.L., Simidu, U., Colwell, R.R., A tissue culture assay for tetrodotoxin, saxitoxin and related toxins. *Toxicon* **1988**, *26*, 191-197.
122. Manger, R.L., Leja, L.S., Lee, S.Y., Hungerford, J.M., Wekell, M.M., Tetrazolium-based cell bioassay for neurotoxins active on voltage sensitive sodium channels - semiautomated assay for saxitoxins, brevetoxins, and ciguatoxins. *Anal. Biochem.* **1993**, *214*, 190-194.
123. Chu, F.S., Huang, X., Hall, S., Production and characterization of antibodies against neosaxitoxin. *J. AOAC Int.* **1992**, *75*, 341-345.
124. Humpage, A.R., Magalhaes, V.F., Froscio, S.M., Comparison of analytical tools and biological assays for detection of paralytic shellfish poisoning toxins. *Anal. Bioanal. Chem.* **2010**, *397*, 1655-1671.
125. Davio, S.R., Fontelo, P.A., A competitive displacement assay to detect saxitoxin and tetrodotoxin. *Anal. Biochem.* **1984**, *141*, 199-204.
126. Doucette, G.J., Logan, M.M., Ramsdell, J.S., VanDolah, F.M., 1997. Development and preliminary validation of a microtiter plate-based receptor binding assay for paralytic shellfish poisoning toxins. *Toxicon* **1997**, *35*, 625-636.
127. Usup, G., Leaw, C.P., Cheah, M.Y., Ahmad, A., Ng, B.K., Analysis of paralytic shellfish poisoning toxin congeners by a sodium channel receptor binding assay. *Toxicon* **2004**, *44*, 37-43.
128. Van Dolan, F.M., Fire, S.E., Leighfield, T.A., Mikulski, C.M., Doucette, G.J., Determination of Paralytic Shellfish Toxins in Shellfish by Receptor Binding Assay: Collaborative Study. *J. AOAC Int.* **2012**, *95*, 795-812.
129. Dell'Aversano, C., Tattaglione, L., Polito, G., Dean, K., Giacobbe, M., Casabianca, S., Capellacci, S., Penna, A., Turner, A.D., First detection of tetrodotoxin and high levels of paralytic shellfish poisoning toxins in shellfish from Sicily (Italy) by three different analytical methods. *Chemosphere* **2019**, *215*, 881-892.
130. Dell'Aversano, C., Hess, P., Quilliam, M.A., Hydrophilic interaction liquid chromatography-mass spectrometry for the analysis of paralytic shellfish poisoning (PSP) toxins. *J. Chromatogr. A.* **2005**, *1081*, 190-201.

131. Dell'Aversano, C., Tattaglione, L., Polito, G., Dean, K., Giacobbe, M., Casabianca, S., Capellacci, S., Penna, A., Turner, A.D., First detection of tetrodotoxin and high levels of paralytic shellfish poisoning toxins in shellfish from Sicily (Italy) by three different analytical methods. *Chemosphere* **2019**, 215, 881-892.
132. Lajeunesse, A., Segura, P.A., Gelinas, M., Hudon, C., Thomas, K., Quilliam, M.A., Gagnon, C., Detection and confirmation of saxitoxin analogues in freshwater benthic *Lyngbya wollei* algae collected in the St. Lawrence River (Canada) by liquid chromatography-tandem mass spectrometry. *J. Chromatogr. A.* **2012**, 1219, 93-103.
133. Foss, A.J., Philips, E.J., Aubel, M.T., Szabo, N.J., Investigation of extraction and analysis techniques for *Lyngbya wollei* derived Paralytic Shellfish Toxins. *Toxicon* **2012b**, 60, 1148-1158.
134. Onodera, H., Oshima, Y., Watanabe, M.F., Watanabe, M., Bolch, C.J., Blackburn, S., Yasumoto, T., Screening of paralytic shellfish toxins in freshwater cyanobacteria and chemical confirmation of the toxins in cultured *Anabaena circinalis* from Australia, In: Yasumoto, T., Oshima, Y., Fukuyo, Y. (Eds.), Harmful and Toxic Algal Blooms. IOS UNESCO, Paris, **1996**, 563-566.



APPENDIX A  
SUPPORTING INFORMATION FOR CHAPTER 2

### **Analytical Method: DBP Quantification.**

For DBP quantification (trihalomethanes, haloacetamides, halonitromethanes, haloacetonitriles, haloketones, haloacetaldehydes, and iodo-trihalomethanes), chlorinated samples were quenched with ammonium chloride based on a chlorine to ammonium chloride molar ratio of 1:1.3. Aliquots of 100 mL were adjusted to pH <1.0 with concentrated sulfuric acid and spiked with 30 g of sodium sulfate and 5 mL of methyl *tert*-butyl ether (MTBE) in 125 mL amber bottles. The extraction was performed as follows: bottles were shaken for 15 min on a mechanical shaker, allowed to settle for 10-min, then the supernatant was removed into a separate container. This process was repeated total of three times, with a total of 15 mL of MTBE collected as the extract. The extract was then passed through a sodium sulfate column to remove water, and concentrated to a final volume of 200  $\mu$ L under nitrogen. Extracts were then spiked with internal standard (1,2-dibromopropane) for analysis of trihalonitromethanes, haloacetamides, haloacetonitriles, haloketones, iodo-trihalomethanes, and trihaloacetaldehydes using an Agilent 7890 GC coupled to an Agilent 5977A mass spectrometer with electron ionization (Agilent Technologies, Santa Clara, CA) in selected ion monitoring mode with an Rtx-200MS GC column (30 m  $\times$  0.25 mm ID  $\times$  0.25  $\mu$ m film thickness; Restek Corporation, Bellefonte, PA, U.S.A.). Minimum reporting limits were mostly 0.1  $\mu$ g/L for DBPs in this study.

**Table A.1.** GC-MS quantifier ions, qualifier ions, and minimum reporting limits (MRLs) for DBPs quantified in this study.

<b>DBP Class</b>	<b>DBP Name</b>	<b>Abbrev.</b>	<b>Quant. Ion (m/z)</b>	<b>Qual. Ion (m/z)</b>	<b>MRL (µg/L)</b>
THM	Trichloromethane	TCM	83.0	85.0	0.1
THM	Tribromomethane	TBM	173.0	252.0	0.1
THM	Dibromochloromethane	DBCM	129.0	126.9	0.1
THM	Bromodichloromethane	BDCM	83.0	129.0	0.1
HAL	Trichloroacetaldehyde	TCAL	82.0	110.9	0.1
HAL	Bromodichloroacetaldehyde	BDCAL	111.0	83.0, 163.8	0.1
HAL	Dibromochloroacetaldehyde	DBCAL	128.9	127.9	0.1
HAL	Tribromoacetaldehyde	TBAL	172.8	171.8	0.1
HAN	Trichloroacetonitrile	TCAN	108.0	110.0	0.1
HAN	Dichloroacetonitrile	DCAN	74.0	82.0	0.1
HAN	Chloroacetonitrile	CAN	75.0	48.0	0.5
HAN	Bromochloroacetonitrile	BCAN	155.0	74.0	0.1
HAN	Bromoacetonitrile	BAN	118.9	120.9	0.1
HAN	Dibromoacetonitrile	DBAN	117.9	199.0	0.1
HAN	Iodoacetonitrile	IAN	167.0	126.9	0.1
HAN	Bromodichloroacetonitrile	BDCAN	154.0	108.0	0.1
HAN	Dibromochloroacetonitrile	DBCAN	154	152	0.1
HAN	Tribromoacetonitrile	TBAN	197.8	195.8	0.1
HK	1,1-Dichloropropanone	1,1-DCP	83.0	43.0	0.1
HK	Chloropropanone	CP	92.0	43.0	0.1
HK	1,1,1-Trichloropropanone	1,1,1-TCP	43.0	125.0	0.1
HK	1,1-Dibromopropanone	1,1-DBP	215.9	43.0	0.1
HK	1-Bromo-1,1-dichloropropanone	1-B-1,1-DCP	125.0	43.0	0.1
HK	1,3-Dichloropropanone	1,3-DCP	77.0	49.0	0.1
HK	1,1,3-Trichloropropanone	1,1,3-TCP	77.0	83.0	0.1
HK	1,1,3,3-Tetrachloropropanone	1,1,3,3-TeCP	83.0	85.0	0.1
HK	1,1,3,3-Tetrabromopropanone	1,1,3,3-TeBP	200.8	119.9	0.1
HNM	Trichloronitromethane	TCNM	116.9	119.0	0.1
HNM	Dichloronitromethane	DCNM	83.0	85.0	0.1
HNM	Bromochloronitromethane	BCNM	129.0	127.0	0.1
HNM	Dibromonitromethane	DBNM	172.8	171.0	0.1
HNM	Bromodichloronitromethane	BDCNM	163.0	161.0	0.1

HNM	Dibromochloronitromethane	DBCNM	206.8	209.0	0.1
HNM	Tribromonitromethane	TBNM	251.0	253.0	0.5
I-THM	Dichloriodomethane	DCIM	83.0	126.9	0.1
I-THM	Bromochloriodomethane	BCIM	128.9	126.9	0.1
I-THM	Dibromiodomethane	DBIM	172.8	299.7	0.1
I-THM	Chlorodiiodomethane	CDIM	174.9	126.9	0.1
I-THM	Bromodiiodomethane	BDIM	218.8	220.8	0.1
I-THM	Iodoform	TIM	266.8	393.7	0.1
HAM	Chloroacetamide	CAM	93.0	44.0	0.1
HAM	Bromoacetamide	BAM	139.0	137.0, 44.0	0.1
HAM	Dichloroacetamide	DCAM	44.0	127.0	0.25
HAM	Bromochloroacetamide	BCAM	44.0	173.0	0.1
HAM	Trichloroacetamide	TCAM	44.0	82.0	0.1
HAM	Iodoacetamide	IAM	185.0	58.0	0.1
HAM	Dibromoacetamide	DBAM	44.0	217.0	0.1
HAM	Chloroiodoacetamide	CIAM	92.0	219.0	0.1
HAM	Bromodichloroacetamide	BDCAM	44.0	128.0	0.1
HAM	Bromiodoacetamide	BIAM	136.0	138.0	0.5
HAM	Dibromochloroacetamide	DBCAM	44.0	128.0	0.1
HAM	Tribromoacetamide	TBAM	44.0	295.0	0.1
HAM	Diiodoacetamide	DIAM	184.0	311.0	0.1

**Table A.2.** Summary of analytical methods.

<b>Parameter</b>	<b>Method</b>
Dissolved organic carbon	Standard Methods
Salinity	Direct analysis of raw water
Total dissolved nitrogen	Standard Methods
Regulated THMs, Haloacetamides (HAMs), haloacetonitriles (HANs), halonitromethanes (HNMs), haloacetaldehydes (HALs), haloketones (HKs), iodo-trihalomethanes (I-THMs)	Liquid-liquid extraction, GC-MS analysis
SUVA	Standard Methods

**Table A.3.** Names and abbreviations of DBPs quantified, with their known cytotoxicity values (LC<sub>50</sub>). DBPs are ordered from most cytotoxic to least cytotoxic.<sup>46</sup>

<b>DBP</b>	<b>Abbreviation</b>	<b>LC<sub>50</sub> (M)</b>
Diiodoacetamide	DIAM	6.78E-07
Iodoacetamide	IAM	1.42E-06
Bromoacetamide	BAM	1.89E-06
Tribromoacetonitrile	TBAN	2.71E-06
Dibromoacetonitrile	DBAN	2.85E-06
Tribromoacetamide	TBAM	3.14E-06
Bromoacetonitrile	BAN	3.21E-06
Iodoacetonitrile	IAN	3.30E-06
Tribromoacetaldehyde	TBAL	3.58E-06
Bromiodoacetamide	BIAM	3.81E-06
Dibromochloroacetamide	DBCAM	4.75E-06
Dibromochloroacetaldehyde	DBCAL	5.15E-06
Chloriodoacetamide	CIAM	5.97E-06
Dibromonitromethane	DBNM	6.09E-06
Bromochloroacetonitrile	BCAN	8.46E-06
Tribromonitromethane	TBNM	8.57E-06
Bromodichloroacetamide	BDCAM	8.68E-06
Dibromoacetamide	DBAM	1.22E-05
Dibromochloronitromethane	DBCNM	1.32E-05
Bromodichloronitromethane	BDCNM	1.32E-05
Bromochloroacetamide	BCAM	1.71E-05
Bromodichloroacetaldehyde	BDCAL	2.04E-05
Bromochloronitromethane	BCNM	4.05E-05
Dichloroacetonitrile	DCAN	5.73E-05

Triiodomethane	TIM	6.60E-05
Chloroacetonitrile	CAN	6.83E-05
Chloroacetamide	CAM	1.48E-04
Trichloroacetonitrile	TCAN	1.60E-04
Dichloronitromethane	DCNM	3.73E-04
Trichloronitromethane	TCNM	5.36E-04
Trichloroacetaldehyde	TCAL	1.16E-03
Bromodiiodomethane	BDIM	1.40E-03
Dibromoiodomethane	DBIM	1.91E-03
Dichloroacetamide	DCAM	1.92E-03
Trichloroacetamide	TCAM	2.05E-03
Chlorodiiodomethane	CDIM	2.41E-03
Bromochloroiodomethane	BCIM	2.42E-03
Tribromomethane	TBM	3.96E-03
Dichloroiodomethane	DCIM	4.13E-03
Dibromochloromethane	DBCM	5.36E-03
Trichloromethane	TCM	9.62E-03
Bromodichloromethane	BDCM	1.15E-02
Bromodichloroacetonitrile	BDCAN	NA
Dibromochloroacetonitrile	DBCAN	NA
Chloropropanone	CP	NA
1,1-Dichloropropanone	1,1-DCP	NA
1,3-Dichloropropanone	1,3-DCP	NA
1,1-Dibromopropanone	1,1-DBP	NA
1,1,1-Trichloropropanone	1,1,1-TCP	NA
1,1,3-Trichloropropanone	1,1,3-TCP	NA
1-Bromo-1,1-Dichloropropanone	1-B-1,1-DCP	NA

1,1,3,3-Tetrachloropropanone	1,1,3,3-TeCP	NA
1,1,3,3-Tetrabromopropanone	1,1,3,3-TeBP	NA

NA = not available.



**Table A.4.** Names and abbreviations of DBPs quantified, with their known genotoxicity values (MTM). DBPs are ordered from most genotoxic to least genotoxic.<sup>46</sup>

<b>DBP</b>	<b>Abbreviation</b>	<b>MTM (M)</b>
Dibromonitromethane	DBNM	2.62E-05
Tribromoacetamide	TBAM	3.25E-05
Diiodoacetamide	DIAM	3.39E-05
Iodoacetamide	IAM	3.41E-05
Bromoacetamide	BAM	3.68E-05
Bromoacetonitrile	BAN	3.85E-05
Dibromoacetonitrile	DBAN	4.71E-05
Bromodichloronitromethane	BDCNM	6.32E-05
Dibromochloronitromethane	DBCNM	6.32E-05
Dibromochloroacetamide	DBCAM	6.94E-05
Tribromonitromethane	TBNM	6.99E-05
Bromiodoacetamide	BIAM	7.21E-05
Trichloronitromethane	TCNM	9.34E-05
Dibromochloroacetaldehyde	DBCAL	1.44E-04
Bromodichloroacetamide	BDCAM	1.46E-04
Bromochloronitromethane	BCNM	1.65E-04
Chloriodoacetamide	CIAM	3.02E-04
Bromochloroacetonitrile	BCAN	3.24E-04
Tribromoacetaldehyde	TBAL	3.40E-04
Dichloronitromethane	DCNM	4.21E-04
Bromodichloroacetaldehyde	BDCAL	4.70E-04
Bromochloroacetamide	BCAM	5.83E-04
Chloroacetonitrile	CAN	6.01E-04
Dibromoacetamide	DBAM	7.44E-04
Trichloroacetonitrile	TCAN	1.01E-03

Chloroacetamide	CAM	1.38E-03
Dichloroacetonitrile	DCAN	2.75E-03
Chlorodiiodomethane	CDIM	2.95E-03
Trichloroacetamide	TCAM	6.54E-03
Trichloroacetaldehyde	TCAL	NA
Dichloroacetamide	DCAM	NA
Iodoacetonitrile	IAN	NA
Tribromoacetonitrile	TBAN	NA
Dibromochloroacetonitrile	DBCAN	NA
Dibromochloromethane	DBCM	NA
Bromodichloromethane	BDCM	NA
Tribromomethane	TBM	NA
Trichloromethane	TCM	NA
Dichloriodomethane	DCIM	NA
Bromochloriodomethane	BCIM	NA
Dibromiodomethane	DBIM	NA
Bromodiiodomethane	BDIM	NA
Triiodomethane	TIM	NA
1,1-Dichloropropanone	1,1-DCP	NA
Chloropropanone	CP	NA
1,1,1-Trichloropropanone	1,1,1-TCP	NA
1,1-Dibromopropanone	1,1-DBP	NA
1-Bromo-1,1-Dichloropropanone	1-B-1,1-DCP	NA
1,3-Dichloropropanone	1,3-DCP	NA
1,1,3-Trichloropropanone	1,1,3-TCP	NA
1,1,3,3-Tetrachloropropanone	1,1,3,3-TeCP	NA
1,1,3,3-Tetrabromopropanone	1,1,3,3-TeBP	NA

NA = not available

**Table A.5.** Total DBPs identified and quantified in Plant 1 waters ( $\mu\text{g/L}$ ).

<b>DBP Class</b>	<b>DBP</b>	<b>RW</b>	<b>PT</b>	<b>BW</b>	<b>ROP</b>	<b>FW</b>
THM	TCM	<0.1	1.1	1.3	<0.1	<0.1
THM	BDCM	<0.1	0.3	0.3	ND	ND
THM	DBCAM	<0.1	<0.1	<0.1	1.3 $\pm$ 0.33	1.4 $\pm$ 0.36
THM	TBM	<0.1	<0.1	<0.1	23.7 $\pm$ 7.05	21.2 $\pm$ 5.34
HAM	CAM	<0.1	<0.1	<0.1	0.5 $\pm$ 0.09	28.5 $\pm$ 8.76
HAM	BAM	<0.1	<0.1	<0.1	ND	<0.1
HAM	IAM	ND	ND	ND	ND	ND
HAM	DCAM	<0.1	<0.1	<0.1	0.3 $\pm$ 0.01	0.3 $\pm$ 0.02
HAM	BCAM	<0.1	0.7	0.1	0.2 $\pm$ 0.00	0.2 $\pm$ 0.01
HAM	CIAM	ND	ND	ND	ND	ND
HAM	DBAM	0.2	<0.1	2.9	0.5 $\pm$ 0.01	0.7 $\pm$ 0.11
HAM	BIAM	ND	ND	ND	ND	ND
HAM	DIAM	<0.1	<0.1	1.3	0.5 $\pm$ 0.00	0.6 $\pm$ 0.00
HAM	TCAM	<0.1	<0.1	<0.1	0.1 $\pm$ 0.00	0.2 $\pm$ 0.02
HAM	BDCAM	<0.1	<0.1	<0.1	0.3 $\pm$ 0.02	0.3 $\pm$ 0.00
HAM	DBCAM	ND	ND	ND	ND	ND
HAM	TBAM	ND	ND	ND	ND	ND
HAN	CAN	<0.1	<0.1	<0.1	0.6 $\pm$ 0.00	2.8 $\pm$ 0.34
HAN	BAN	<0.1	<0.1	0.6	0.6 $\pm$ 0.00	0.9 $\pm$ 0.07
HAN	IAN	<0.1	<0.1	<0.1	ND	<0.1
HAN	DCAN	<0.1	<0.1	<0.1	<0.1	0.3 $\pm$ 0.06
HAN	BCAN	<0.1	<0.1	<0.1	0.2 $\pm$ 0.00	0.6 $\pm$ 0.05
HAN	DBAN	<0.1	<0.1	<0.1	0.2 $\pm$ 0.04	0.2 $\pm$ 0.01
HAN	TCAN	<0.1	<0.1	<0.1	0.1 $\pm$ 0.02	0.3 $\pm$ 0.07
HAN	BDCAN	ND	ND	ND	ND	ND

HAN	DBCAN	ND	ND	ND	ND	0.4±0.00
HAN	TBAN	ND	ND	ND	ND	0.5±0.00
HNM	DCNM	<0.1	<0.1	<0.1	0.2±0.00	4.5±1.24
HNM	DBNM	<0.1	<0.1	<0.1	0.3±0.00	0.3±0.00
HNM	BCNM	<0.1	<0.1	<0.1	0.3±0.00	0.3±0.01
HNM	TCNM	ND	ND	ND	ND	0.2±0.01
HNM	BDCNM	ND	ND	ND	0.1±0.00	0.2±0.01
HNM	DBCNM	ND	ND	ND	0.5±0.01	0.5±0.00
HNM	TBNM	ND	ND	ND	<0.1	<0.1
HK	CP	ND	<0.1	ND	ND	1.8±0.42
HK	1,1-DCP	1.4	<0.1	2.4	1.0±1.05	1.7±0.69
HK	1,3-DCP	<0.1	0.4	0.2	0.4±0.00	3.5±1.38
HK	1,1-DBP	<0.1	<0.1	<0.1	ND	ND
HK	1,1,1-TCP	<0.1	<0.1	<0.1	0.2±0.01	0.3±0.06
HK	1,1,3-TCP	<0.1	<0.1	<0.1	0.1±0.00	0.2±0.05
HK	1-B-1,1-DCP	0.3	<0.1	<0.1	0.3±0.01	6.0±1.40
HK	1,1,3,3-TeCP	<0.1	<0.1	0.01	0.1±0.00	0.8±0.19
HK	1,1,3,3-TeBP	<0.1	<0.1	<0.1	0.1±0.00	0.4±0.10
HAL	TCAL	<0.1	<0.1	<0.1	0.1±0.01	0.1±0.03
HAL	BDCAL	<0.1	<0.1	<0.1	0.2±0.00	14.3±4.80
HAL	DBCAL	<0.1	<0.1	<0.1	ND	0.6±0.07
HAL	TBAL	<0.1	<0.1	0.2	0.3±0.00	0.6±0.10
I-THM	DCIM	<0.1	<0.1	<0.1	0.4±0.00	2.2±0.48

I-THM	BCIM	<0.1	<0.1	<0.1	0.3±0.00	0.3±0.00
I-THM	DBIM	<0.1	0.4	0.2	<0.1	<0.1
I-THM	CDIM	<0.1	<0.1	<0.1	ND	0.5±0.00
I-THM	BDIM	<0.1	<0.1	<0.1	0.4±0.00	0.4±0.00
I-THM	TIM	<0.1	<0.1	<0.1	0.5±0.00	0.5±0.00

ND = not detected

**Table A.6.** Plant 1 Calculated Toxicity Index (CTI) values for cytotoxicity.

<b>DBP Class</b>	<b>DBP</b>	<b>RW</b>	<b>PT</b>	<b>BW</b>	<b>ROP</b>	<b>FW</b>
THM	TCM	0	9.33E-01	1.09E+00	0	0
THM	BDCM	0	1.60E-01	1.48E-01	0	0
THM	DBCM	0	0	0	1.16E+00	1.25E+00
THM	TBM	0	0	0	2.37E+01	2.12E+01
HAM	CAM	0	0	0	3.61E+01	2.06E+03
HAM	BAM	0	0	0	0	0
HAM	DCAM	0	0	0	1.22E+00	1.22E+00
HAM	BCAM	0	2.19E+02	4.46E+01	6.78E+01	6.78E+01
HAM	TCAM	0	0	0	3.00E-01	6.01E-01
HAM	IAM	0	0	0	0	0
HAM	DBAM	6.06E+01	0	1.11E+03	1.89E+02	2.65E+02
HAM	CIAM	0	0	0	0	0
HAM	BDCAM	0	0	0	1.67E+02	1.67E+02
HAM	BIAM	0	0	0	0	0
HAM	DBCAM	0	0	0	0	0
HAM	TBAM	0	0	0	0	0
HAM	DIAM	0	0	6.07E+03	2.37E+03	2.85E+03
HAN	TCAN	0	0	0	4.33E+00	1.30E+01
HAN	DCAN	0	0	0	0	4.76E+01
HAN	CAN	0	0	0	1.16E+02	5.43E+02
HAN	BCAN	0	0	0	1.53E+02	4.59E+02
HAN	BAN	0	0	1.47E+03	1.56E+03	2.34E+03
HAN	DBAN	0	0	0	3.53E+02	3.53E+02
HAN	IAN	NA	NA	NA	NA	NA
HAN	TBAN	NA	NA	NA	NA	NA

HNM	TCNM	0	0	0	0	2.27E+00
HNM	DCNM	0	0	0	4.13E+00	9.29E+01
HNM	BCNM	0	0	0	4.25E+01	4.25E+01
HNM	DBNM	0	0	0	2.25E+02	2.25E+02
HNM	BDCNM	0	0	0	3.63E+01	7.26E+01
HNM	DBCNM	0	0	0	1.50E+02	1.50E+02
HNM	TBNM	0	0	0	0	0
HK	1,1-DCP	NA	NA	NA	NA	NA
HK	CP	NA	NA	NA	NA	NA
HK	1,1,1-TCP	NA	NA	NA	NA	NA
HK	1,1-DBP	NA	NA	NA	NA	NA
HK	1-B-1,1-DCP	NA	NA	NA	NA	NA
HK	1,3-DCP	NA	NA	NA	NA	NA
HK	1,1,3-TCP	NA	NA	NA	NA	NA
HK	1,1,3,3-TeCP	NA	NA	NA	NA	NA
HK	1,1,3,3-TeBP	NA	NA	NA	NA	NA
HAL	TCAL	0	0	0	5.85E-01	5.85E-01
HAL	BDCAL	0	0	0	5.11E+01	3.65E+03
HAL	DBCAL	0	0	0	0	4.93E+02
HAL	TBAL	0	0	1.85E+02	2.98E+02	5.97E+02
HAL	CAL	0	0	0	0	0
HAL	DCAL	0	0	0	0	0
HAL	BAL	0	0	0	0	0
HAL	BCAL	0	0	0	0	0

HAL	DBAL	0	0	0	0	0
I-THM	DCIM	0	0	0	4.59E-01	2.53E+00
I-THM	BCIM	0	0	0	4.86E-01	4.86E-01
I-THM	DBIM	0	7.39E-01	3.25E-01	0	0
I-THM	CDIM	0	0	0	0	6.86E-01
I-THM	BDIM	0	0	0	8.24E-01	8.24E-01
I-THM	TIM	0	0	0	1.92E+01	1.92E+01

NA = not applicable due to a lack of cytotoxicity index values.



**Table A.7.** Plant 1 Calculated Toxicity Index (CTI) values for genotoxicity.

<b>DBP Class</b>	<b>DBP</b>	<b>RW</b>	<b>PT</b>	<b>BW</b>	<b>ROP</b>	<b>FW</b>
THM	TCM	NA	NA	NA	NA	NA
THM	BDCM	NA	NA	NA	NA	NA
THM	DBCAM	NA	NA	NA	NA	NA
THM	TBM	NA	NA	NA	NA	NA
HAM	CAM	0	0	0	3.87E+00	2.21E+02
HAM	BAM	0	0	0	0	0
HAM	DCAM	NA	NA	NA	NA	NA
HAM	BCAM	0	6.43E+00	1.31E+00	1.99E+00	1.99E+00
HAM	TCAM	0	0	0	9.42E-02	1.88E-01
HAM	IAM	0	0	0	0	0
HAM	DBAM	9.93E-01	0	1.82E+01	3.10E+00	4.34E+00
HAM	CIAM	0	0	0	0	0
HAM	BDCAM	0	0	0	9.93E+00	9.93E+00
HAM	BIAM	0	0	0	0	0
HAM	DBCAM	0	0	0	0	0
HAM	TBAM	0	0	0	0	0
HAM	DIAM	0	0	1.21E+02	4.74E+01	5.69E+01
HAN	TCAN	0	0	0	6.86E-01	2.06E+00
HAN	DCAN	0	0	0	0	9.92E-01
HAN	CAN	0	0	0	1.32E+01	6.17E+01
HAN	BCAN	0	0	0	4.00E+00	1.20E+01
HAN	BAN	0	0	1.23E+02	1.30E+02	1.95E+02
HAN	DBAN	0	0	0	2.14E+01	2.14E+01
HAN	IAN	NA	NA	NA	NA	NA

HAN	TBAN	NA	NA	NA	NA	NA
HNM	TCNM	0	0	0	0	1.30E+01
HNM	DCNM	0	0	0	3.66E+00	8.23E+01
HNM	BCNM	0	0	0	1.04E+01	1.04E+01
HNM	DBNM	0	0	0	5.23E+01	5.23E+01
HNM	BDCNM	0	0	0	7.58E+00	1.52E+01
HNM	DBCNM	0	0	0	3.12E+01	3.12E+01
HNM	TBNM	0	0	0	0	0
HK	1,1-DCP	NA	NA	NA	NA	NA
HK	CP	NA	NA	NA	NA	NA
HK	1,1,1-TCP	NA	NA	NA	NA	NA
HK	1,1-DBP	NA	NA	NA	NA	NA
HK	1-B-1,1-DCP	NA	NA	NA	NA	NA
HK	1,3-DCP	NA	NA	NA	NA	NA
HK	1,1,3-TCP	NA	NA	NA	NA	NA
HK	1,1,3,3-TeCP	NA	NA	NA	NA	NA
HK	1,1,3,3-TeBP	NA	NA	NA	NA	NA
HAL	TCAL	0	0	0	0	0
HAL	BDCAL	0	0	0	2.22E+00	1.59E+02
HAL	DBCAL	0	0	0	0	1.76E+01
HAL	TBAL	0	0	1.95E+00	3.14E+00	6.29E+00
HAL	CAL	0	0	0	0	0
HAL	DCAL	0	0	0	0	0
HAL	BAL	0	0	0	0	0

HAL	BCAL	0	0	0	0	0
HAL	DBAL	0	0	0	0	0
I-THM	DCIM	NA	NA	NA	NA	NA
I-THM	BCIM	NA	NA	NA	NA	NA
I-THM	DBIM	NA	NA	NA	NA	NA
I-THM	CDIM	0	0	0	0	5.61E-01
I-THM	BDIM	NA	NA	NA	NA	NA
I-THM	TIM	NA	NA	NA	NA	NA

NA = not applicable due to a lack of genotoxicity index values.

**Table A.8.** DBPs quantified and identified in Plant 2 waters ( $\mu\text{g/L}$ ).

<b>DBP Class</b>	<b>DBP</b>	<b>RW</b>	<b>RW + Cl<sub>2</sub></b>	<b>BW</b>	<b>BW + Cl<sub>2</sub></b>
THM	TCM	0.3	0.8	0.6	0.6
THM	BDCM	ND	<0.1	<0.1	0.1
THM	DBCM	0.1	<0.1	ND	0.8
THM	TBM	1.4	<0.1	ND	ND
HAM	CAM	ND	<0.1	ND	ND
HAM	BAM	0.1	ND	ND	ND
HAM	IAM	ND	0.6	ND	1.1
HAM	DCAM	ND	0.5	ND	2.5
HAM	BCAM	ND	ND	ND	<0.1
HAM	CIAM	ND	ND	ND	ND
HAM	DBAM	0.1	<0.1	ND	1.7
HAM	BIAM	ND	ND	ND	ND
HAM	DIAM	ND	ND	ND	<0.1
HAM	TCAM	ND	<0.1	ND	<0.1
HAM	BDCAM	0.5	ND	ND	<0.1
HAM	DBCAM	<0.1	0.2	0.2	<0.1
HAM	TBAM	ND	ND	<0.1	0.3
HAN	CAN	ND	<0.1	ND	ND
HAN	BAN	ND	ND	ND	ND
HAN	IAN	ND	ND	ND	<0.1
HAN	DCAN	ND	<0.1	ND	ND
HAN	BCAN	ND	<0.1	ND	0.1
HAN	DBAN	0.6	<0.1	ND	3.2
HAN	TCAN	ND	<0.1	ND	<0.1
HAN	BDCAN	<0.1	0.17	ND	ND

HAN	DBCAN	<0.1	0.24	ND	ND
HAN	TBAN	0.2	ND	0.6	ND
HNM	DCNM	ND	<0.1	ND	<0.1
HNM	DBNM	<0.1	ND	ND	0.2
HNM	BCNM	ND	<0.1	ND	0.1
HNM	TCNM	ND	<0.1	ND	0.1
HNM	BDCNM	0.2	1.1	ND	ND
HNM	DBCNM	<0.1	3.0	ND	ND
HNM	TBNM	0.9	2.8	3.7	0.4
HK	CP	ND	<0.1	ND	<0.1
HK	1,1-DCP	ND	<0.1	<0.1	0.10
HK	1,3-DCP	0.2	<0.1	ND	ND
HK	1,1-DBP	ND	<0.1	ND	0.30
HK	1,1,1-TCP	ND	<0.1	ND	0.13
HK	1,1,3-TCP	ND	ND	ND	<0.1
HK	1-B-1,1-DCP	0.5	0.2	ND	ND
HK	1,1,3,3-TeCP	<0.1	ND	ND	ND
HK	1,1,3,3-TeBP	ND	ND	ND	ND
HAL	TCAL	ND	<0.1	ND	0.2
HAL	BDCAL	ND	ND	ND	0.3
HAL	DBCAL	ND	ND	ND	0.1
HAL	TBAL	<0.1	ND	ND	0.9
I-THM	DCIM	ND	<0.1	ND	<0.1
I-THM	BCIM	ND	<0.1	ND	<0.1
I-THM	DBIM	ND	<0.1	ND	0.3
I-THM	CDIM	ND	<0.1	ND	<0.1
I-THM	BDIM	ND	ND	<0.1	ND

I-THM	TIM	0.9	ND	ND	0.2
-------	-----	-----	----	----	-----

ND = not detected

**Table A.9.** Plant 2 Calculated Toxicity Index (CTI) values for cytotoxicity.

<b>DBP Class</b>	<b>DBP</b>	<b>RW</b>	<b>RW + Cl2</b>	<b>BW</b>	<b>BW + Cl2</b>
THM	TCM	2.55E-01	6.55E-01	4.83E-01	4.90E-01
THM	BDCM	0	1.73E-02	2.99E-03	5.10E-02
THM	DBCM	1.11E-01	1.51E-02	0	7.07E-01
THM	TBM	1.39E+00	6.39E-02	0	0
HAM	CAM	0	4.08E+00	0	0
HAM	BAM	3.96E+02	0	0	0
HAM	DCAM	0	2.16E+00	0	1.01E+01
HAM	BCAM	0	0	0	1.50E+01
HAM	TCAM	0	1.25E-01	0	2.21E-01
HAM	IAM	0	2.19E+03	0	4.16E+03
HAM	DBAM	4.05E+01	2.48E+01	0	6.58E+02
HAM	CIAM	0	0	0	0
HAM	BDCAM	2.79E+02	0	0	5.54E+00
HAM	BIAM	0	0	0	0
HAM	DBCAM	2.45E+00	1.99E+02	1.24E+02	6.59E+01
HAM	TBAM	0	0	1.07E+01	3.38E+02
HAM	DIAM	0	0	0	1.26E+02
HAN	TCAN	0	2.44E-01	0	3.20E+00
HAN	DCAN	0	2.84E+00	0	0
HAN	CAN	0	1.19E+01	0	0
HAN	BCAN	0	1.51E+01	0	7.90E+01
HAN	BAN	0	0	0	0
HAN	DBAN	1.02E+03	1.18E+01	0	5.72E+03
HAN	IAN	NA	NA	NA	NA
HAN	TBAN	NA	NA	NA	NA

HNM	TCNM	0	2.65E-01	0	1.33E+00
HNM	DCNM	0	5.02E-01	0	9.11E-01
HNM	BCNM	0	1.19E+00	0	2.01E+01
HNM	DBNM	3.18E+01	0	0	1.13E+02
HNM	BDCNM	8.08E+01	4.02E+02	0	0
HNM	DBCNM	7.34E+00	9.03E+02	0	0
HNM	TBNM	3.57E+02	1.11E+03	1.46E+03	1.73E+02
HK	1,1-DCP	NA	NA	NA	NA
HK	CP	NA	NA	NA	NA
HK	1,1,1-TCP	NA	NA	NA	NA
HK	1,1-DBP	NA	NA	NA	NA
HK	1-B-1,1-DCP	NA	NA	NA	NA
HK	1,3-DCP	NA	NA	NA	NA
HK	1,1,3-TCP	NA	NA	NA	NA
HK	1,1,3,3-TeCP	NA	NA	NA	NA
HK	1,1,3,3-TeBP	NA	NA	NA	NA
HAL	TCAL	0	8.26E-02	0	1.22E+00
HAL	BDCAL	0	0	0	6.45E+01
HAL	DBCAL	0	0	0	7.96E+01
HAL	TBAL	5.27E+01	0	0	9.05E+02
HAL	CAL	0	0	0	0
HAL	DCAL	0	0	0	0
HAL	BAL	0	0	0	0
HAL	BCAL	0	0	0	0
HAL	DBAL	0	0	0	0



I-THM	DCIM	0	2.29E-02	0	3.09E-02
I-THM	BCIM	0	5.43E-02	0	9.18E-02
I-THM	DBIM	0	3.59E-02	0	5.03E-01
I-THM	CDIM	0	1.24E-02	0	5.73E-03
I-THM	BDIM	0	0	7.25E-02	0
I-THM	TIM	3.28E+01	0	0	6.56E+00

NA = not applicable due to a lack of cytotoxicity index values.

**Table A.10.** Plant 2 Calculated Toxicity Index (CTI) values for genotoxicity.

<b>DBP Class</b>	<b>DBP</b>	<b>RW</b>	<b>RW + CI2</b>	<b>BW</b>	<b>BW + CI2</b>
THM	TCM	NA	NA	NA	NA
THM	BDCM	NA	NA	NA	NA
THM	DBCM	NA	NA	NA	NA
THM	TBM	NA	NA	NA	NA
HAM	CAM	0	4.38E-01	0	0
HAM	BAM	2.03E+01	0	0	0
HAM	DCAM	0	0	0	0
HAM	BCAM	0	0	0	4.39E-01
HAM	TCAM	0	3.93E-02	0	6.91E-02
HAM	IAM	0	9.12E+01	0	1.73E+02
HAM	DBAM	6.63E-01	4.07E-01	0	1.08E+01
HAM	CIAM	0	0	0	0
HAM	BDCAM	1.66E+01	0	0	3.29E-01
HAM	BIAM	0	0	0	0
HAM	DBCAM	1.67E-01	1.36E+01	8.50E+00	4.51E+00
HAM	TBAM	0	0	1.04E+00	3.27E+01
HAM	DIAM	0	0	0	2.52E+00
HAN	TCAN	0	3.87E-02	0	5.07E-01
HAN	DCAN	0	5.92E-02	0	0
HAN	CAN	0	1.36E+00	0	0
HAN	BCAN	0	3.95E-01	0	2.06E+00
HAN	BAN	0	0	0	0
HAN	DBAN	6.18E+01	7.13E-01	0	3.46E+02
HAN	IAN	NA	NA	NA	NA
HAN	TBAN	NA	NA	NA	NA

HNM	TCNM	0	1.52E+00	0	7.65E+00
HNM	DCNM	0	4.45E-01	0	8.07E-01
HNM	BCNM	0	2.93E-01	0	4.93E+00
HNM	DBNM	7.40E+00	0	0	2.62E+01
HNM	BDCNM	1.69E+01	8.40E+01	0	0
HNM	DBCNM	1.53E+00	1.89E+02	0	0
HNM	TBNM	4.37E+01	1.36E+02	1.79E+02	2.12E+01
HK	1,1-DCP	NA	NA	NA	NA
HK	CP	NA	NA	NA	NA
HK	1,1,1-TCP	NA	NA	NA	NA
HK	1,1-DBP	NA	NA	NA	NA
HK	1-B-1,1-DCP	NA	NA	NA	NA
HK	1,3-DCP	NA	NA	NA	NA
HK	1,1,3-TCP	NA	NA	NA	NA
HK	1,1,3,3-TeCP	NA	NA	NA	NA
HK	1,1,3,3-TeBP	NA	NA	NA	NA
HAL	TCAL	0	0	0	0
HAL	BDCAL	0	0	0	2.80E+00
HAL	DBCAL	0	0	0	2.85E+00
HAL	TBAL	5.55E-01	0	0	9.53E+00
HAL	CAL	0	0	0	0
HAL	DCAL	0	0	0	0
HAL	BAL	0	0	0	0
HAL	BCAL	0	0	0	0
HAL	DBAL	0	0	0	0

I-THM	DCIM	NA	NA	NA	NA
I-THM	BCIM	NA	NA	NA	NA
I-THM	DBIM	NA	NA	NA	NA
I-THM	CDIM	0	1.01E-02	0	4.68E-03
I-THM	BDIM	NA	NA	NA	NA
I-THM	TIM	NA	NA	NA	NA

NA = not applicable due to the lack of genotoxicity index values.

**Table A.11.** DBPs quantified and identified in Plant 3 ( $\mu\text{g/L}$ ).

<b>DBP Class</b>	<b>DBP</b>	<b>RW</b>	<b>RW + Cl<sub>2</sub></b>	<b>BW</b>	<b>BW + Cl<sub>2</sub></b>	<b>FW</b>
THM	TCM	0.35	3.3	<0.1	0.8	0.5±0.01
THM	BDCM	ND	8	ND	ND	<0.1
THM	DBCAM	<0.1	<0.1	<0.1	0.3	1.4±0.03
THM	TBM	ND	<0.1	ND	<0.1	0.8±0.03
HAM	CAM	ND	ND	ND	ND	ND
HAM	BAM	ND	ND	ND	ND	ND
HAM	IAM	ND	ND	ND	ND	ND
HAM	DCAM	ND	ND	ND	ND	ND
HAM	BCAM	ND	ND	ND	ND	ND
HAM	CIAM	ND	ND	ND	<0.1	ND
HAM	DBAM	ND	ND	ND	ND	ND
HAM	BIAM	ND	ND	ND	<0.1	<0.1
HAM	DIAM	ND	ND	ND	ND	ND
HAM	TCAM	ND	ND	ND	ND	ND
HAM	BDCAM	ND	ND	ND	<0.1	ND
HAM	DBCAM	ND	ND	ND	ND	ND
HAM	TBAM	ND	ND	ND	ND	ND
HAN	CAN	ND	<0.1	ND	<0.1	1.4±0.02
HAN	BAN	ND	ND	ND	2.2	0.7±0.00
HAN	IAN	ND	ND	ND	ND	ND
HAN	DCAN	ND	9.6	ND	ND	0.2±0.02
HAN	BCAN	ND	2.3	ND	ND	0.4±0.02
HAN	DBAN	ND	ND	ND	<0.1	0.5±0.02
HAN	TCAN	<0.1	<0.1	<0.1	<0.1	0.3±0.00
HAN	BDCAN	ND	ND	ND	ND	ND

HAN	DBCAN	ND	ND	ND	ND	<0.1
HAN	TBAN	ND	ND	ND	ND	0.2±0.01
HNM	DCNM	ND	7.8	ND	ND	<0.1
HNM	DBNM	ND	ND	ND	ND	0.2±0.00
HNM	BCNM	ND	ND	ND	2.2	0.4±0.02
HNM	TCNM	ND	<0.1	ND	<0.1	0.3±0.02
HNM	BDCNM	ND	ND	ND	ND	0.2±0.00
HNM	DBCNM	ND	ND	ND	ND	0.4±0.00
HNM	TBNM	ND	ND	ND	ND	ND
HK	CP	ND	1.9	ND	6.9	0.9±0.01
HK	1,1-DCP	ND	3.1	ND	ND	0.3±0.00
HK	1,3-DCP	ND	ND	ND	<0.1	ND
HK	1,1-DBP	ND	ND	ND	ND	0.2±0.00
HK	1,1,1-TCP	ND	1	ND	<0.1	0.2±0.00
HK	1,1,3-TCP	ND	ND	ND	ND	ND
HK	1-B-1,1-DCP	ND	ND	<0.1	<0.1	0.1±0.00
HK	1,1,3,3-TeCP	ND	ND	<0.1	ND	<0.1
HK	1,1,3,3-TeBP	ND	ND	ND	ND	4.3±0.03
HAL	TCAL	ND	ND	ND	<0.1	<0.1
HAL	BDCAL	ND	ND	ND	ND	0.2±0.02
HAL	DBCAL	ND	ND	ND	ND	0.3±0.00
HAL	TBAL	ND	0.4	ND	ND	0.8±0.00
I-THM	DCIM	ND	<0.1	ND	<0.1	0.2±0.00
I-THM	BCIM	ND	2	ND	<0.1	ND
I-THM	DBIM	ND	ND	ND	<0.1	0.4±0.00

I-THM	CDIM	ND	ND	ND	ND	ND
I-THM	BDIM	ND	ND	ND	ND	ND
I-THM	TIM	ND	ND	ND	ND	ND

ND = not detected

**Table A.12.** Plant 3 Calculated Toxicity Index (CTI) values for cytotoxicity.

<b>DBP Class</b>	<b>DBP</b>	<b>RW</b>	<b>RW + CI2</b>	<b>BW</b>	<b>BW + CI2</b>	<b>FW</b>
THM	TCM	3.05E-01	2.87E+00	0	6.96E-01	0
THM	BDCM	0	4.25E+00	0	0	0
THM	DBCM	0	0	0	2.69E-01	0
THM	TBM	0	0	0	0	0
HAM	CAM	0	0	0	0	0
HAM	BAM	0	0	0	0	0
HAM	DCAM	0	0	0	0	0
HAM	BCAM	0	0	0	0	0
HAM	TCAM	0	0	0	0	0
HAM	IAM	0	0	0	0	0
HAM	DBAM	0	0	0	0	0
HAM	CIAM	0	0	0	0	0
HAM	BDCAM	0	0	0	0	0
HAM	BIAM	0	0	0	0	0
HAM	DBCAM	0	0	0	0	0
HAM	TBAM	0	0	0	0	0
HAM	DIAM	0	0	0	0	0
HAN	TCAN	0	0	0	0	1.30E+01
HAN	DCAN	0	1.52E+03	0	0	3.17E+01
HAN	CAN	0	0	0	0	2.71E+02
HAN	BCAN	0	1.76E+03	0	0	3.06E+02
HAN	BAN	0	0	0	5.71E+03	1.82E+03
HAN	DBAN	0	0	0	0	8.82E+02
HAN	IAN	NA	NA	NA	NA	NA
HAN	TBAN	NA	NA	NA	NA	NA



HNM	TCNM	0	0	0	0	3.40E+00
HNM	DCNM	0	1.61E+02	0	0	0
HNM	BCNM	0	0	0	3.12E+02	5.66E+01
HNM	DBNM	0	0	0	0	1.50E+02
HNM	BDCNM	0	0	0	0	7.26E+01
HNM	DBCNM	0	0	0	0	1.20E+02
HNM	TBNM	0	0	0	0	0
HK	1,1-DCP	NA	NA	NA	NA	NA
HK	CP	NA	NA	NA	NA	NA
HK	1,1,1-TCP	NA	NA	NA	NA	NA
HK	1,1-DBP	NA	NA	NA	NA	NA
HK	1-B-1,1-DCP	NA	NA	NA	NA	NA
HK	1,3-DCP	NA	NA	NA	NA	NA
HK	1,1,3-TCP	NA	NA	NA	NA	NA
HK	1,1,3,3-TeCP	NA	NA	NA	NA	NA
HK	1,1,3,3-TeBP	NA	NA	NA	NA	NA
HAL	TCAL	0	0	0	0	0
HAL	BDCAL	0	0	0	0	5.11E+01
HAL	DBCAL	0	0	0	0	2.47E+02
HAL	TBAL	0	3.98E+02	0	0	7.96E+02
HAL	CAL	0	0	0	0	0
HAL	DCAL	0	0	0	0	0
HAL	BAL	0	0	0	0	0
HAL	BCAL	0	0	0	0	0

HAL	DBAL	0	0	0	0	0
I-THM	DCIM	0	0	0	0	0
I-THM	BCIM	0	3.24E+00	0	0	0
I-THM	DBIM	0	0	0	0	6.99E-01
I-THM	CDIM	0	0	0	0	0
I-THM	BDIM	0	0	0	0	0
I-THM	TIM	0	0	0	0	0

NA = not applicable due to a lack of cytotoxicity index values.

**Table A.13.** Plant 3 Calculated Toxicity Index (CTI) values for genotoxicity.

<b>DBP Class</b>	<b>DBP</b>	<b>RW</b>	<b>RW + CI2</b>	<b>BW</b>	<b>BW + CI2</b>	<b>FW</b>
THM	TCM	NA	NA	NA	NA	NA
THM	BDCM	NA	NA	NA	NA	NA
THM	DBCM	NA	NA	NA	NA	NA
THM	TBM	NA	NA	NA	NA	NA
HAM	CAM	0	0	0	0	0
HAM	BAM	0	0	0	0	0
HAM	DCAM	0	0	0	0	0
HAM	BCAM	0	0	0	0	0
HAM	TCAM	0	0	0	0	0
HAM	IAM	0	0	0	0	0
HAM	DBAM	0	0	0	0	0
HAM	CIAM	0	0	0	0	0
HAM	BDCAM	0	0	0	0	0
HAM	BIAM	0	0	0	0	0
HAM	DBCAM	0	0	0	0	0
HAM	TBAM	0	0	0	0	0
HAM	DIAM	0	0	0	0	0
HAN	TCAN	0	0	0	0	2.06E+00
HAN	DCAN	0	3.18E+01	0	0	6.62E-01
HAN	CAN	0	0	0	0	3.09E+01
HAN	BCAN	0	4.60E+01	0	0	8.00E+00
HAN	BAN	0	0	0	4.76E+02	1.52E+02
HAN	DBAN	0	0	0	0	5.34E+01
HAN	IAN	NA	NA	NA	NA	NA

HAN	TBAN	NA	NA	NA	NA	NA
HNM	TCNM	0	0	0	0	1.95E+01
HNM	DCNM	0	1.43E+02	0	0	0
HNM	BCNM	0	0	0	7.65E+01	1.39E+01
HNM	DBNM	0	0	0	0	3.49E+01
HNM	BDCNM	0	0	0	0	1.52E+01
HNM	DBCNM	0	0	0	0	2.50E+01
HNM	TBNM	0	0	0	0	0
HK	1,1-DCP	NA	NA	NA	NA	NA
HK	CP	NA	NA	NA	NA	NA
HK	1,1,1-TCP	NA	NA	NA	NA	NA
HK	1,1-DBP	NA	NA	NA	NA	NA
HK	1-B-1,1-DCP	NA	NA	NA	NA	NA
HK	1,3-DCP	NA	NA	NA	NA	NA
HK	1,1,3-TCP	NA	NA	NA	NA	NA
HK	1,1,3,3-TeCP	NA	NA	NA	NA	NA
HK	1,1,3,3-TeBP	NA	NA	NA	NA	NA
HAL	TCAL	0	0	0	0	0
HAL	BDCAL	0	0	0	0	2.22E+00
HAL	DBCAL	0	0	0	0	8.82E+00
HAL	TBAL	0	4.19E+00	0	0	8.38E+00
HAL	CAL	0	0	0	0	0
HAL	DCAL	0	0	0	0	0
HAL	BAL	0	0	0	0	0
HAL	BCAL	0	0	0	0	0

HAL	DBAL	0	0	0	0	0
I-THM	DCIM	NA	NA	NA	NA	NA
I-THM	BCIM	NA	NA	NA	NA	NA
I-THM	DBIM	NA	NA	NA	NA	NA
I-THM	CDIM	0	0	0	0	0
I-THM	BDIM	NA	NA	NA	NA	NA
I-THM	TIM	NA	NA	NA	NA	NA

NA = not applicable due to a lack of genotoxicity index values.

APPENDIX B  
SUPPORTING INFORMATION FOR CHAPTER 3

**Table B.1.** UHPLC Parameters.

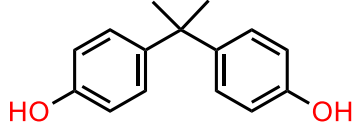
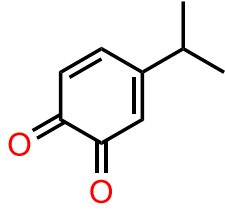
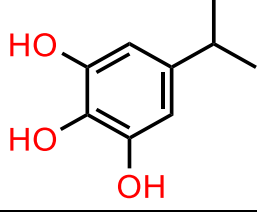
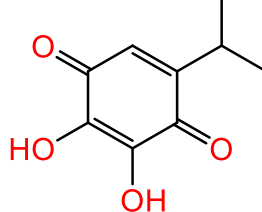
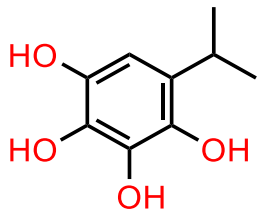
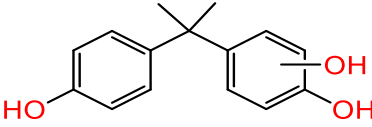
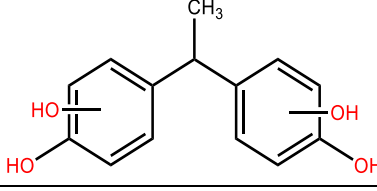
Parameter	Value	
Instrument	1290 Infinity II UHPLC Binary Pump	
Mobile Phase	Positive	A) 0.1% formic acid, 5 mM ammonium acetate in water  B) 0.1% formic acid, 5 mM ammonium acetate in methanol
	Negative	A) 0.02% ammonium hydroxide in water  B) 0.02% ammonium hydroxide in methanol
Gradient	Time (min)	%B
	0	5
	1	5
	10	95
	12	95
	12.1	5
Flow rate	0.35 mL/min	
Column	Agilent InfinityLab Poroshell 120 EC-C18 column (2.1 x 50 mm, 1.9 $\mu$ m)	
Temperature	30 °C	
Injection Volume	10 $\mu$ L	

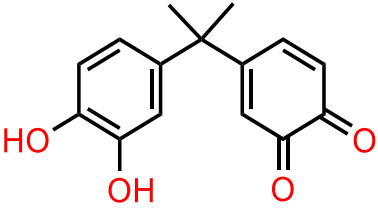
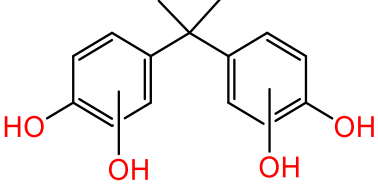
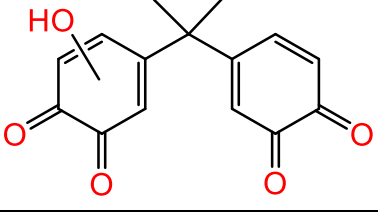
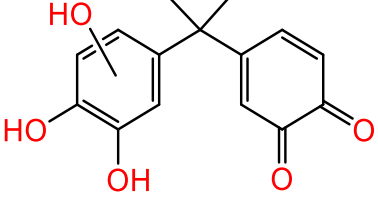

**Table B.2.** Q-TOF LC-MS Parameters.

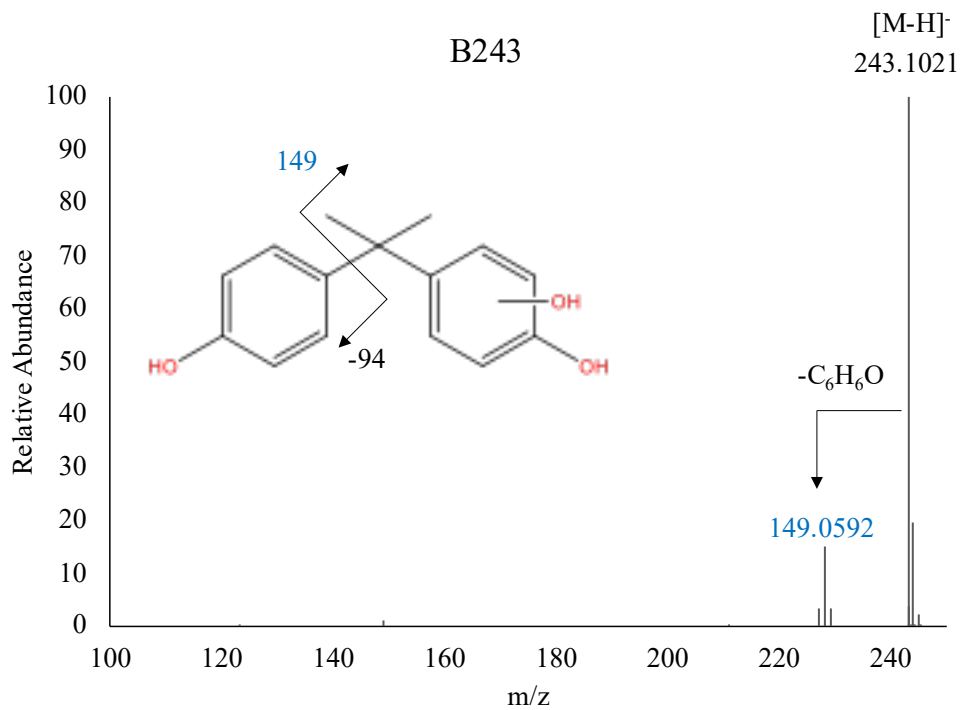
Parameter	Value
Instrument	6545 LC/Q-TOF
MS1 mass range	100-3000 m/z
MS2 mass range	50-3000 m/z
MS1 acquisition rate	4.5 spectra/s
MS2 acquisition rate	1 spectra/s
Collision energy	30 eV
Dry gas temperature	300 °C
Drying gas flow rate	12 l/min
Sheath gas temperature	375 °C
Sheath gas flow rate	12 l/min
Nebulizer gas	35 psi
Skimmer voltage	40 V
Octopole RF	750 V
Fragmentor voltage	110 V
Capillary voltage	4 kV



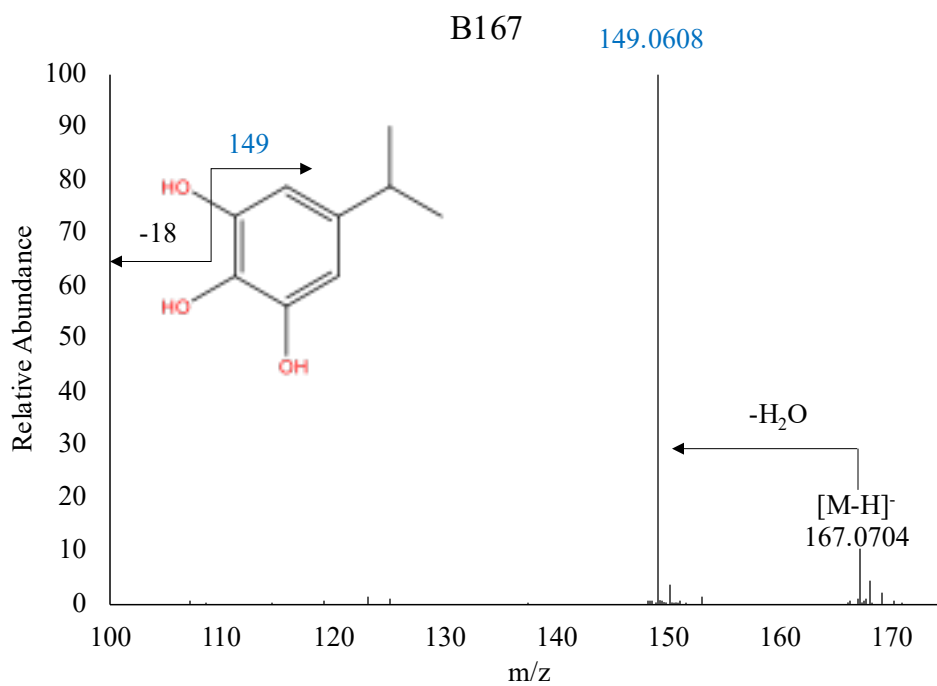
**Table B.3.** Detected transformation products of bisphenol-A during UV/H<sub>2</sub>O<sub>2</sub> treatment.

	RT (min)	[M-H] <sup>-</sup>		Chemical Formula	Proposed Structure
		Theoretical <i>m/z</i>	Observed <i>m/z</i>		
BPA	4.98	227.1078	227.1102	C <sub>15</sub> H <sub>16</sub> O <sub>2</sub>	
B <sub>149</sub>	1.55	149.0608	149.0620	C <sub>9</sub> H <sub>10</sub> O <sub>2</sub>	
B <sub>167</sub>	1.56	167.0714	167.0704	C <sub>9</sub> H <sub>12</sub> O <sub>3</sub>	
B <sub>181</sub>	4.14	181.0506	181.0521	C <sub>9</sub> H <sub>10</sub> O <sub>4</sub>	
B <sub>183</sub>	1.38	183.0663	183.0680	C <sub>9</sub> H <sub>12</sub> O <sub>4</sub>	
B <sub>243a</sub>	3.59	243.1027	243.1021	C <sub>15</sub> H <sub>16</sub> O <sub>3</sub>	
B <sub>243b</sub>	4.59	243.1027	243.1021	C <sub>15</sub> H <sub>16</sub> O <sub>3</sub>	
B <sub>245</sub>		245.0819	245.0817	C <sub>14</sub> H <sub>14</sub> O <sub>4</sub>	
B <sub>257a</sub>	3.17	257.0819	257.0850	C <sub>15</sub> H <sub>14</sub> O <sub>4</sub>	

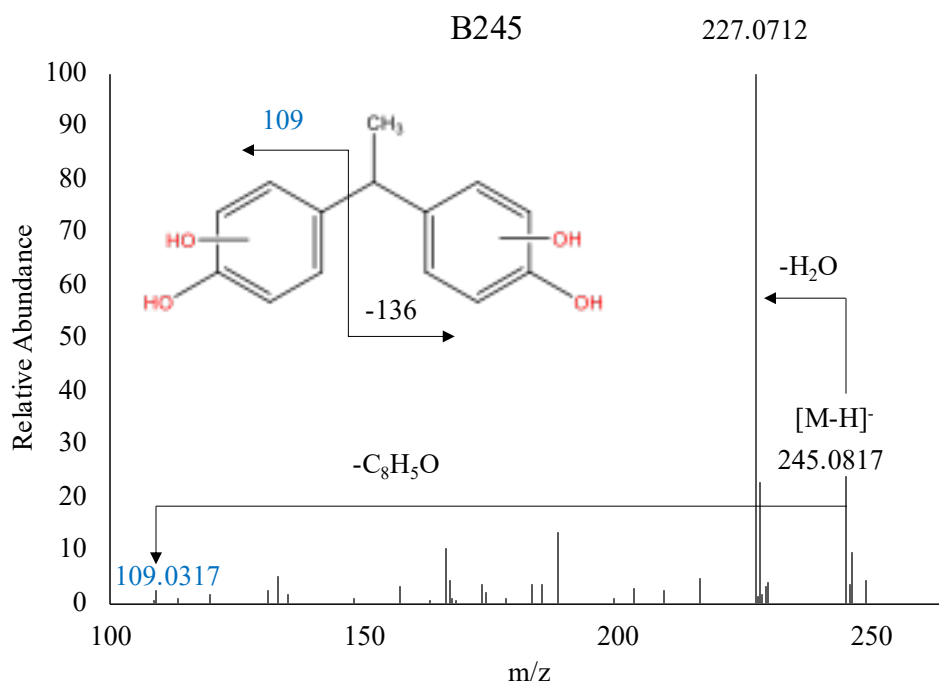
B <sub>257b</sub>	5.48	257.0819	257.0849	C <sub>15</sub> H <sub>14</sub> O <sub>4</sub>	
B <sub>259a</sub>	3.24	259.0976	259.1009	C <sub>15</sub> H <sub>16</sub> O <sub>4</sub>	
B <sub>259b</sub>	3.46	259.0976	259.1009	C <sub>15</sub> H <sub>16</sub> O <sub>4</sub>	
B <sub>271</sub>	2.08	271.0612	271.0644	C <sub>15</sub> H <sub>12</sub> O <sub>5</sub>	
B <sub>273</sub>	5.19	273.0768	273.0799	C <sub>15</sub> H <sub>14</sub> O <sub>5</sub>	



**Figure B.1.** High resolution MS/MS mass spectrum and tentative structure of B<sub>243</sub>.

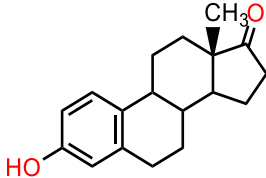
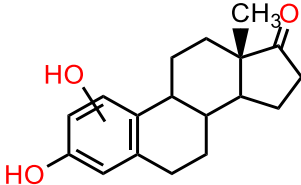
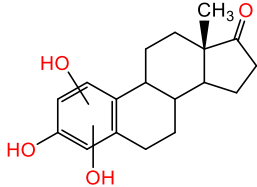


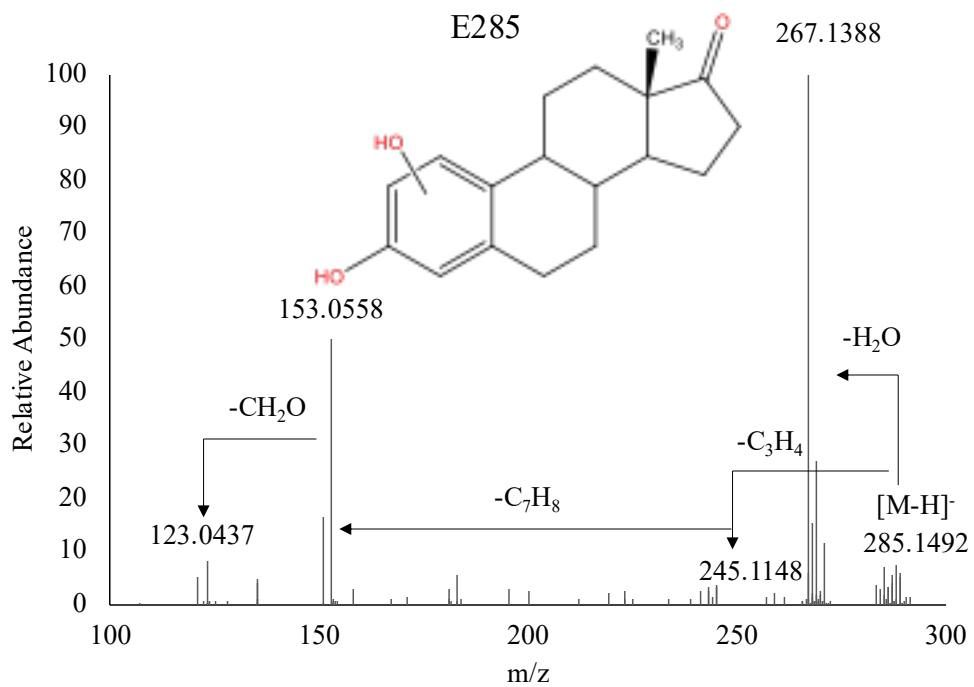
**Figure B.2.** High resolution MS/MS mass spectrum and tentative structure of B<sub>167</sub>.



**Figure B.3.** High resolution MS/MS mass spectrum and tentative structure of B<sub>245</sub>.

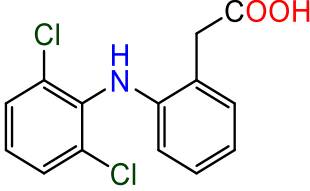
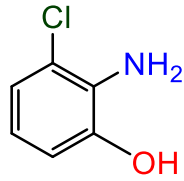
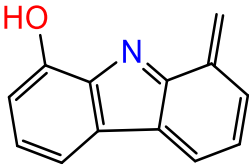
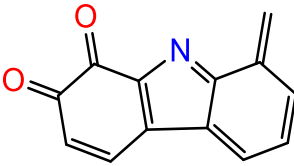
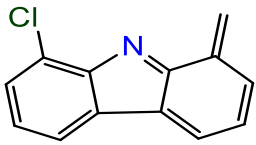
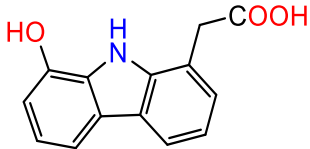
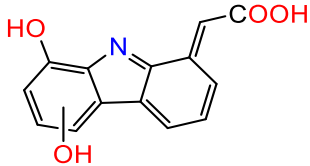
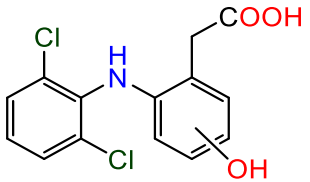
**Table B.4.** Detected transformation products of estrone during UV/H<sub>2</sub>O<sub>2</sub> treatment.

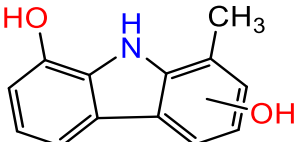
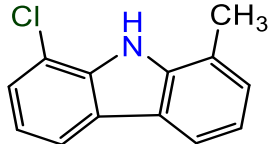
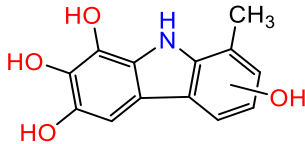
	RT (min)	[M-H] <sup>-</sup>		Chemical Formula	Proposed Structure
		Theoretical <i>m/z</i>	Observed <i>m/z</i>		
Estrone	5.62	269.1547	269.1544	C <sub>18</sub> H <sub>22</sub> O <sub>2</sub>	
E <sub>285</sub>	4.58	285.1496	285.1492	C <sub>18</sub> H <sub>22</sub> O <sub>3</sub>	
E <sub>301</sub>	3.45	301.1445	301.1461	C <sub>18</sub> H <sub>22</sub> O <sub>4</sub>	

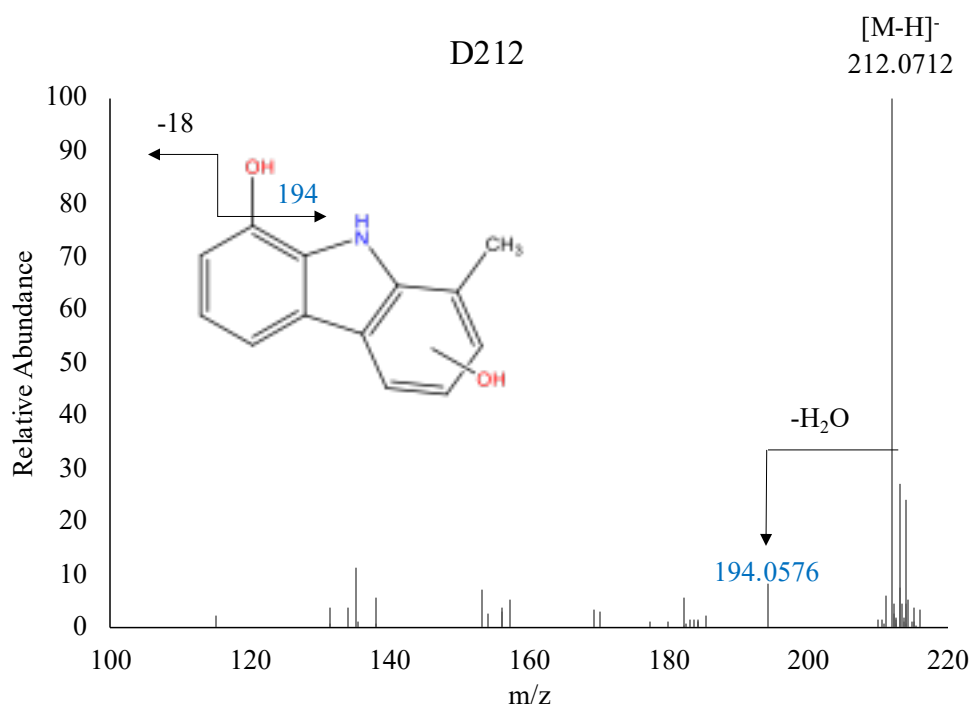


**Figure B.4.** High resolution MS/MS mass spectrum and tentative structure of E<sub>285</sub>.

**Table B.5.** Detected transformation products of diclofenac during UV/H<sub>2</sub>O<sub>2</sub> treatment.

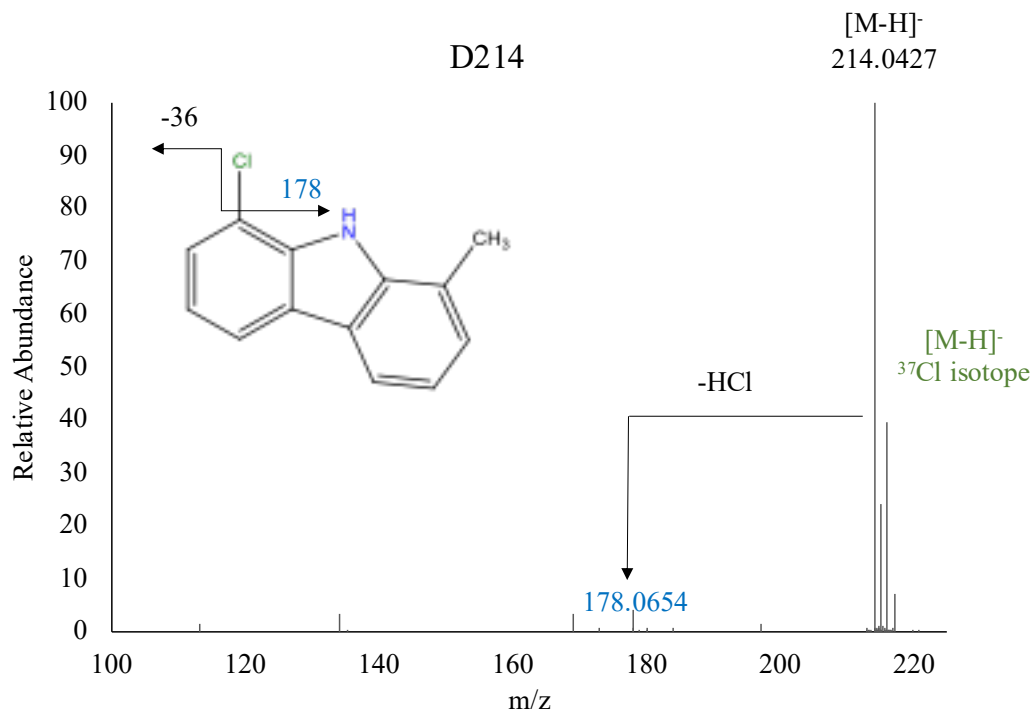
	RT (min)	[M+H] <sup>+</sup>		Chemical Formula	Proposed Structure
		Theoretical <i>m/z</i>	Observed <i>m/z</i>		
DCF	5.91	296.0240	296.0242	C <sub>14</sub> H <sub>11</sub> Cl <sub>2</sub> NO <sub>2</sub>	
D <sub>144</sub>	3.00	144.0211	144.0210	C <sub>6</sub> H <sub>6</sub> ClNO	
D <sub>196</sub>	4.24	196.0757	196.0752	C <sub>13</sub> H <sub>9</sub> NO	
D <sub>210</sub>	3.51	210.0550	210.0548	C <sub>13</sub> H <sub>7</sub> NO <sub>2</sub>	
D <sub>214(+)</sub>	5.47	214.0418	214.0415	C <sub>13</sub> H <sub>8</sub> ClN	
D <sub>242</sub>	4.23	242.0812	242.0811	C <sub>14</sub> H <sub>11</sub> NO <sub>3</sub>	
D <sub>256</sub>	3.50	256.0604	256.0601	C <sub>14</sub> H <sub>9</sub> NO <sub>4</sub>	
D <sub>312</sub>	4.81	312.0189	312.0187	C <sub>14</sub> H <sub>11</sub> Cl <sub>2</sub> NO <sub>3</sub>	

D <sub>212</sub> (-)	212.0717	212.0712	C <sub>13</sub> H <sub>11</sub> NO <sub>2</sub>	
D <sub>214</sub> (-)	214.0429	214.0427	C <sub>13</sub> H <sub>10</sub> ClN	
D <sub>244</sub> (-)	244.0615	244.0613	C <sub>13</sub> H <sub>11</sub> NO <sub>4</sub>	

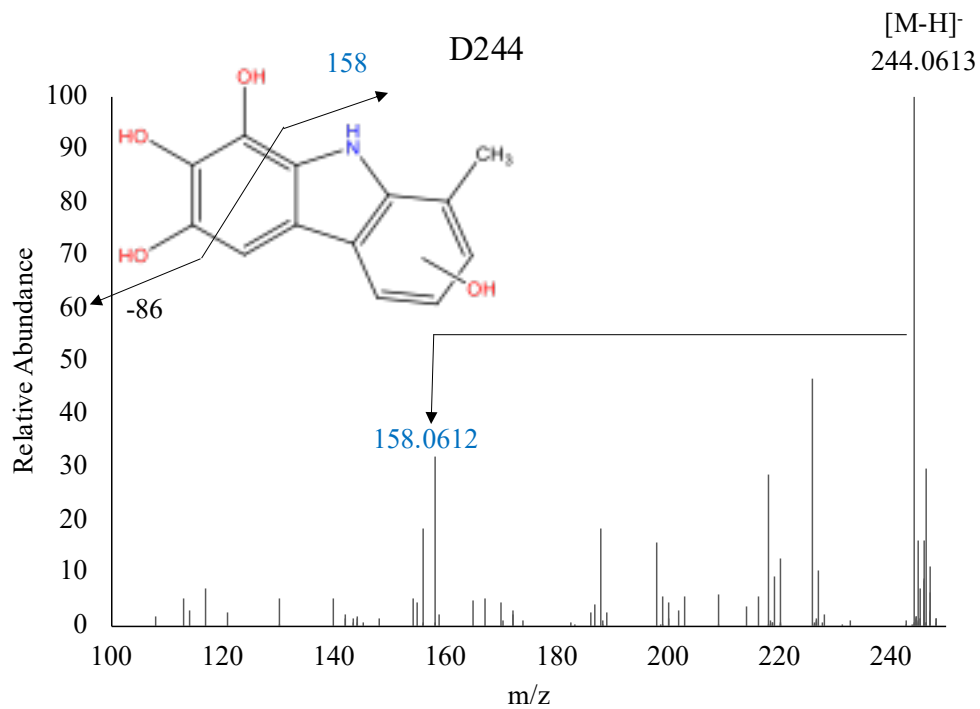


**Figure B.5.** High resolution MS/MS mass spectrum and tentative structure of D<sub>212</sub>.





**Figure B.6.** High resolution MS/MS mass spectrum and tentative structure of D<sub>214</sub>.

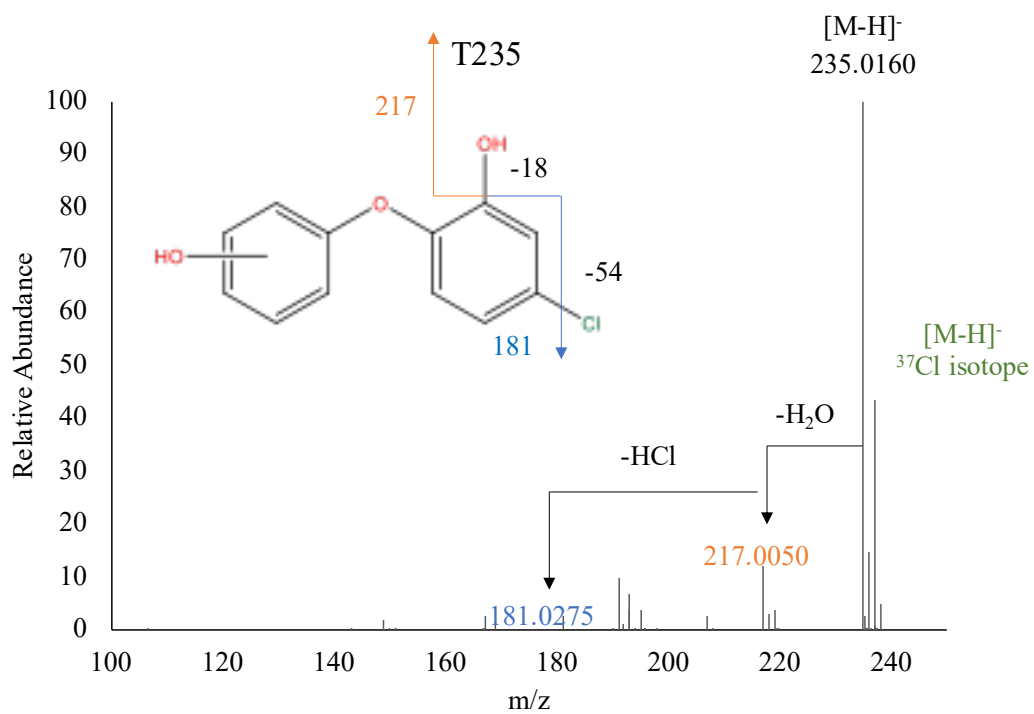


**Figure B.7.** High resolution MS/MS mass spectrum and tentative structure of D<sub>244</sub>.

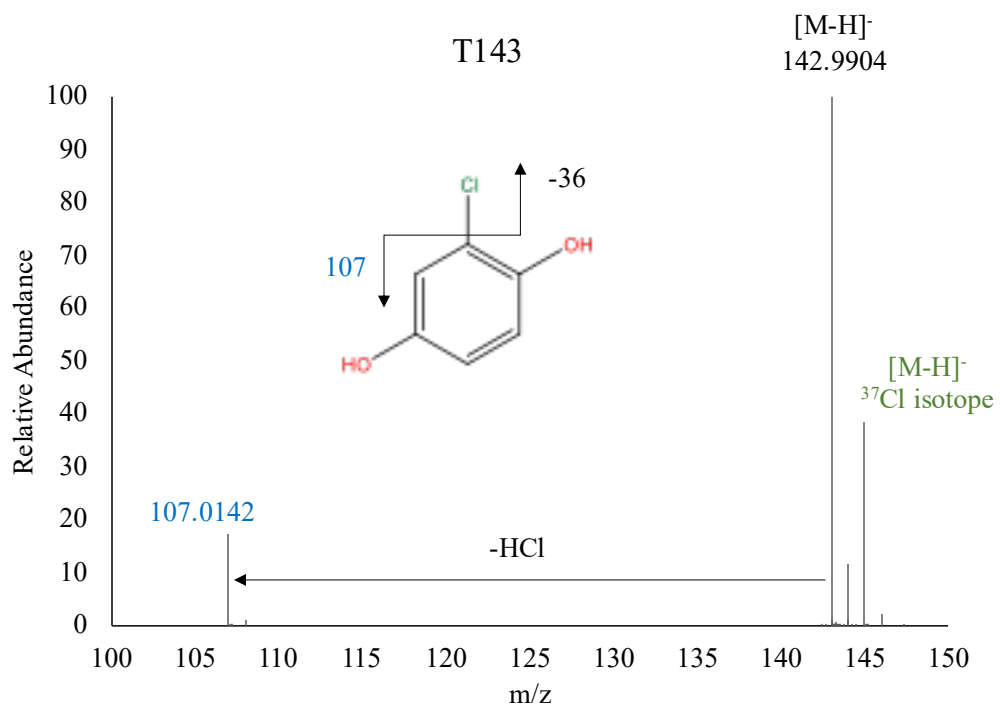
**Table B.6.** Detected transformation products of triclosan during UV/H<sub>2</sub>O<sub>2</sub> treatment.

	RT (min)	[M-H] <sup>-</sup>		Chemical Formula	Proposed Structure
		Theoretical <i>m/z</i>	Observed <i>m/z</i>		
Triclosan	6.31	286.9439	286.9467	C <sub>12</sub> H <sub>7</sub> Cl <sub>3</sub> O <sub>2</sub>	
T <sub>127a</sub>	2.62	126.9956	126.9966	C <sub>6</sub> H <sub>5</sub> ClO	
T <sub>127b</sub>	2.76	126.9956	126.9965	C <sub>6</sub> H <sub>5</sub> ClO	
T <sub>143</sub>	2.21	142.9905	142.9904	C <sub>6</sub> H <sub>5</sub> ClO <sub>2</sub>	
T <sub>161</sub>	2.54	160.9566	160.9576	C <sub>6</sub> H <sub>4</sub> Cl <sub>2</sub> O	
T <sub>201</sub>	3.83	201.0557	201.0573	C <sub>12</sub> H <sub>10</sub> O <sub>3</sub>	
T <sub>235</sub>	4.57	235.0167	235.0160	C <sub>12</sub> H <sub>9</sub> ClO <sub>3</sub>	
T <sub>249a</sub>	3.18	248.9960	248.9979	C <sub>12</sub> H <sub>7</sub> ClO <sub>4</sub>	
T <sub>249b</sub>	3.73	248.9960	248.9983	C <sub>12</sub> H <sub>7</sub> ClO <sub>4</sub>	
T <sub>253a</sub>	4.95	252.9829	252.9854	C <sub>12</sub> H <sub>8</sub> Cl <sub>2</sub> O <sub>2</sub>	
T <sub>253b</sub>	5.53	252.9829	252.9852	C <sub>12</sub> H <sub>8</sub> Cl <sub>2</sub> O <sub>2</sub>	
T <sub>267-1</sub>	8.10	266.9621	266.9647	C <sub>12</sub> H <sub>6</sub> Cl <sub>2</sub> O <sub>3</sub>	

T <sub>267-2</sub>	1.92	267.0066	267.0090	C <sub>12</sub> H <sub>9</sub> ClO <sub>5</sub>	
T <sub>269</sub>	5.78	268.9778	268.9802	C <sub>12</sub> H <sub>8</sub> Cl <sub>2</sub> O <sub>3</sub>	
T <sub>283</sub>	4.05	282.9570	282.9598	C <sub>12</sub> H <sub>6</sub> Cl <sub>2</sub> O <sub>4</sub>	



**Figure B.8.** High resolution MS/MS mass spectrum and tentative structure of T<sub>235</sub>.



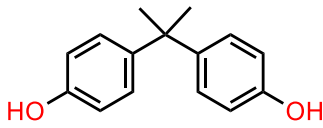

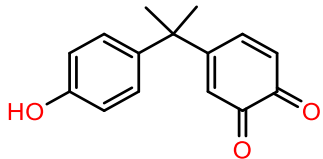
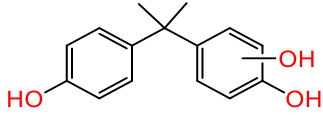
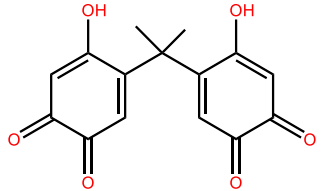
**Figure B.9.** High resolution MS/MS mass spectrum and tentative structure of T<sub>143</sub>.

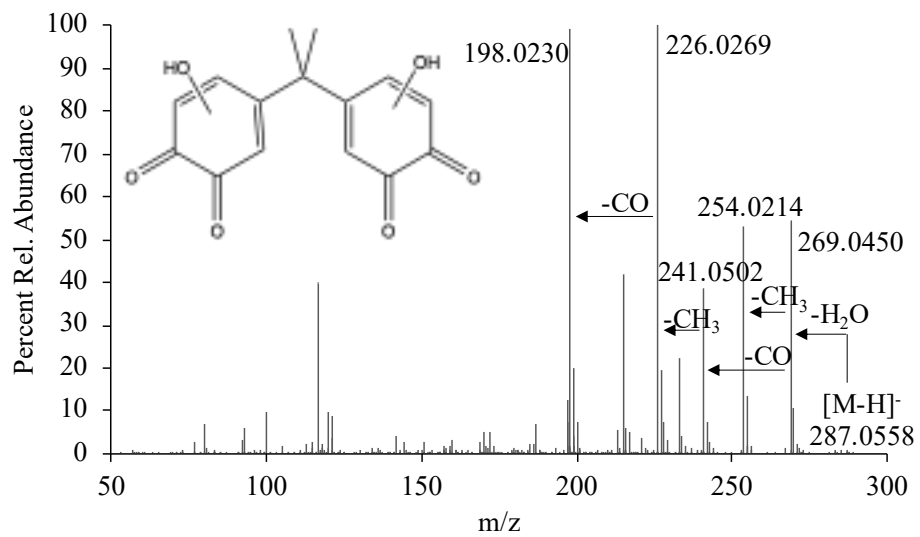
**Table B.7.** Individual cytotoxicity of BPA, IBP, DCF, TCS, and E1 during the UV/H<sub>2</sub>O<sub>2</sub> treatment in Milli-Q water.

Reaction conditions: [EC]<sub>0</sub> = 1 μM, [H<sub>2</sub>O<sub>2</sub>]<sub>0</sub> = 1 mM, pH = 7.3, no buffer.

ECs	Cytotoxicity		
	<i>Concentration</i>	<i>p</i>	Direction
<b>Bisphenol A</b>	5%	0.741	Increased
<b>Diclofenac</b>	1%	<0.0001	Decreased
<b>Ibuprofen</b>	5%	0.998	Increased
<b>Triclosan</b>	5%	0.813	Increased
<b>Estrone</b>	5%	0.625	Decreased

**Table B.8.** Detected transformation products of bisphenol-A in UV/NO<sub>3</sub><sup>-</sup>/HCO<sub>3</sub><sup>-</sup>.

	RT (min)	[M-H] <sup>-</sup>		Chemical Formula	Proposed Structure
		Theoretical <i>m/z</i>	Observed <i>m/z</i>		
Bisphenol A	4.98	227.1078	227.1103	C <sub>15</sub> H <sub>16</sub> O <sub>2</sub>	
B <sub>138a</sub>	2.83	138.0197	138.0211	C <sub>6</sub> H <sub>5</sub> NO <sub>3</sub>	
B <sub>241</sub>	4.27	241.0870	241.0895	C <sub>15</sub> H <sub>14</sub> O <sub>3</sub>	
B <sub>243</sub>	4.59	243.1027	243.1053	C <sub>15</sub> H <sub>16</sub> O <sub>3</sub>	
B <sub>287</sub>	*	287.0561	287.0558	C <sub>15</sub> H <sub>12</sub> O <sub>6</sub>	

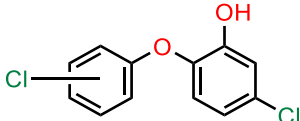
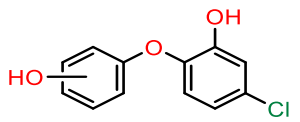
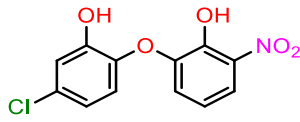
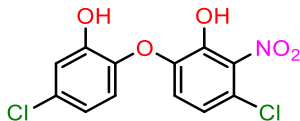
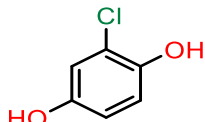
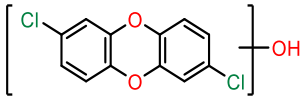


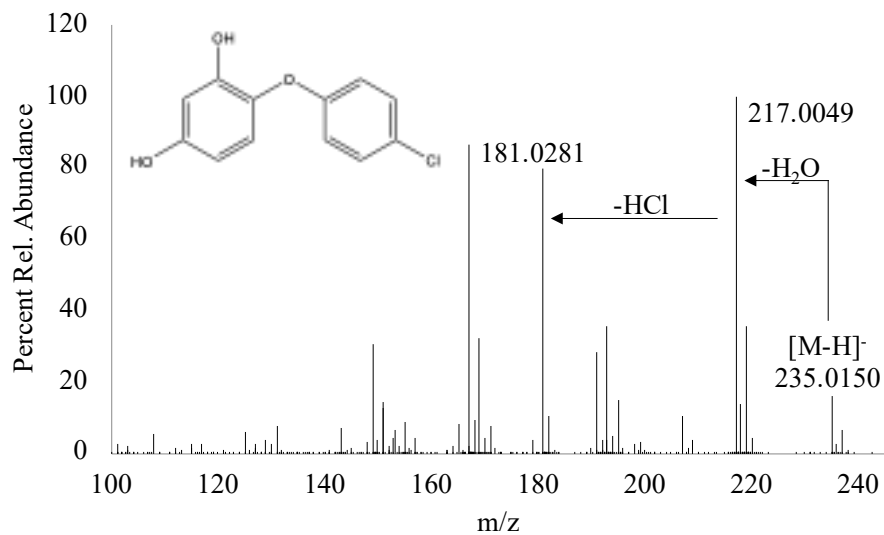
**Figure B.10.** High resolution MS/MS mass spectrum and tentative structure of B<sub>287</sub>.

**Table B.9.** Detected transformation products of triclosan in UV/NO<sub>3</sub><sup>-</sup>/HCO<sub>3</sub><sup>-</sup>.

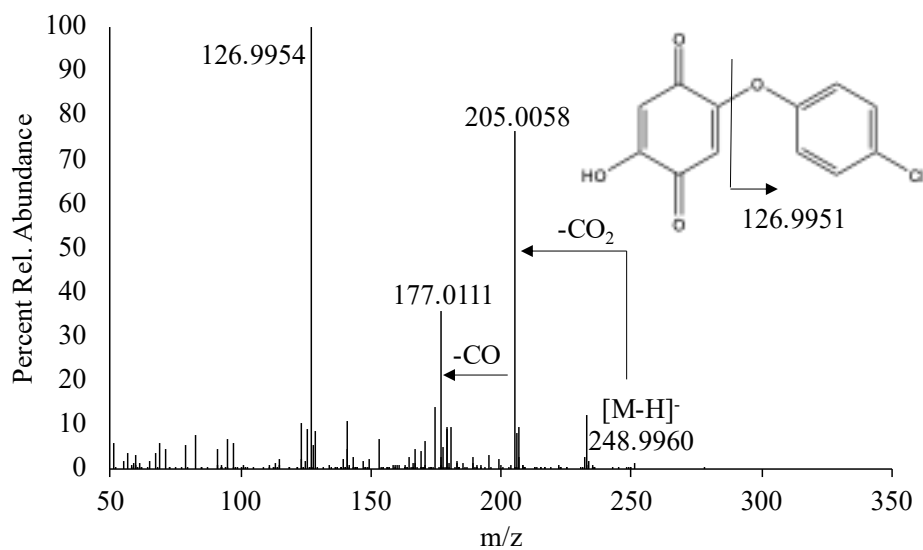
	RT (min)	[M-H] <sup>-</sup>		Chemical Formula	Proposed Structure
		Theoretical <i>m/z</i>	Observed <i>m/z</i>		
Triclosan	6.31	286.9439	286.9459	C <sub>12</sub> H <sub>7</sub> Cl <sub>3</sub> O <sub>2</sub>	
T <sub>127a</sub>	2.18	126.9956	126.9968	C <sub>6</sub> H <sub>5</sub> ClO	
T <sub>127b</sub>	2.58	126.9956	126.9967	C <sub>6</sub> H <sub>5</sub> ClO	
T <sub>161</sub>	2.54	160.9566	160.9579	C <sub>6</sub> H <sub>4</sub> Cl <sub>2</sub> O	
T <sub>317</sub>	2.71	316.9181	316.9180	C <sub>12</sub> H <sub>5</sub> Cl <sub>3</sub> O <sub>4</sub>	
T <sub>249</sub>	3.13	248.9960	248.9960	C <sub>12</sub> H <sub>7</sub> ClO <sub>4</sub>	
T <sub>264</sub>	3.84	264.0069	264.0095	C <sub>12</sub> H <sub>8</sub> ClNO <sub>4</sub>	
T <sub>283</sub>	4.03	282.9570	282.9589	C <sub>12</sub> H <sub>6</sub> Cl <sub>2</sub> O <sub>4</sub>	
T <sub>253a</sub>	4.53	252.9829	252.9850	C <sub>12</sub> H <sub>8</sub> Cl <sub>2</sub> O <sub>2</sub>	
T <sub>253b</sub>	4.91	252.9829	252.9850	C <sub>12</sub> H <sub>8</sub> Cl <sub>2</sub> O <sub>2</sub>	



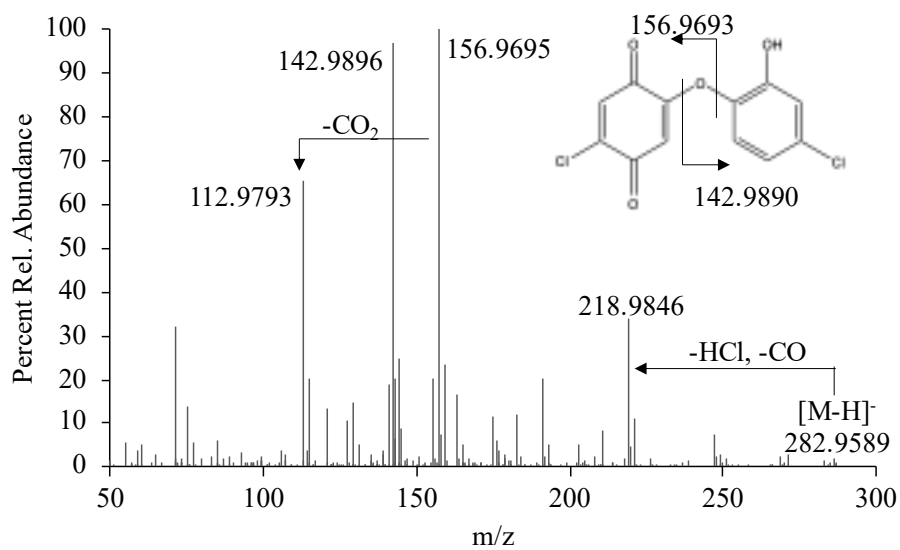
T <sub>253c</sub>	5.52	252.9829	252.9850	C <sub>12</sub> H <sub>8</sub> Cl <sub>2</sub> O <sub>2</sub>	
T <sub>235</sub>	4.57	235.0167	235.0150	C <sub>12</sub> H <sub>9</sub> ClO <sub>3</sub>	
T <sub>280</sub>	4.58	280.0018	280.0005	C <sub>12</sub> H <sub>8</sub> ClNO <sub>5</sub>	
T <sub>314</sub>	4.91	313.9629	313.9659	C <sub>12</sub> H <sub>7</sub> Cl <sub>2</sub> NO <sub>5</sub>	
T <sub>143</sub>	6.58	142.9905	142.9915	C <sub>6</sub> H <sub>5</sub> ClO <sub>2</sub>	
T <sub>267</sub>	8.10	266.9621	266.9645	C <sub>12</sub> H <sub>6</sub> Cl <sub>2</sub> O <sub>3</sub>	



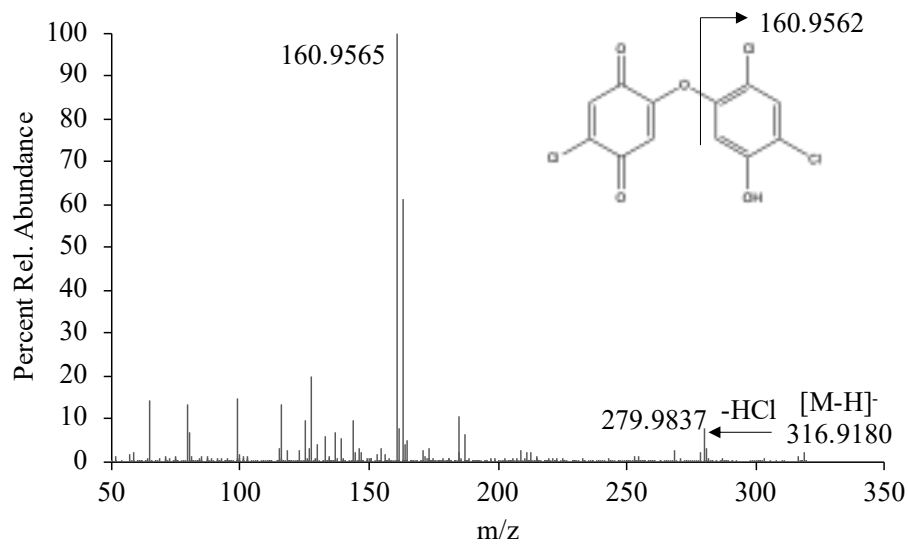
**Figure B.11.** High resolution MS/MS mass spectrum and tentative structure of T<sub>235</sub>.



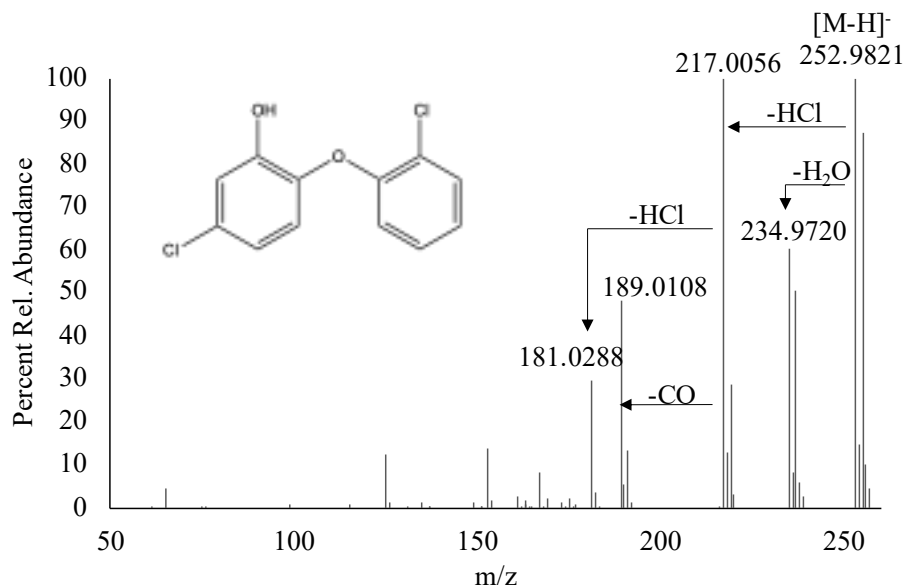
**Figure B.12.** High resolution MS/MS mass spectrum and tentative structure of T<sub>249</sub>.



**Figure B.13.** High resolution MS/MS mass spectrum and tentative structure of T<sub>283</sub>.



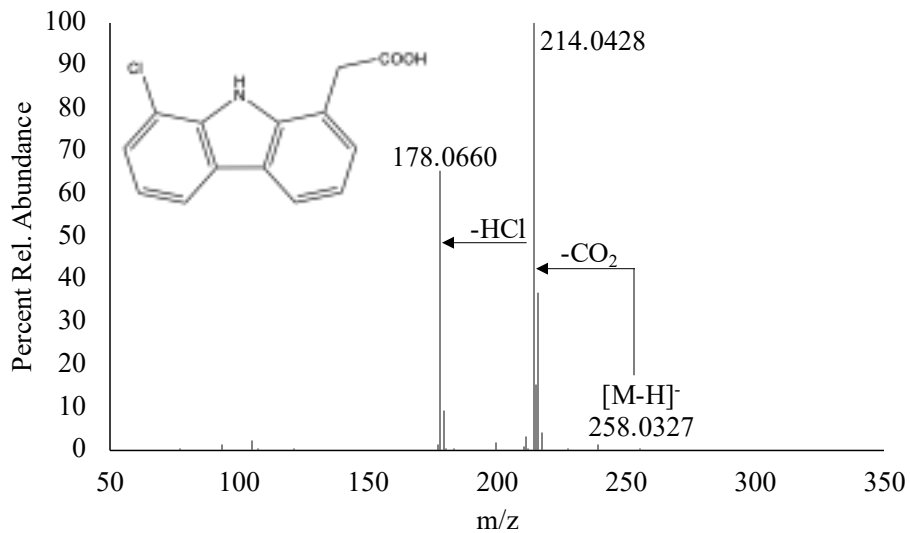
**Figure B.14.** High resolution MS/MS mass spectrum and tentative structure of T<sub>317</sub>.



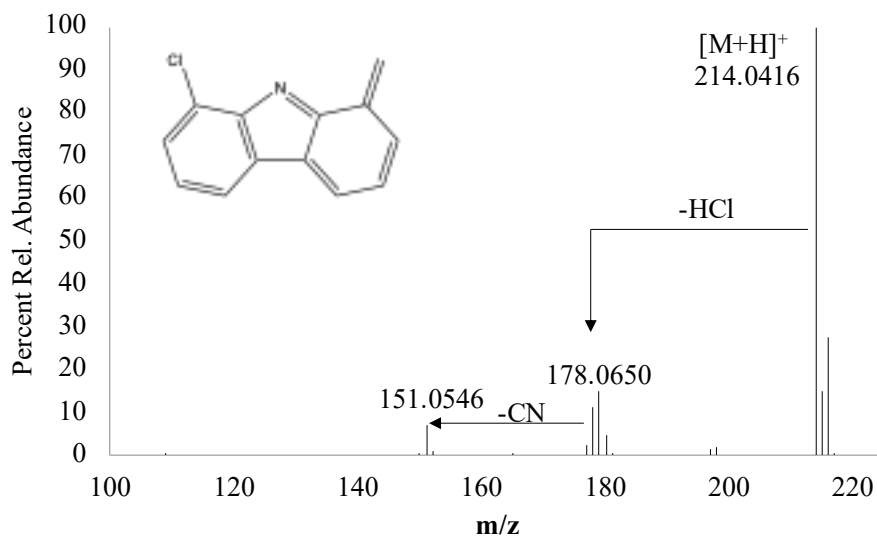
**Figure B.15.** High resolution MS/MS mass spectrum and tentative structure of T<sub>253</sub>.

**Table B.10.** Detected transformation products of diclofenac in UV/NO<sub>3</sub><sup>-</sup>/HCO<sub>3</sub><sup>-</sup>.

	RT (min)	[M+H] <sup>+</sup>		Chemical Formula	Proposed Structure
		Theoretical <i>m/z</i>	Observed <i>m/z</i>		
Diclofenac	4.98	296.0240	296.0242	C <sub>14</sub> H <sub>11</sub> Cl <sub>2</sub> NO <sub>2</sub>	
D <sub>214</sub>	5.47	214.0418	214.0416	C <sub>13</sub> H <sub>8</sub> ClN	
D <sub>260</sub>	2.94	260.0473	260.0475	C <sub>14</sub> H <sub>10</sub> ClNO <sub>2</sub>	

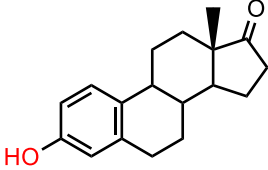
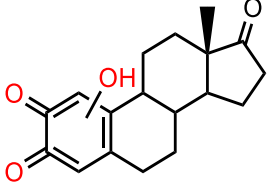
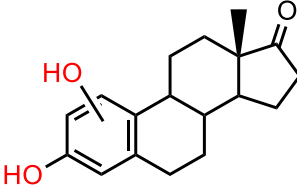
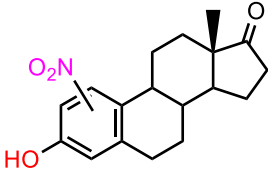
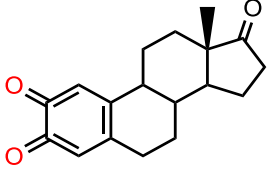


**Figure B.16.** High resolution MS/MS mass spectrum and tentative structure of D<sub>260</sub>.

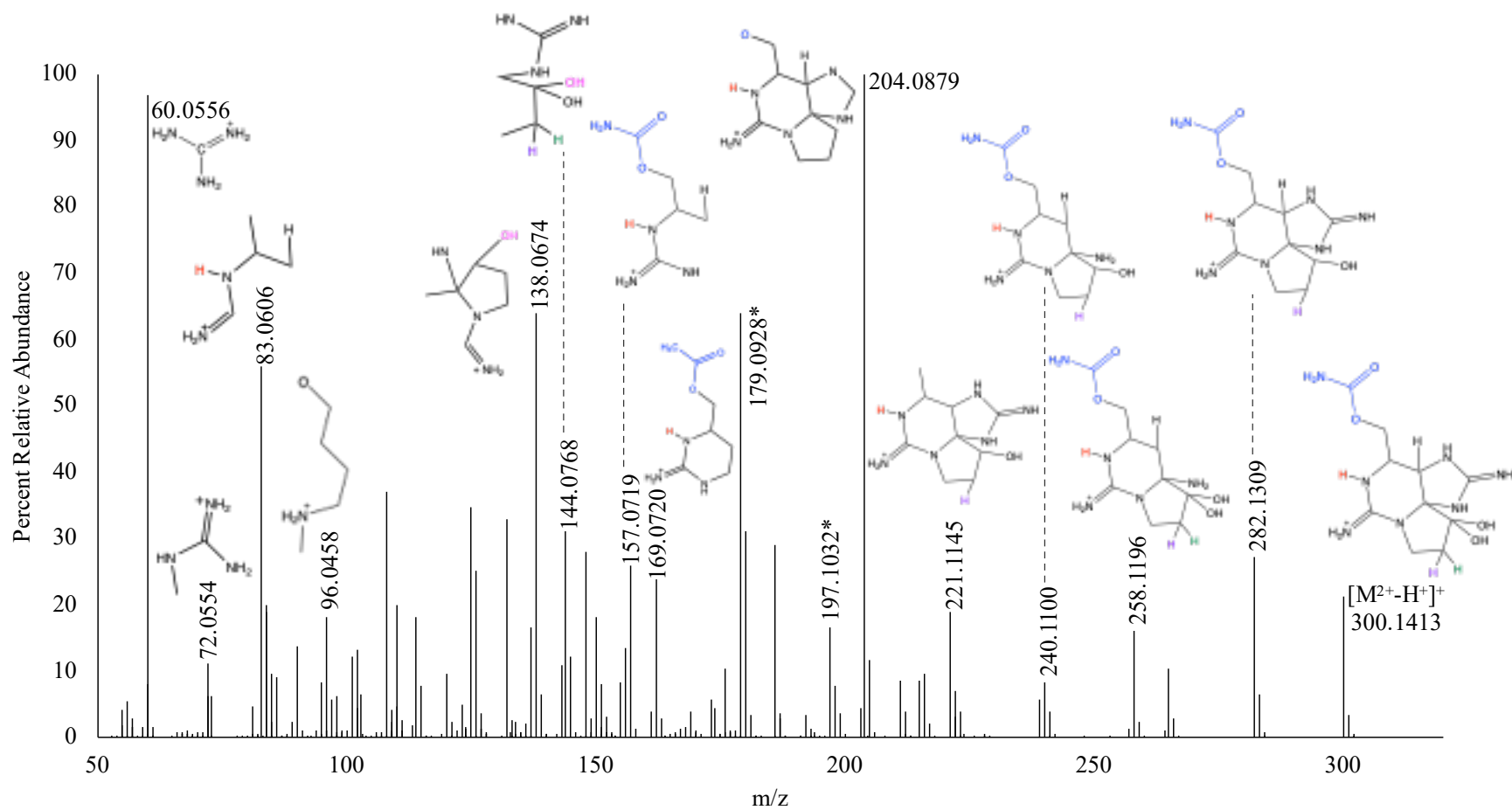


**Figure B.17.** High resolution MS/MS mass spectrum and tentative structure of D<sub>214</sub>.

**Table B.11.** Detected transformation products of estrone in UV/NO<sub>3</sub><sup>-</sup>/HCO<sub>3</sub><sup>-</sup>.

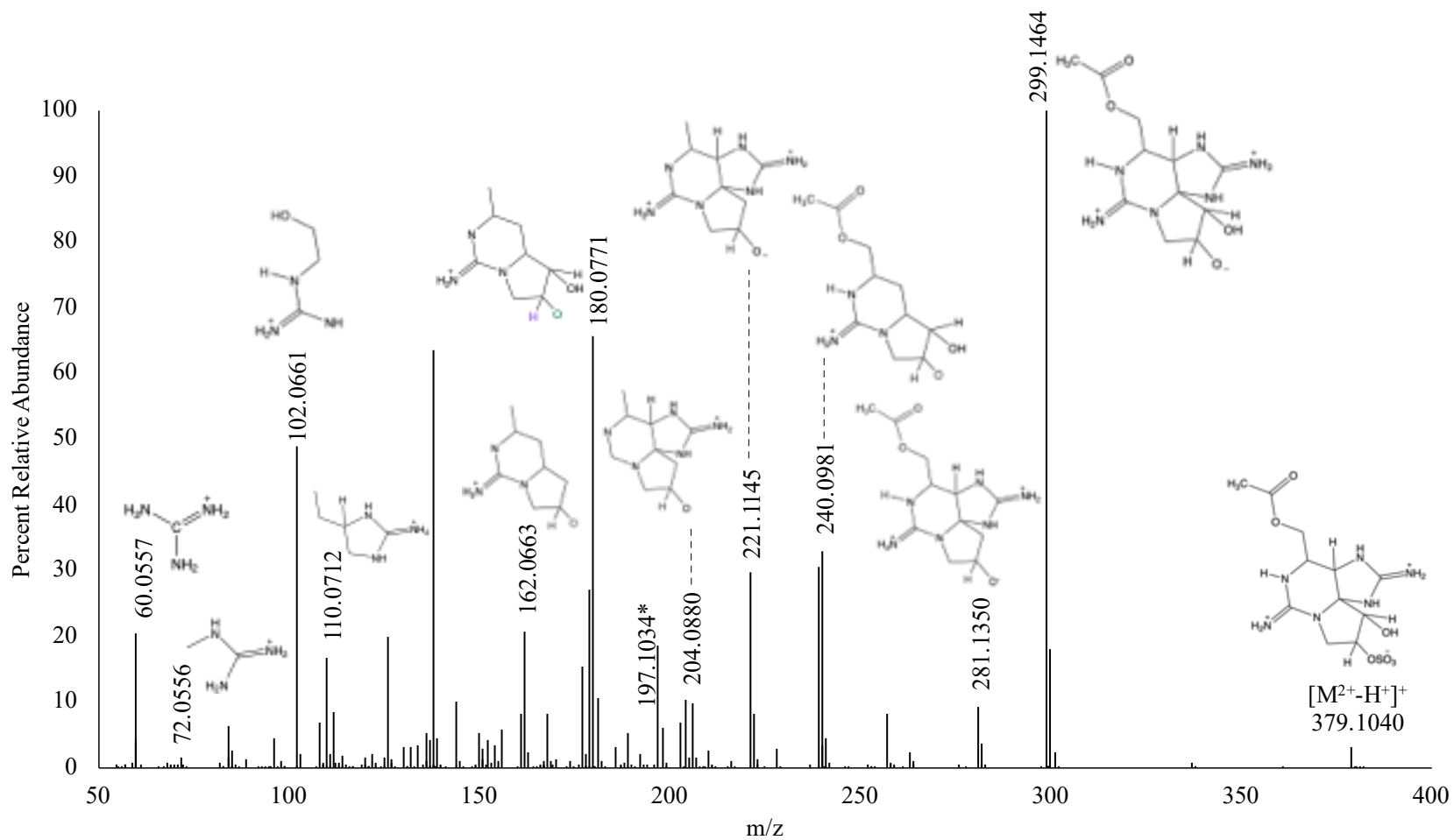
	RT (min)	[M-H] <sup>-</sup>		Chemical Formula	Proposed Structure
		Theoretical <i>m/z</i>	Observed <i>m/z</i>		
Estrone	5.62	269.1547	269.1544	C <sub>18</sub> H <sub>22</sub> O <sub>2</sub>	
E <sub>299</sub>	3.35	299.1289	299.1288	C <sub>18</sub> H <sub>20</sub> O <sub>4</sub>	
E <sub>285a</sub>	2.96	285.1496	285.1495	C <sub>18</sub> H <sub>22</sub> O <sub>3</sub>	
E <sub>285b</sub>	3.77	285.1496	285.1494	C <sub>18</sub> H <sub>22</sub> O <sub>3</sub>	
E <sub>314a</sub>	3.79	314.1398	314.1398	C <sub>18</sub> H <sub>21</sub> NO <sub>4</sub>	
E <sub>314b</sub>	6.11	314.1398	314.1392	C <sub>18</sub> H <sub>21</sub> NO <sub>4</sub>	
E <sub>283</sub>	4.25	283.1340	283.1338	C <sub>18</sub> H <sub>20</sub> O <sub>3</sub>	

APPENDIX C  
SUPPORTING INFORMATION FOR CHAPTER 4

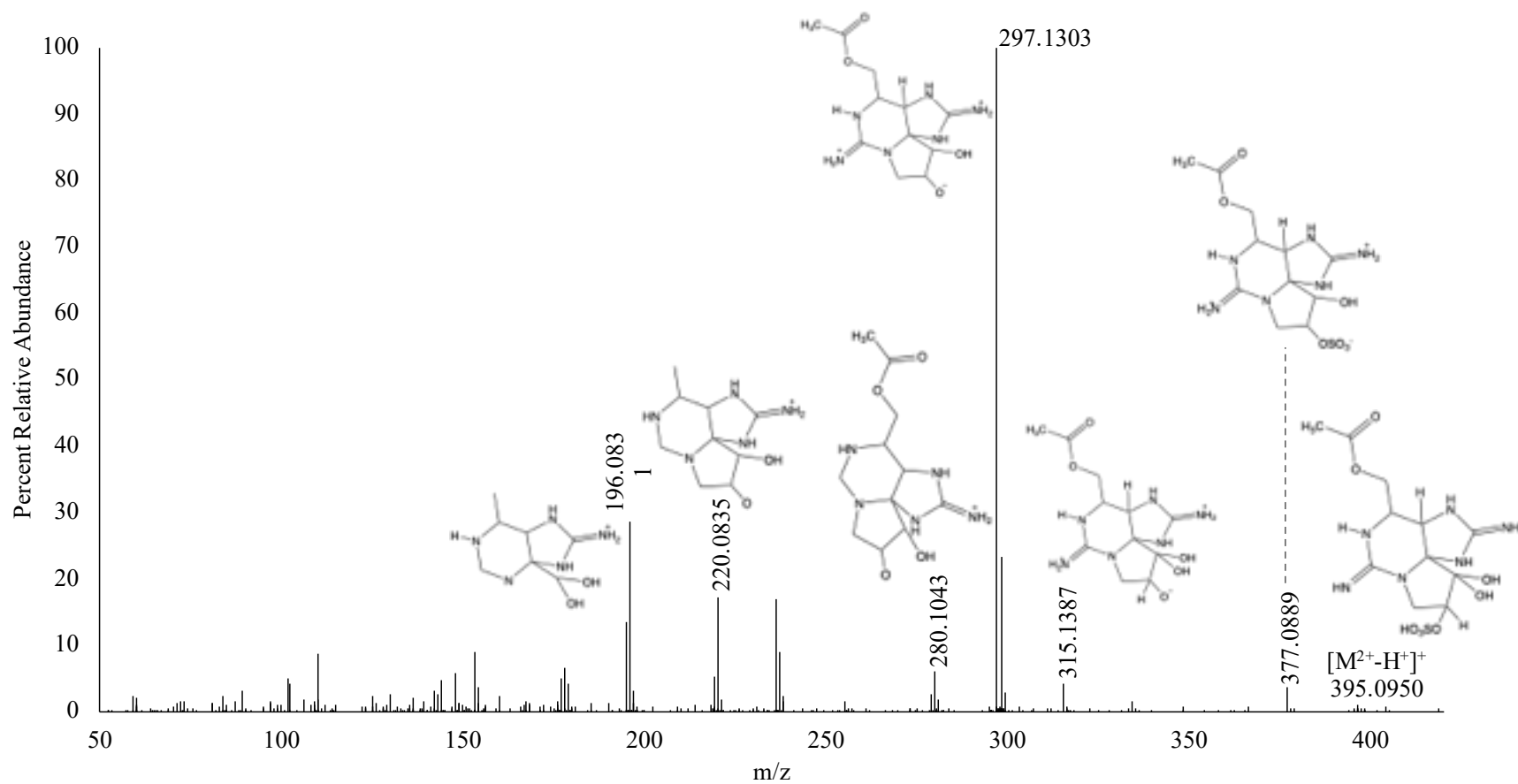


**Figure C.1.** +ESI High resolution mass spectra of LWT 2/3 at 3.87 min obtained from the UHPLC-QTOF.

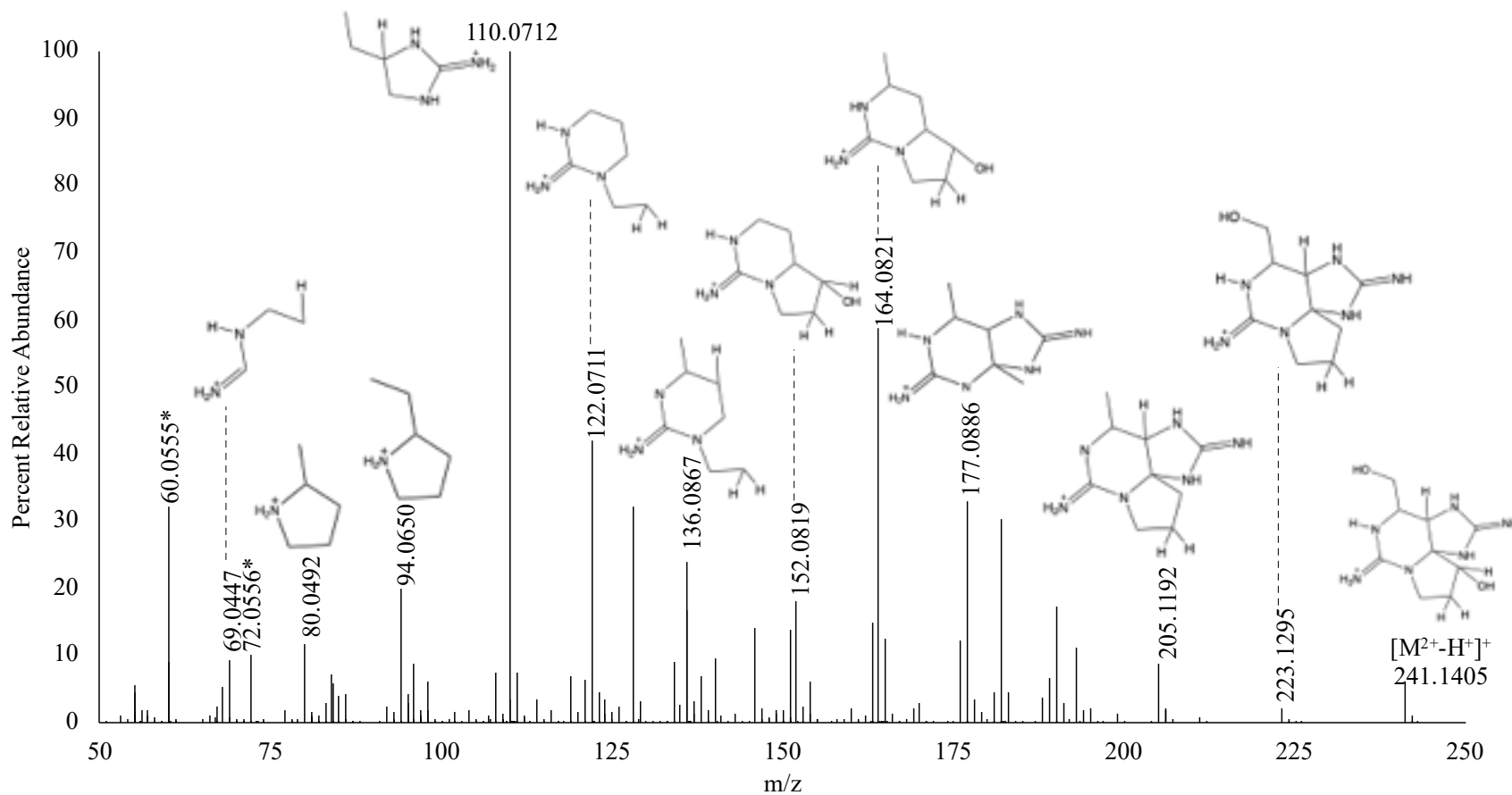




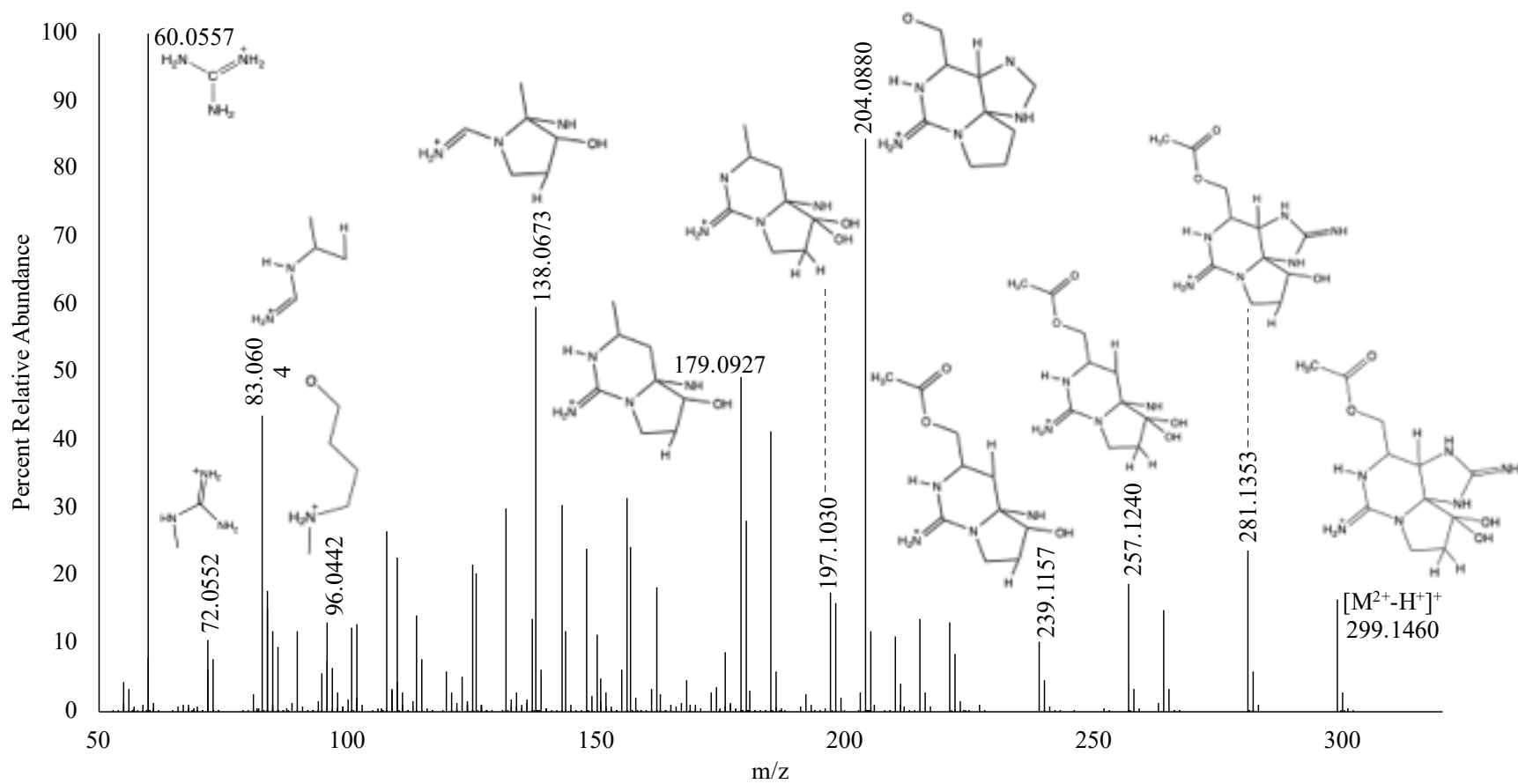
**Figure C.2.** +ESI High resolution mass spectra of LWT1 at 3.87 min obtained from the UHPLC-QTOF.



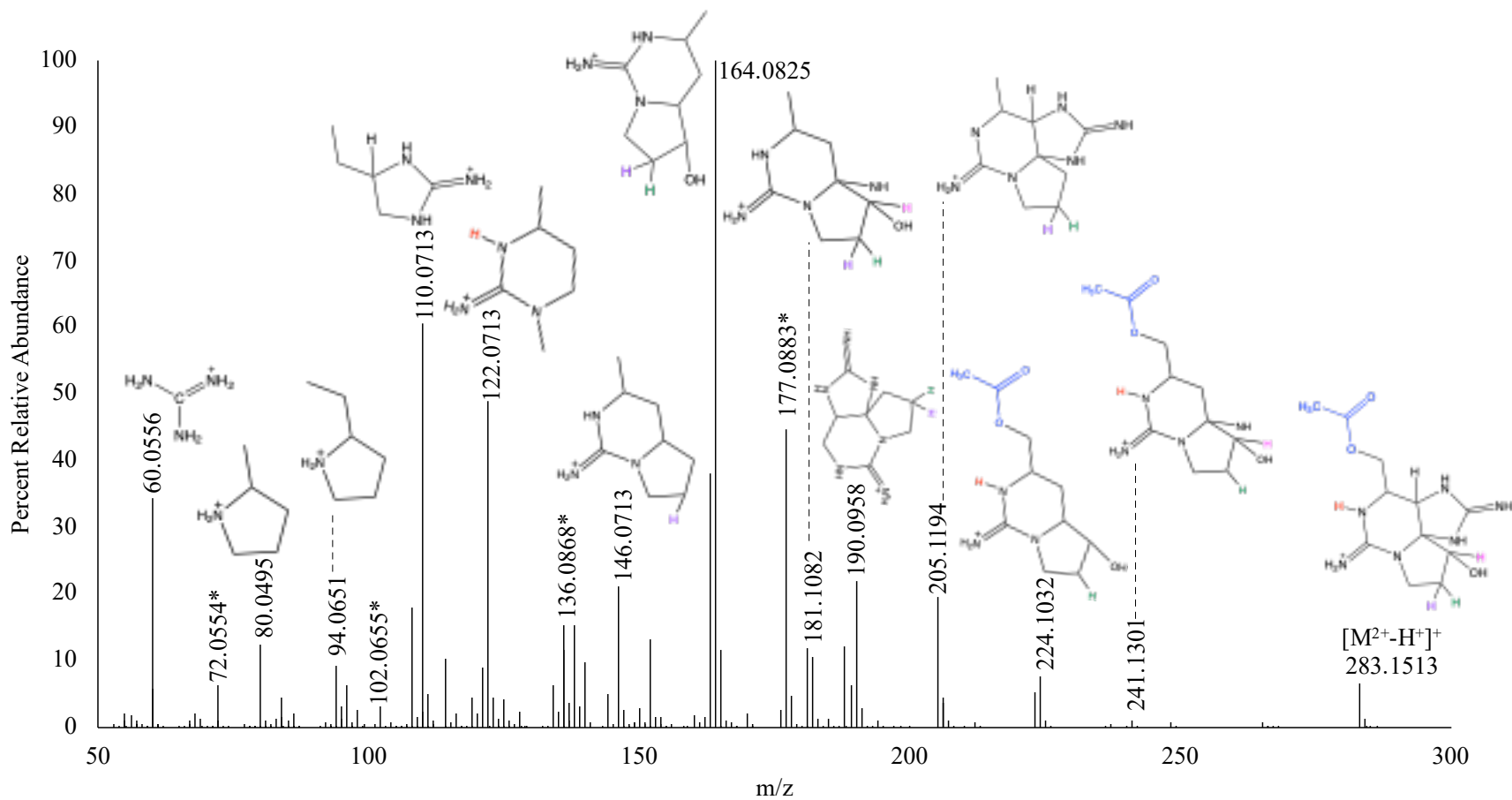
**Figure C.3.** +ESI High resolution mass spectra of LWT 2/3 at 3.87 min obtained from the UHPLC-QTOF.



**Figure C.4.** +ESI High resolution mass spectra of LWT4 at 6.13 min obtained from the UHPLC-QTOF.



**Figure C.5.** +ESI High resolution mass spectra of LWT5 at 5.84 min obtained from the UHPLC-QTOF.



**Figure C.6.** +ESI High resolution mass spectra of LWT6 at 4.96 min obtained from the UHPLC-QTOF.

## APPENDIX D

### REPRINT PERMISSIONS



RightsLink®



Home



Help



Live Chat



Sign in



Create Account



#### Degradation of contaminants of emerging concern by UV/H<sub>2</sub>O<sub>2</sub> for water reuse: Kinetics, mechanisms, and cytotoxicity analysis

**Author:** Ying Huang, Minghao Kong, Scott Coffin, Kristin H. Cochran, Danielle C. Westerman, Daniel Schlenk, Susan D. Richardson, Lecheng Lei, Dionysios D. Dionysiou

**Publication:** Water Research

**Publisher:** Elsevier

**Date:** 1 May 2020

© 2020 Elsevier Ltd. All rights reserved.

#### Journal Author Rights

Please note that, as the author of this Elsevier article, you retain the right to include it in a thesis or dissertation, provided it is not published commercially. Permission is not required, but please ensure that you reference the journal as the original source. For more information on this and on your other retained rights, please visit: <https://www.elsevier.com/about/our-business/policies/copyright#Author-rights>

BACK

CLOSE WINDOW

© 2021 Copyright - All Rights Reserved | Copyright Clearance Center, Inc. | Privacy statement | Terms and Conditions  
Comments? We would like to hear from you. E-mail us at [customer-care@copyright.com](mailto:customer-care@copyright.com)



RightsLink®



Home



Help



Live Chat



Sign in



Create Account



#### Effects of HCO<sub>3</sub><sup>-</sup> on Degradation of Toxic Contaminants of Emerging Concern by UV/NO<sub>3</sub><sup>-</sup>

**Author:** Ying Huang, Minghao Kong, Danielle Westerman, et al

**Publication:** Environmental Science & Technology

**Publisher:** American Chemical Society

**Date:** Nov 1, 2018

Copyright © 2018, American Chemical Society

#### PERMISSION/LICENSE IS GRANTED FOR YOUR ORDER AT NO CHARGE

This type of permission/license, instead of the standard Terms & Conditions, is sent to you because no fee is being charged for your order. Please note the following:

- Permission is granted for your request in both print and electronic formats, and translations.
- If figures and/or tables were requested, they may be adapted or used in part.
- Please print this page for your records and send a copy of it to your publisher/graduate school.
- Appropriate credit for the requested material should be given as follows: "Reprinted (adapted) with permission from (COMPLETE REFERENCE CITATION). Copyright (YEAR) American Chemical Society." Insert appropriate information in place of the capitalized words.
- One-time permission is granted only for the use specified in your request. No additional uses are granted (such as derivative works or other editions). For any other uses, please submit a new request.

BACK

CLOSE WINDOW

© 2021 Copyright - All Rights Reserved | Copyright Clearance Center, Inc. | Privacy statement | Terms and Conditions  
Comments? We would like to hear from you. E-mail us at [customer-care@copyright.com](mailto:customer-care@copyright.com)



**Emerging Lyngbya wollei toxins: A new high resolution mass spectrometry method to elucidate a potential environmental threat**

Author: Meagan L. Smith, Danielle C. Westerman, Samuel P. Putnam, Susan D. Richardson, John L. Ferry

Publication: Harmful Algae

Publisher: Elsevier

Date: December 2019

© 2019 Elsevier B.V. All rights reserved.

**Journal Author Rights**

Please note that, as the author of this Elsevier article, you retain the right to include it in a thesis or dissertation, provided it is not published commercially. Permission is not required, but please ensure that you reference the journal as the original source. For more information on this and on your other retained rights, please visit: <https://www.elsevier.com/about/our-business/policies/copyright#Author-rights>

BACK

CLOSE WINDOW



**Ultrafast photodegradation of isoxazole and isothiazolinones by UV254 and UV254/H2O2 photolysis in a microcapillary reactor**

Author: Danilo Russo, Kristin H. Cochran, Danielle Westerman, Gianluca Li Puma, Raffaele Marotta, Roberto Andreozzi, Susan D. Richardson

Publication: Water Research

Publisher: Elsevier

Date: 1 February 2020

© 2019 Elsevier Ltd. All rights reserved.

**Journal Author Rights**

Please note that, as the author of this Elsevier article, you retain the right to include it in a thesis or dissertation, provided it is not published commercially. Permission is not required, but please ensure that you reference the journal as the original source. For more information on this and on your other retained rights, please visit: <https://www.elsevier.com/about/our-business/policies/copyright#Author-rights>

BACK

CLOSE WINDOW



High-Resolution Mass Spectrometry Identification of Novel Surfactant-Derived Sulfur-Containing Disinfection Byproducts from Gas Extraction Wastewater

Author: Hannah K. Liberatore, Danielle C. Westerman, Joshua M. Allen, et al

Publication: Environmental Science & Technology

Publisher: American Chemical Society

Date: Aug 1, 2020

Copyright © 2020, American Chemical Society

PERMISSION/LICENSE IS GRANTED FOR YOUR ORDER AT NO CHARGE

This type of permission/license, instead of the standard Terms & Conditions, is sent to you because no fee is being charged for your order. Please note the following:

- Permission is granted for your request in both print and electronic formats, and translations.
- If figures and/or tables were requested, they may be adapted or used in part.
- Please print this page for your records and send a copy of it to your publisher/graduate school.
- Appropriate credit for the requested material should be given as follows: "Reprinted (adapted) with permission from (COMPLETE REFERENCE CITATION). Copyright (YEAR) American Chemical Society." Insert appropriate information in place of the capitalized words.
- One-time permission is granted only for the use specified in your request. No additional uses are granted (such as derivative works or other editions). For any other uses, please submit a new request.

BACK

CLOSE WINDOW

**\*Publication: "Tracking the formation of new brominated disinfection by-products during the seawater desalination process," published through the Royal Society of Chemistry, does not require permission/licesnse to be included in a thesis/dissertation.**



APPENDIX E  
PUBLICATIONS





## Degradation of contaminants of emerging concern by UV/H<sub>2</sub>O<sub>2</sub> for water reuse: Kinetics, mechanisms, and cytotoxicity analysis



Ying Huang<sup>a,b</sup>, Minghao Kong<sup>a</sup>, Scott Coffin<sup>c,e</sup>, Kristin H. Cochran<sup>d</sup>, Danielle C. Westerman<sup>d</sup>, Daniel Schlenk<sup>c,f</sup>, Susan D. Richardson<sup>d</sup>, Lecheng Lei<sup>b</sup>, Dionysios D. Dionysiou<sup>a,\*</sup>

<sup>a</sup> Department of Chemical and Environmental Engineering, University of Cincinnati, Cincinnati, OH, 45221, United States

<sup>b</sup> College of Chemical and Biological Engineering, Key Laboratory of Biomass Chemical Engineering of Ministry of Education, Zhejiang University, Zhejiang, 310012, China

<sup>c</sup> Department of Environmental Sciences, University of California, Riverside, CA, 92521, United States

<sup>d</sup> Department of Chemistry and Biochemistry, University of South Carolina, Columbia, SC, 29208, United States

<sup>e</sup> California State Water Resources Control Board, Sacramento, CA, 95814, United States

<sup>f</sup> Institute of Environmental Health, College of Environmental and Resource Sciences, Zhejiang University, Hangzhou 310058, China

### ARTICLE INFO

#### Article history:

Received 2 November 2019

Received in revised form

31 January 2020

Accepted 2 February 2020

Available online 4 February 2020

#### Keywords:

UV/H<sub>2</sub>O<sub>2</sub> AOP

Water reuse

Transformation products

Cytotoxicity

Contaminants of emerging concern

### ABSTRACT

Advanced oxidation using UV and hydrogen peroxide (UV/H<sub>2</sub>O<sub>2</sub>) has been widely applied to degrade contaminants of emerging concern (CECs) in wastewater for water reuse. This study investigated the degradation kinetics of mixed CECs by UV/H<sub>2</sub>O<sub>2</sub> under variable H<sub>2</sub>O<sub>2</sub> doses, including bisphenol A, estrone, diclofenac, ibuprofen, and triclosan. Reverse osmosis (RO) treated water samples from Orange County Water District's Groundwater Replenishment System (GWRS) potable reuse project were collected on different dates and utilized as reaction matrices with spiked additions of chemicals (CECs and H<sub>2</sub>O<sub>2</sub>) to assess the application of UV/H<sub>2</sub>O<sub>2</sub>. Possible degradation pathways of selected CECs were proposed based on high resolution mass spectrometry identification of transformation products (TPs). Toxicity assessments included cytotoxicity, aryl hydrocarbon receptor-binding activity, and estrogen receptor-binding activity, in order to evaluate potential environmental impacts resulting from CEC degradation by UV/H<sub>2</sub>O<sub>2</sub>. Cytotoxicity and estrogenic activity were significantly reduced during the degradation of mixed CECs in Milli-Q water by UV/H<sub>2</sub>O<sub>2</sub> with high UV fluence (3200 mJ cm<sup>-2</sup>). However, in GWRS RO-treated water samples collected in April 2017, the cytotoxicity and estrogen activity of spiked CEC-mixture after UV/H<sub>2</sub>O<sub>2</sub> treatment were not significantly eliminated; this might be due to the high concentration of target CEC and their TPs, which was possibly affected by the varied quality of the secondary treatment influent at this facility such as sewer-shed and wastewater discharges. This study aimed to provide insight on the impacts of post-UV/H<sub>2</sub>O<sub>2</sub> CECs and TPs on human and ecological health at cellular level.

© 2020 Elsevier Ltd. All rights reserved.

### 1. Introduction

Wastewater reuse has been increasingly utilized globally to alleviate water shortages, especially in regions with heightened water scarcity (Binz et al., 2016). In typical wastewater treatment trains for potable reuse, microfiltration (MF) or ultrafiltration (UF) are used to remove microorganisms and colloidal particles, and

reverse osmosis (RO) is utilized to reject viruses, salts and small molecules, and is often followed by a UV/hydrogen peroxide advanced oxidation process (UV/H<sub>2</sub>O<sub>2</sub> AOP) for disinfection and destruction of remaining contaminants of emerging concern (CECs) (Chuang et al., 2017; Patton et al., 2018). A serious limitation for water reuse is the incomplete removal of certain organic contaminants by conventional wastewater treatment, resulting in the presence of many contaminants in the source water to the AOP, including pharmaceuticals, antibacterial compounds, hormones, and plasticizers (Wols et al., 2013). A list of CECs was recommended by a State of California expert panel for monitoring indirect potable

\* Corresponding author.

E-mail address: [dionysios.d.dionysiou@uc.edu](mailto:dionysios.d.dionysiou@uc.edu) (D.D. Dionysiou).

<https://doi.org/10.1016/j.watres.2020.115587>

0043-1354/© 2020 Elsevier Ltd. All rights reserved.

## Effects of $\text{HCO}_3^-$ on Degradation of Toxic Contaminants of Emerging Concern by $\text{UV}/\text{NO}_3^-$

Ying Huang,<sup>†</sup> Minghao Kong,<sup>†</sup> Danielle Westerman,<sup>‡</sup> Elvis Genbo Xu,<sup>§</sup> Scott Coffin,<sup>§</sup> Kristin H. Cochran,<sup>†</sup> Yiqing Liu,<sup>†,||</sup> Susan D. Richardson,<sup>†</sup> Daniel Schlenk,<sup>§</sup> and Dionysios D. Dionysiou<sup>\*,†</sup>

<sup>†</sup>Environmental Engineering and Science, Department of Chemical and Environmental Engineering, University of Cincinnati, Cincinnati, Ohio 45221, United States

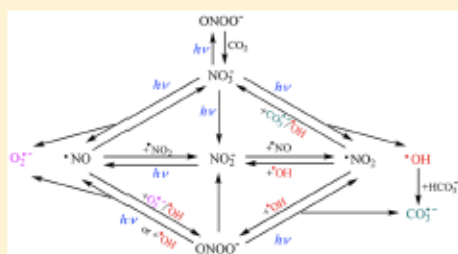
<sup>‡</sup>Department of Chemistry and Biochemistry, University of South Carolina, Columbia, South Carolina 29208, United States

<sup>§</sup>Department of Environmental Sciences, University of California, Riverside, California 92521, United States

<sup>||</sup>Faculty of Geosciences and Environmental Engineering, Southwest Jiaotong University, Chengdu 611756, China

### Supporting Information

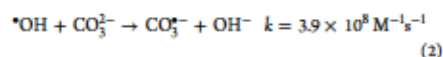
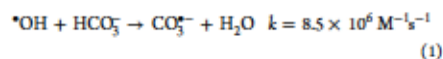
**ABSTRACT:** This study investigated the significant influence of  $\text{HCO}_3^-$  on the degradation of contaminants of emerging concern (CECs) during nitrate photolysis at 254 nm for water reuse applications. The second-order rate constants for the reactions between selected contaminants with carbonate radical ( $\text{CO}_3^{\bullet-}$ ) were determined at pH 8.8 and  $T = 20^\circ\text{C}$ : estrone ( $(5.3 \pm 1.1) \times 10^8 \text{ M}^{-1} \text{ s}^{-1}$ ), bisphenol A ( $(2.8 \pm 0.2) \times 10^8 \text{ M}^{-1} \text{ s}^{-1}$ ), 17 $\alpha$ -ethynylestradiol ( $(1.6 \pm 0.3) \times 10^8 \text{ M}^{-1} \text{ s}^{-1}$ ), triclosan ( $(4.2 \pm 1.4) \times 10^7 \text{ M}^{-1} \text{ s}^{-1}$ ), diclofenac ( $(2.7 \pm 0.7) \times 10^7 \text{ M}^{-1} \text{ s}^{-1}$ ), atrazine ( $(5.7 \pm 0.1) \times 10^6 \text{ M}^{-1} \text{ s}^{-1}$ ), carbamazepine ( $(4.2 \pm 0.01) \times 10^6 \text{ M}^{-1} \text{ s}^{-1}$ ), and ibuprofen ( $(1.2 \pm 1.1) \times 10^6 \text{ M}^{-1} \text{ s}^{-1}$ ). Contributions from UV, reactive nitrogen species (RNS), hydroxyl radical ( $^{\bullet}\text{OH}$ ), and  $\text{CO}_3^{\bullet-}$  to the CEC decomposition in  $\text{UV}/\text{NO}_3^-$  in the presence and absence of  $\text{HCO}_3^-$  were investigated. In addition, possible transformation products and degradation pathways of triclosan, diclofenac, bisphenol A, and estrone in  $\text{UV}/\text{NO}_3^-/\text{HCO}_3^-$  were proposed based on the mass (MS) and  $\text{MS}^2$  spectra. Significant reduction in the cytotoxicity of bisphenol A was observed after the treatment with  $\text{UV}/\text{NO}_3^-/\text{HCO}_3^-$ .



### INTRODUCTION

Nitrate ( $\text{NO}_3^-$ ) photolysis causes the formation of reactive oxygen species (ROS) and nitrogen species (RNS), nitrite ( $\text{NO}_2^-$ ) and peroxy nitrite ( $\text{ONOO}^-$ ), which may pose a health threat in water undergoing treatment.<sup>1,2</sup> Irradiation of water containing  $\text{NO}_3^-$  under low-pressure (LP)-UV at 254 nm ( $\text{UV}/\text{NO}_3^-$ ) primarily leads to the formation of  $\text{ONOO}^-$ , nitrogen dioxide radical ( $^{\bullet}\text{NO}_2$ ), and hydroxyl radical ( $^{\bullet}\text{OH}$ ).<sup>3–6</sup> Nitrite formation is mainly ascribed to the decomposition of peroxy nitrite when the irradiation wavelength is lower than 280 nm.<sup>2,4</sup> Nitrogen oxide radical ( $^{\bullet}\text{NO}$ ) is subsequently produced via the photolysis of nitrate, nitrite, peroxy nitrite, and the substantial oxidation of peroxy nitrite by  $^{\bullet}\text{OH}$ .<sup>7–9</sup> Nitrate photolysis is highly dependent on the reaction pH and the irradiation wavelength.<sup>6</sup> The primary reactions of nitrate photolysis at 254 nm and high pH ( $7 \leq \text{pH} < 9$ ) in solutions containing dissolved  $\text{O}_2$  are summarized in Figure 1. Carbonate radical ( $\text{CO}_3^{\bullet-}$ ) can also be formed with low yield during the  $\text{NO}_3^-$  photolysis in surface water due to the presence of  $\text{CO}_2$  via the decomposition of an adduct  $\text{ONOOOC(O)O}^-$  produced.<sup>2</sup> As prevalent anions in natural

waters,  $\text{HCO}_3^-/\text{CO}_3^{2-}$  play a significant role in  $\text{NO}_3^-$  photolysis, affecting the RNS speciation via enhancing the  $\text{ONOOOC(O)O}^-$  formation and quenching  $^{\bullet}\text{OH}$  with the generation of  $\text{CO}_3^{\bullet-}$  (eqs 1 and 2).<sup>5,4,10,11</sup>



Among the reactive species in  $\text{UV}/\text{NO}_3^-$  in the presence of  $\text{HCO}_3^-$  ( $\text{UV}/\text{NO}_3^-/\text{HCO}_3^-$ ),  $^{\bullet}\text{OH}$  ( $E^0 = 2.0 \text{ V}$ )<sup>12</sup> is a nonselective oxidant, which could react with various contaminants at high rate constants ( $>10^9 \text{ M}^{-1} \text{ s}^{-1}$ ) through electron transfer, H-abstraction, and radical addition.<sup>13</sup> These three routes are favorable for  $^{\bullet}\text{NO}_2$  ( $E^0 = 1.03 \text{ V}$ ) as well, but it

Received: August 6, 2018

Revised: September 30, 2018

Accepted: October 4, 2018

Published: October 4, 2018



## Ultrafast photodegradation of isoxazole and isothiazolinones by UV<sub>254</sub> and UV<sub>254</sub>/H<sub>2</sub>O<sub>2</sub> photolysis in a microcapillary reactor



Daniilo Russo <sup>a,\*</sup>, Kristin H. Cochran <sup>a</sup>, Danielle Westerman <sup>a</sup>, Gianluca Li Puma <sup>b</sup>, Raffaele Marotta <sup>c</sup>, Roberto Andreozzi <sup>c</sup>, Susan D. Richardson <sup>a,\*\*</sup>

<sup>a</sup> Department of Chemistry and Biochemistry, University of South Carolina, USA

<sup>b</sup> Environmental Nanocatalysis & Photoreaction Engineering, Department of Chemical Engineering, Loughborough University, UK

<sup>c</sup> Dipartimento di Ingegneria Chimica, Dei Materiali e Della Produzione Industriale, Università di Napoli Federico II, Italy

### ARTICLE INFO

#### Article history:

Received 28 June 2019

Received in revised form

14 October 2019

Accepted 15 October 2019

Available online 18 October 2019

#### Keywords:

Microcontaminants

Advanced oxidation processes

Isoxazole

Water reclamation

Water treatment

Isothiazolinones

### ABSTRACT

The photodegradation process of methylisothiazolinone (MIT), benzisothiazolinone (BIT), and isoxazole (ISOX) in ultrapure water and synthetic wastewater by means of UV<sub>254</sub> photolysis and by UV<sub>254</sub>/H<sub>2</sub>O<sub>2</sub> advanced oxidation process were investigated in a microcapillary photoreactor designed for ultrafast photochemical transformation of microcontaminants. For the first time, we estimated key photo-kinetic parameters, i.e. quantum yields (354 mmol·ein<sup>-1</sup> for MIT, and 13.5 and 55.8 mmol·ein<sup>-1</sup> for BIT at pH = 4–6 and 8, respectively) and rate constants of the reaction of photo-generated OH radicals with MIT and BIT (2.09·10<sup>9</sup> and 5.9·10<sup>9</sup> L·mol<sup>-1</sup>·s<sup>-1</sup> for MIT and BIT). The rate constants of the reaction of photo-generated OH radicals with ISOX in MilliQ water was also estimated (2.15·10<sup>9</sup> L·mol<sup>-1</sup>·s<sup>-1</sup>) and it was in good agreement with literature indications obtained in different aqueous matrices. The models were extended and validated to the case of simultaneous degradation of mixtures of these compounds and using synthetic wastewater as an aqueous matrix. High resolution-accurate mass spectrometry analysis enabled identification of the main intermediates (BIT200, B200, saccharin, BIT166) and enabled proposal of a novel degradation pathway for BIT under UV<sub>254</sub>/H<sub>2</sub>O<sub>2</sub> treatment. This study demonstrates an ultrafast method to determine key photo-kinetic parameters of contaminants of emerging concern in water and wastewater, which are needed for design and validation of photochemical water treatment processes of municipal and industrial wastewaters.

© 2019 Elsevier Ltd. All rights reserved.

### 1. Introduction

Isoxazole and isothiazolinones are five-membered heterocyclic compounds having various pharmacological and antimicrobial properties (Harnad and Sharshira, 2011; Lee and Kim, 2002; Clerici et al., 2008). The large interest in these substances and their derivatives is due to their versatility as synthetic building blocks (Gribble and Joule, 2003). As a result of their massive adoption in a wide variety of commonly used products, such compounds have been included in the class of emerging pollutants (Ghattas et al.,

2017; Shi et al., 2012). The current broad definition of emerging pollutants includes a significant number of chemicals normally employed in detergents, personal care products, pharmaceuticals and drugs, which are usually present in wastewater and surface water at levels from ng to µg per liter (Miraji et al., 2016; Wanda et al., 2017; McCance et al., 2018; Guo et al., 2018). Despite their low levels, their potential ecotoxicological effect cannot be ruled out (Kohanski et al., 2010; Lin et al., 2010) and several studies addressed the problem of their removal from liquid and solid compartments (Stamm et al., 2015; Boliman et al., 2014; Luo et al., 2014; Margot et al., 2015).

2-Methyl-1,2-thiazol-3(2H)-one, also named methylisothiazolinone (MIT) and 1,2-Benzisothiazol-3(2H)-one, or benzisothiazolinone (BIT) are very common biocides employed in personal care products, detergents (Li et al., 2016a; García-Hidalgo et al., 2016), roof and outdoor paints, paper materials, and in other important industrial applications (Jungnickel et al., 2008; Wieck

\* Corresponding author.

\*\* Corresponding author.

E-mail addresses: [daniilo.russo@uscar.edu](mailto:daniilo.russo@uscar.edu), [ds473@cam.ac.uk](mailto:ds473@cam.ac.uk) (D. Russo),

[RCHAS45@mailbox.usc.edu](mailto:RCHAS45@mailbox.usc.edu) (S.D. Richardson).

<sup>†</sup> Present address: Department of Chemical Engineering and Biotechnology, University of Cambridge, UK.





## Emerging *Lyngbya wollei* toxins: A new high resolution mass spectrometry method to elucidate a potential environmental threat



Meagan L. Smith<sup>a,b</sup>, Danielle C. Westerman<sup>a,b</sup>, Samuel P. Putnam<sup>a,b</sup>, Susan D. Richardson<sup>a,b</sup>, John L. Ferry<sup>a,b,\*</sup>

<sup>a</sup> University of South Carolina, Department of Chemistry and Biochemistry, 631 Sumter Street Columbia, SC 29208, United States

<sup>b</sup> University of South Carolina, Center for Innovations of Climate Change on Oceans and Human Health, 623 Assembly St. Ste. 401, Columbia, SC 29208, United States

### ARTICLE INFO

**Keywords:**  
Cyanobacteria  
Saxitoxin  
Benthic  
Flamnetion  
Quantification  
Liquid chromatography

### ABSTRACT

Mass spectrometric methods for the quantitative and qualitative analyses of algal biotoxins are often complicated by co-eluting compounds that present analytically as interferences. This issue is particularly critical for organic polyamines, whose co-eluting materials can suppress the formation of cations during electrospray ionization. Here we present an extraction procedure designed specifically to overcome matrix-derived ion suppression of algal toxins in samples of *Lyngbya wollei*, a filamentous benthic algae known to produce several saxitoxin analogues. *Lyngbya wollei* samples were collected from a large, persistent harmful algal bloom in Lake Wateree, SC. Six known *Lyngbya wollei*-specific toxins (LWT1–6) were successfully resolved and quantified against saxitoxin using hydrophilic interaction liquid chromatography coupled with triple quadrupole and quadrupole time-of-flight mass spectrometry. The parent ions  $[M^{2+} - H^+]$  were observed for LWTs 1–6 and the  $[M]^{2+}$  ion was observed for LWT5. High resolution mass spectra and unique fragmentation ions were obtained for LWTs 1–6. A dilution factor of 50 resulted in a linear calibration of saxitoxin in the algae matrix. Ion suppression was resolved by sample dilution, which led to linear, positive correlations between peak area and mass of the extracted sample ( $R^2 > 0.96$ ). Optimized sample extraction method and instrument parameters are presented.

### 1. Introduction

Analogues of the neurotoxic alkaloid saxitoxin, also known as paralytic shellfish toxins are members of a class of naturally occurring secondary metabolites produced by freshwater cyanobacteria and marine dinoflagellates (Hamada et al., 1982; Oshima et al., 1987). Saxitoxin is a selective sodium channel blocker that has been documented to be extremely toxic to a wide range of species, including humans (Carmichael, 1994; Jochimsen et al., 1998; Kao, 1993; Landsberg, 2002; Negri et al., 1995). To date, there are at least 57 known analogues of saxitoxin (Wiese et al., 2010) with varying levels of toxicity (by mouse bioassay), produced by a variety of genera including *Anabaena* (Al-Tobrini et al., 2010; Humpage et al., 1994; Onodera et al., 1996), *Cylinodermopsis* (Lagos et al., 1999), *Aphanizomenon* (Jackim and Gentile, 1968; Mahmood and Carmichael, 1986; Sawyer et al., 1968), *Planktoerix* (Pomati et al., 2003), and *Lyngbya* (Dell'Aversano, 2011). *Lyngbya wollei* (Farlow ex Gomont) Speziale &

Dyck, a filamentous, benthic cyanobacteria, is a source of saxitoxin analogues known as *Lyngbya wollei* toxins (Carmichael et al., 1997; Cowell and Botts, 1994; Foss et al., 2012b; Onodera et al., 1997; Yin et al., 1997) (LWTs, Fig. 1 and Fig. S1).

The qualification and quantification of saxitoxin analogues can be challenging. Effect based assays, including the mouse bioassay (Cusick and Saylor, 2013; Schantz et al., 1958; Turner et al., 2012), in-vitro cell viability assays (Gallacher and Hirkbeck, 1992; Jellitt et al., 1992; Kogure et al., 1988; Manger et al., 1993), enzyme-linked immune sorbent assay (Chu et al., 1992; Humpage et al., 2010), and receptor binding assay (Davio and Fontelo, 1984; Doucette et al., 1997; Usup et al., 2004; Van Dolan et al., 2012) can provide qualitative and quantitative toxicity information (Cusick and Saylor, 2013). However, these techniques report concentrations as summed saxitoxin equivalents and do not report the relative concentrations of different structural analogues. The latter is key for developing a detailed understanding of the relevant toxin biosynthetic pathways and understanding

Abbreviations: LWT, *Lyngbya wollei* toxin; UPLC-TQ, ultra performance liquid chromatograph – triple quadrupole; UPLC-QTOF, ultrahigh performance liquid chromatograph – quadrupole time-of-flight; ESI, electrospray ionization; MS/MS, tandem mass spectrometry

\* Corresponding author at: University of South Carolina, Department of Chemistry and Biochemistry, 631 Sumter Street Columbia, SC 29208, United States.

E-mail address: [ferry@sc.edu](mailto:ferry@sc.edu) (J.L. Ferry).

<https://doi.org/10.1016/j.hal.2019.101700>

Received 24 July 2019; Received in revised form 16 October 2019; Accepted 25 October 2019

Available online 20 November 2019

1568-9883/ © 2019 Elsevier B.V. All rights reserved.

## High-Resolution Mass Spectrometry Identification of Novel Surfactant-Derived Sulfur-Containing Disinfection Byproducts from Gas Extraction Wastewater

Hannah K. Liberatore, Danielle C. Westerman, Joshua M. Allen, Michael J. Plewa, Elizabeth D. Wagner, Amy M. McKenna, Chad R. Weisbrod, James P. McCord, Richard J. Liberatore, David B. Bumett, Leslie H. Cizmas, and Susan D. Richardson\*

Cite This: *Environ. Sci. Technol.* 2020, 54, 9374–9386

Read Online

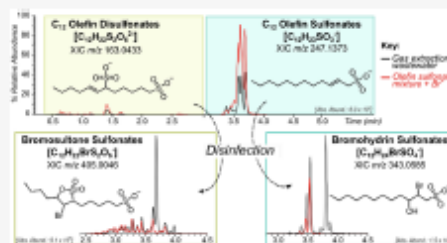
ACCESS |

Metrics & More

Article Recommendations

Supporting Information

**ABSTRACT:** Introduction of oil and gas extraction wastewaters (OGWs) to surface water leads to elevated halide levels from geogenic bromide and iodide, as well as enhanced formation of brominated and iodinated disinfection byproducts (DBPs) when treated. OGWs contain high levels of chemical additives used to optimize extraction activities, such as surfactants, which have the potential to serve as organic DBP precursors in OGW-impacted water sources. We report the first identification of olefin sulfonate surfactant-derived DBPs from laboratory-disinfected gas extraction wastewater. Over 300 sulfur-containing DBPs, with 43 unique molecular formulas, were found by high-resolution mass spectrometry, following bench-scale chlor(am)ination. DBPs consisted of mostly brominated species, including bromohydrin sulfonates, dihalo-bromosulfonates, and bromosulfone sulfonates, with chlorinated/iodinated analogues formed to a lesser extent. Disinfection of a commercial  $C_{12}$  olefin sulfonate surfactant mixture revealed dodecene sulfonate as a likely precursor for most detected DBPs; disulfur-containing DBPs, like bromosulfone sulfonate and bromohydrin disulfonate, originated from olefin disulfonate species, present as side-products of olefin sulfonate production. Disinfection of wastewaters increased mammalian cytotoxicity several orders of magnitude, with chloraminated water being more toxic. This finding is important to OGW-impacted source waters because drinking water plants with high-bromide source waters may switch to chloramination to meet DBP regulations.



### INTRODUCTION

Oil and gas extraction activities have become increasingly common due to enhanced gas extraction from shale. Millions of liters of water are injected per well, which return to the surface containing components released from the shale, including bromide and iodide. With the large volumes of wastewater being created, transported, and disposed, concerns have been raised about the potential for contamination of drinking water sources.<sup>1,2</sup> In most source waters, the major organic disinfection byproduct (DBP) precursor is natural organic matter (NOM), which is composed of fulvic and humic acids.<sup>3</sup> However, disinfectants can also react with organic contaminants to form DBPs,<sup>4–5</sup> and oil and gas extraction wastewaters (OGWs) tend to be highly concentrated with dissolved organic matter (DOM) contributed by both anthropogenic and geogenic constituents.<sup>5,6</sup> DBP speciation and concentrations depend on organic precursor species, bromide/iodide concentration, and the type of disinfectant used. In general, chlorine- and chloramine-

disinfection of halide-rich waters, including saline<sup>7–9</sup> and oil/gas extraction wastewaters,<sup>1,2,5</sup> enhance the formation of brominated (and iodinated, especially with chloramination) DBPs, which are more toxic than their chlorinated analogues that predominantly form during chlor(am)ination of low-salinity waters.<sup>10–14</sup> Flowback and produced waters from oil and gas activities have been reported to contain tens to thousands of parts-per-million (ppm) bromide and tens of ppm iodide from shale,<sup>1,5,15</sup> as well as up to thousands of ppm total organic carbon (TOC), mostly from fluid additives.<sup>1,15</sup>

Oil and gas extraction fluids (and their wastewaters) contain chemical additives (biocides, friction reducers, corrosion

Received: March 31, 2020

Revised: June 18, 2020

Accepted: June 29, 2020

Published: June 29, 2020

